BATTERIES FOR ADVANCED TRANSPORTATION TECHNOLOGIES (HIGH-ENERGY BATTERY)

2001
ANNUAL
PROGRESS
REPORT

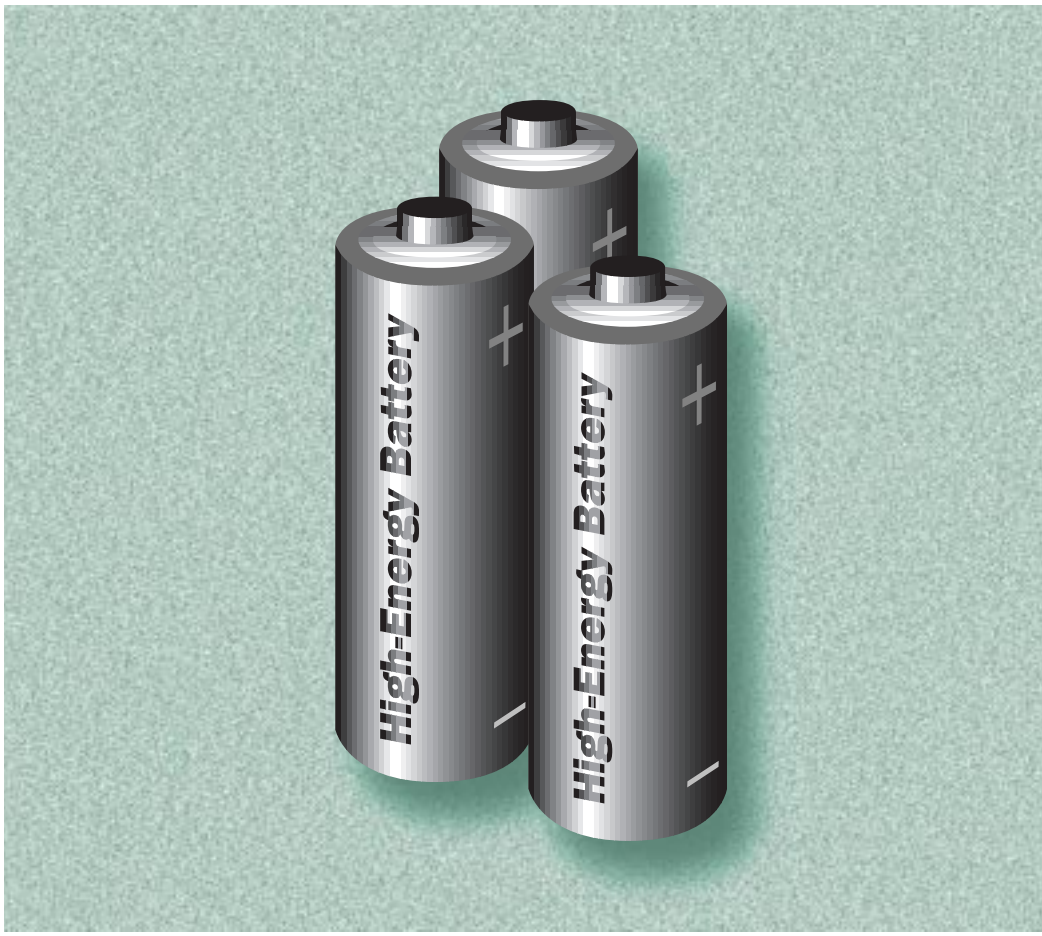

U.S. Department of Energy

Energy Efficiency and Renewable Energy

Office of Transportation Technologies

ACKNOWLEDGEMENT

We would like to express our sincere appreciation to Lawrence Berkeley National Laboratory, to Argonne National Laboratory, and to Sentech, Inc., for their artistic and technical contributions in preparing and publishing this report.

In addition, we would like to thank all our program participants for their contributions to the programs and all the authors who prepared the project abstracts that comprise this report.

U.S. Department of Energy
Office of Advanced Automotive Technologies
1000 Independence Avenue, S.W.
Washington, D.C. 20585-0121

FY 2001

Progress Report for the Batteries for Advanced Transportation Technologies (High-Energy Battery)

Energy Efficiency and Renewable Energy
Office of Transportation Technologies
Office of Advanced Automotive Technologies
Energy Management Team

Raymond A. Sutula **Energy Management Team Leader**

December 2001

CONTENTS

INTRODUCTION

The Batteries for Advanced Transportation Technologies (BATT) Program is supported by the U.S. Department of Energy Office of Advanced Automotive Technologies (DOE/OAAT) to help develop high-performance rechargeable batteries for use in electric vehicles (EVs) and hybrid-electric vehicles (HEVs). The work is carried out by the Lawrence Berkeley National Laboratory (LBNL) and several other organizations, and is organized into six separate research tasks.

Background and Program Context

The development of an advanced battery for automotive applications is a difficult undertaking. There is a strong need to identify and understand performance and lifetime limitations to help guide battery scale-up and development activities. High cell potentials and demanding cycling requirements lead to chemical and mechanical instabilities, which are important issues that must be addressed. The BATT Program addresses fundamental issues of chemistries and materials that face all lithium battery candidates for DOE EV and HEV applications. The Program emphasizes synthesis of components into battery cells with determination of failure modes, coupled with strong efforts in materials synthesis and evaluation, advanced diagnostics, and improved electrochemical models. The selected battery chemistries are monitored continuously with periodic substitution of more-promising components. This is done with advice from within the BATT Program, from outside experts, and from assessments of world-wide battery R&D. The BATT Program also educates battery and electrochemical scientists who move on to work for battery developers.

Task Descriptions

The six primary BATT Program task areas are: (1) Cell Development, (2) Anodes, (3) Electrolytes, (4) Cathodes, (5) Diagnostics, and (6) Modeling. Task 1 comprises cell fabrication, testing and characterization, Tasks 2-4 are aimed at identifying new materials, and Tasks 5-6 support all BATT Program work. Brief summary descriptions of each task follow.

The Cell Development task has identified three "baseline" rechargeable Li cell chemistries. The polymer-electrolyte cell chemistry includes a Li negative electrode, $Li(CF_3SO_2)_2N$ + cross-linked poly(ethylene) oxide (PEO)-based polymer electrolyte, and V_6O_{13} or a tunnel-structure Li_xMnO_2 positive electrolyte. The gel-electrolyte cell chemistry includes a natural graphite negative electrode or a high-capacity tin-based electrode with acceptable stability, $LiBF_4$ + cross-linked gel electrolyte, and a $LiFePO_4$ or $Li_{1.02}Al_{0.25}Mn_{1.75}O_{3.92}S_{0.03}$ positive electrode. The baseline Li-ion chemistry is based on the DOE Advanced Technology Development (ATD) Program "Generation 2" chemistry: a negative electrode composed of graphite + poly(vinylidene) fluoride (PVDF) binder, a $LiPF_6$ + ethylene carbonate-ethyl methyl carbonate (EC-EMC) electrolyte, and a positive electrode composed of $LiAl_{0.05}Ni_{0.80}Co_{0.15}O_2$ + graphite + acetylene black + PVDF binder. A web page is under development for reporting cell test data.

The Anodes task seeks to characterize and improve graphitic and other carbon materials, as well as conduct exploratory research on non-carbonaceous anode materials. Every commercial Li-ion battery uses some form of carbon as its anode material, and these batteries suffer from safety, cycle life, and storage-life problems. It is for these reasons that either improved carbons or non-

carbonaceous anodes must be developed as possible alternatives. Low-cost metal alloys with acceptable capacity, rate, cyclability, and calendar life are under investigation.

Polymer Electrolyte research aims to understand performance characteristics by studies of the transport properties of the electrolyte as a function of polymer and salt structure, polymer structural changes as a function of temperature, and interactions at the electrode/electrolyte interface related to transport and chemical/mechanical stability. A multi-pronged approach involving chemical synthesis, advanced diagnostic tools, and coordinated modeling studies is being used. The development of non-flammable electrolytes (NFEs) and novel electrolyte additives is recognized as a critical need for Li-ion battery technology. We seek to identify advanced NFEs and electrolyte additives to determine their effectiveness for liquid-based Li-ion batteries.

The identification and development of novel Cathodes is critical because of the fundamental limitations of cobalt-based and vanadium-based materials used in present-day rechargeable Li batteries. For example, Co is priced at $140/kg, which is inconsistent with EV and HEV cost targets. The focus of this effort is to develop a high-rate and stable MnO_2 cathode. Although manganese is a low-cost constituent, MnO_2 cathodes tend to lose capacity at an unacceptable rate. Research is directed at understanding the reasons for the capacity fade and developing methods to stabilize this material, as well as the evaluation of novel forms of MnO_2 cathodes.

Advanced Diagnostics are essential to investigate life-limiting and performance-limiting processes in batteries. We use post-test analyses and enhanced spectroscopic and microscopic techniques to investigate morphology, structure, and compositional changes of electrode materials. Examples include providing better understanding of the solid electrolyte interphase (SEI) layers formed on carbon through ellipsometric techniques, and a detailed investigation of the Li/polymer interface *via* advanced microscopies and spectroscopies.

Sophisticated Modeling is required to support BATT Program Tasks 1-5. This effort brings physical understanding to complex interactions through the development of comprehensive phenomenological models. Models are being advanced to elucidate the failure mechanisms of Li battery components and to understand the mechanisms for thermal runaway.

This report (originally published in June 2001 as the Final Report for CY 2000) summarizes the research activities and accomplishments of the BATT Program in FY 2001. The BATT Program is a reorganized version of the Exploratory Technology Research (ETR) Program. ETR Program reports for prior years have been published; and they are listed at the end of this Program Summary. A website for the BATT Program, which provides Internet links to recent quarterly and annual reports, is found at http://www.berc.lbl.gov/BATT/BATT.html.

Tien Q. Duong
Program Manager
Office of Advanced Automotive Technologies
Office of Transportation Technologies
Department of Energy.

TASK AREA 1: CELL DEVELOPMENT

Cell Fabrication and Testing

Kathryn A. Striebel

Lawrence Berkeley National Laboratory, 70-108B, Berkeley CA 94720

(510) 486-4385, fax: (510) 486-7303; email: kastriebel@lbl.gov

Objective

- Evaluate baseline new materials for high-power and low-cost Li-ion cells.

Approach

- Prepare uniform electrodes from novel battery materials, assemble them into baseline cells with proven components and a reference electrode, and test them with a standard protocol.
- Disassemble the cells, after testing, for analysis by the diagnostic tasks within the BATT Program.

Accomplishments

- Visited Argonne National Laboratory (ANL), Quallion Corp. and Mine Safety Appliances to evaluate techniques and materials required for pouch cell manufacture.
- Developed and used a test protocol for the evaluation of 640 mAh commercial Li-ion cells provided by DooYoun Corp. in Korea.

Future Directions

- Prepare pouch cells from commercial cell components and LBNL-prepared electrodes in liquid and gel electrolyte formulations for testing with set protocols.
- Receive and test novel materials from other projects within the BATT Program.

The testing of novel materials in a standard cell with preset protocols will provide the necessary link between the invention of novel battery components and the diagnostic evaluation of failure modes, and will accelerate the development of a battery-powered EV. This task is a collaborative effort, which includes the development of an appropriate test vehicle (cell geometry), electrochemical cycling, and cell disassembly. Novel components will be developed in BATT Program Tasks 2, 3, and 4 (anodes, electrolytes, and cathodes) for baseline liquid and gel electrolyte chemistries. These components are incorporated into a standardized cell with appropriate ratios of components (*i.e.*, active materials/electrolyte volume) and tested with a consistent protocol to determine capacity, energy, power, and lifetime characteristics. Components are then delivered to the scientists who carry out BATT Program diagnostics. Fabrication and testing of the third baseline cell, Li metal/polymer/V_6O_{13}, will be carried out in the electrolyte Task.

The test protocol was developed for 640 mAh cells received from Doo Youn Corp., Korea. The protocol involves characterization tests to establish actual *vs.* rated capacity, open circuit voltage (OCV) *vs.* depth of discharge (DoD), and power capability. The cells are then cycled at different temperatures with constant current (C/2) charge and discharge until less than 60% of the rated capacity remains, with periodic interruptions to monitor power performance.

A decision was made to pursue the pouch cell as a test vehicle for both Li-ion liquid and gel

electrolyte cells. In the case of the liquid electrolyte cells, external compression will be applied. This vehicle lends itself to the preparation of cells of varying sizes and precise determination of electrolyte volumes. In addition, there should be good flexibility on the location of reference electrodes and cell disassembly is straightforward.

This is a new project (started October 2000) and the equipment necessary for the production of laboratory pouch cells is being assembled/ordered. Site visits were made to Quallion Corp. in Los Angeles, Mine Safety Appliances in Maryland, and ANL in Chicago to gather input into this process.

A preliminary web site has been established at http://Battdata.lbl.gov/ for the posting of data generated in this task. The data will be contained in a database for ease of maintenance.

Active Materials Characterization Using X-Ray Diffraction and Chemical Analysis

Thomas J. Richardson

Lawrence Berkeley National Laboratory, 62-203, Berkeley, CA 94720

(510) 486-8619, fax: (510) 486-8619, e-mail: tjrichardson@lbl.gov

Objectives

- Determine the products and mechanisms of deterioration of active electrode materials that result in failure or lost capacity.
- Accelerate evaluation of electrode materials for in-house cell development by structural characterization of active components.

Approach

- Analyze cycled electrodes removed from BATT Program cells to ascertain phase transformations in the bulk of the active material and accumulated inactive decomposition products.

Accomplishments

- Recorded and analyzed baseline X-ray diffraction (XRD) patterns for commercial cells received from LBNL cell fabrication and testing projects; no new phases were detected in cells that failed short-term, high-temperature cycling tests.
- Design and fabrication of hardware for *in situ* XRD studies were completed.
- Prepared and characterized some alternative cathode materials.

Future Directions

- Examine BATT and commercial battery electrodes subjected to long-term cycling.
- Establish presence or absence of inactive phases and decomposition products in cycled cells.
- Carry out exploratory studies on potentially useful alternative electrode materials in support of cell fabrication and cathode development tasks.

A small number of electrodes from $LiCoO_2$ commercial cells that have completed cycling tests were received and analyzed by XRD. No new phases were detected in the cycled cathodes, as expected from the nature of the cycling tests performed to date.

Sampling hardware for *in situ* XRD experiments has been designed and built. Planar cells with beryllium windows will be studied in reflection mode.

TASK AREA 2: ANODES

Carbon Electrochemistry

Kim Kinoshita
Lawrence Berkeley National Laboratory, 90-1142, Berkeley CA 94720
(510) 486-7389, fax: (510) 486-4260; email: k_kinoshita@lbl.gov

•Objective

Identify a low-cost carbon (<$10/kg) for negative electrodes in Li-ion batteries for Evs and HEVs.

Approach

- Explore chemical procedures to develop low-cost carbons for Li-ion batteries.
- Use analytical and spectroscopic techniques such as high-resolution electron microscopy, scanning electron microscopy, Raman spectroscopy, X-ray diffraction analysis, and thermal analysis to determine the physicochemical properties of carbon.

Accomplishments

- Investigated the intercalation rate of Li^+-ions in flake natural graphite with particle sizes that ranged from 2 to 40 μm.
- Investigated how flake natural graphite with a particle size of 12 μm may provide the optimum combination of reversible capacity and irreversible capacity loss in the electrolyte and discharge rates used in this study.

Future Directions

- Continue collaboration with Superior Graphite and HydroQuébec to identify a low-cost carbon with improved rate capability in Li-ion batteries.
- Identify a chemical procedure that is less expensive than thermal processes to produce purified natural graphite for Li-ion batteries..

The intercalation rate of Li^+-ions in flake natural graphite with particle sizes that ranged from 2 to 40 μm was investigated. The amount of Li^+ ions that intercalated at different rates was determined by measurement of the reversible capacity during de-intercalation in 1 M $LiClO_4$/1:1 (volume ratio) ethylene carbonate-dimethyl carbonate (EC-DMC). The key issues in this study were the roles of particle size and the fraction of edge sites on the rate of intercalation and de-intercalation of Li^+ ions.

The working electrode was fabricated from a mixture of natural graphite and PVDF dissolved in 1-methyl-2-pyrrolidinone (NMP). The slurry was spread onto a copper grid (Exmet Corp., Naugatuck, CT) and dried under vacuum at 95°C for 24 h. A typical electrode thickness was about 200 μm, and the electrode area was 12 cm^2 (6 cm^2 per side). The working electrodes were evaluated in a three-electrode cell that contained metallic Li as both the counter and reference electrodes. The cells were built in a glove box under an Ar atmosphere containing less than 5-ppm water. Electrochemical measurements of the charge/discharge of graphite were conducted in cells cycled between 2.5 and 0 V *vs*. Li/Li^+.

Figure 1 shows representative charge-discharge profiles for NG2 and NG30 at a discharge rate of 46.5 mA/g (C/8 rate) and a charge rate of 31 mA/g (C/12 rate). The profiles show that NG2 discharged for 8 h before the potential reached 0 V, and the corresponding time for NG30 was 6 h. The time for charge of NG2 was equal to the rate (C/12), whereas the time for NG30 was less (8 h) because the Li^+-ion content in the intercalated graphite was less. At the higher discharge rates, the potential of the samples reached 0 V much sooner than the time indicated by the C-rate. Because of the slow transport rate of Li^+ ions in the graphene layer planes, the time is too short for the ions to completely intercalate the larger graphite particles to the theoretical limit. Slow solid-state diffusion of Li^+ ions produces concentration polarization in graphite that drives the potential towards 0 V, and this cut-off potential is reached before intercalation is complete.

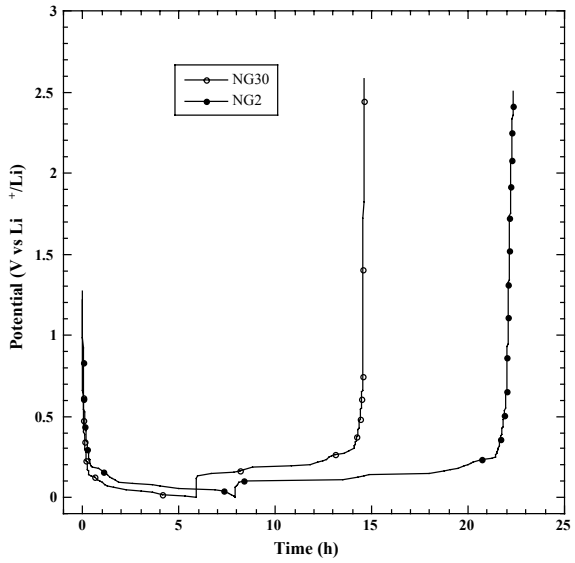

Figure 1. Charge-discharge profiles for NG2 and NG30 at a discharge rate of 46.5 mA/g (C/8 rate) and a charge rate of 31 mA/g (C/12 rate).

The composition of intercalated graphite, x in Li_xC_6, which is obtained with natural graphite of different particle size is presented in Fig. 2 as a function of discharge rate. At low specific currents, the composition of lithiated graphite approaches the theoretical value, x = 1, except for natural graphite with the largest particle size. However, x decreases with an increase in specific current for all particle sizes. This trend suggests that solid-state diffusion of Li^+ ions is limiting the intercalation capacity in graphite. At this time, we have no good explanation for the higher reversible capacity of NG12 compared to NG7. The particle size distribution of the particles in an electrode has an influence on the electrode capacity at a given intercalation rate. The presence of a small fraction of large particles in a composite electrode with a majority of monodisperse small particles lowers the overall intercalation capacity. The particle size distribution of the natural graphite was not considered in the present study, but this factor could play a role in the scatter observed in the data.

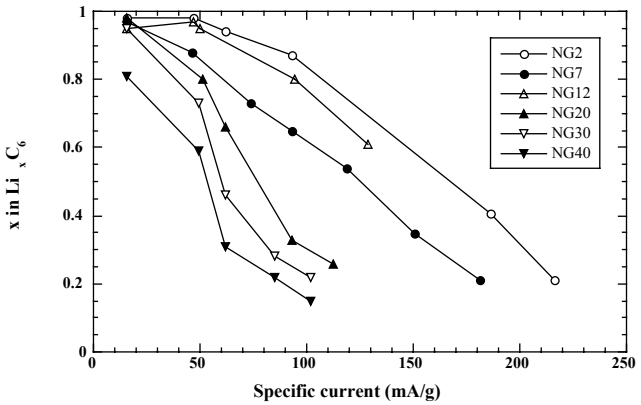

Figure 2. Composition of intercalated graphites, x in Li_xC_6, *vs.* discharge rate of natural graphite. Parameter is particle size.

The flake natural graphite with a particle size of 12 μm may provide the optimum combination of reversible capacity and irreversible capacity loss in the electrolyte and discharge rates used in this study.

PUBLICATIONS

W. Jiang, T. Tran, X. Song and K. Kinoshita, "Thermal and Electrochemical Studies of Carbons for Li-Ion Batteries. 1. Thermal Analysis of Petroleum and Pitch Cokes," *J. Power Sources,* **85**, 261 (2000).

T. Tran, B. Yebka, X. Song, G. Nazri, K. Kinoshita and D. Curtis, "Thermal and Electrochemical Studies of Carbons for Li-Ion Batteries. 2. Correlation of Active Sites and Irreversible Capacity Loss," *J. Power Sources*, **85**, 269 (2000).

W. Jiang, G. Nadeau, K. Zaghib and K. Kinoshita, "Thermal Analysis of the Oxidation of Natural Graphite – Effect of Particle Size," *Thermochim. Acta*, **351**, 85 (2000).

K. Zaghib, G. Nadeau and K. Kinoshita, "Effects of Graphite Particle Size on Irreversible Capacity Loss," *J. Electrochem. Soc.*, **147**, 2110 (2000).

S.E. Sloop, J.K. Pugh, S. Wang, J.B. Kerr and K. Kinoshita, "Chemical Reactivity of PF_5 and $LiPF_6$ in Ethylene Carbonate/Dimethyl Carbonate Solutions," *Electrochem. and Solid-State Lett.,* **4**, A42 (2001).

T. Tran and K. Kinoshita, "Surface Modifications for Carbon Lithium Intercalation Anodes," *U.S. Patent 6,096,454*, August 1, 2000.

.

Optimization of Anodes for Li-Ion Batteries

M. David Curtis and Gholam-Abbas Nazri

University of Michigan, Department of Chemistry, Ann Arbor MI 48109-1055

(734) 763-2132; fax: (734) 763-2307; e-mail: mdcurtis@umich.edu

Objectives

- Develop new surface coatings for carbonaceous anodes in order to minimize electrolyte decomposition and enhance Li-ion conduction for application in advanced Li batteries.
- Improve safety aspects of Li-ion technology by incorporating electron- and ion-conducting polymers with fire-retardant properties in the construction of carbonaceous anodes.

Approach

- Establish a baseline for thermal behavior of carbonaceous anodes at various states of charge, and compare thermal and electrochemical properties of the modified electrodes with the baseline data.
- Simulate lithiated graphite anodes by chemical intercalation and evaluate thermal behavior of the modified surface-coated graphitic anodes.
- Evaluate reactivity of modified surface-coated anodes toward electrolyte decomposition, gas generation, and surface film formation.
- Improve surface coating and binder technology for large-surface-area electrodes.

Accomplishments

- Completed the determination of thermal stability and reactivity of various graphitic anodes as a function of the electrolyte composition and degree of lithiation. These data constitute the baseline behavior against which further modifications of anode surface behavior will be compared.
- Synthesized and evaluated new lithium phosphonate materials for use as artificial SEI coatings on carbon anodes.
- Developing new polymers that are both ionic and electronic conductors and that can serve simultaneously as anode surface passivators and binder.

Future Directions

- Use the new polymer systems as described above to construct test cells for comparison against our baseline data.
- Optimize the overall performance of graphitic anodes for high-power and high-energy applications.

Carbonaceous anodes are currently the material of choice for use in Li-ion batteries. However, these materials react with the electrolyte to produce flammable organic gases during initial charge cycles. This reaction also produces a gelatinous surface coating (SEI layer) that eventually passivates the carbon surface towards reaction with the electrolyte. Although this coating has the beneficial property of passivation, the coating also increases the internal impedance of the cell, leads to irreversible capacity loss in the first cycles, and can cause mechanical instability and loss of electrical contact between the carbon particles.

We have established a baseline data set against which future modifications of the carbon anode can be compared. This baseline includes the nature and amounts of the various gases that are released during the initial passivation reactions, as well as the thermal stability and chemical compositions of the SEI, and the nature of the sites on the carbon particles that lead to deleterious electrolyte decompositions. The thermal stability of chemically prepared LiC_x electrodes was determined as function of Li content.

Most of the work in the past year has been focused on the synthesis and testing of new Li-phosphonates for use as artificial SEI coatings and/or binders for carbon anodes. It is our working hypothesis that the active sites on the carbon particles can be blocked from reaction with electrolyte, thus diminishing or eliminating the release of flammable gases. These coatings must conduct Li ions in order that the internal impedance not be increased unduly. Furthermore, if the coating can act as binder, a step in the anode manufacturing process could be avoided. For high-power applications, the binder itself should be electronically conductive in order for all carbon particles to be in electrical contact with each other and with the current collector. We are therefore now focusing our efforts on the development of new binder-SEI coatings that will simultaneously passivate the carbon surface, allow facile transport of Li ions, and serve as an electron-conducting binder.

The types of materials that are under development are conjugated polymers (electrically conducting in the doped or charged state) that have pendant ionic groups to facilitate Li-ion transport. Examples of these polymers are shown in the following figures.

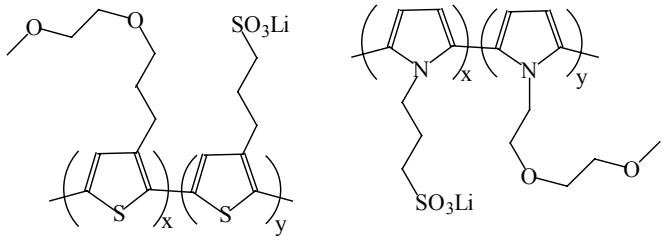

Figure 3.

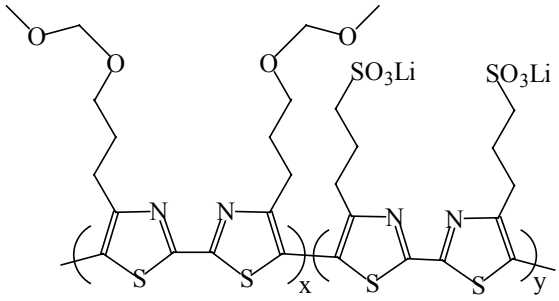

Figure 4.

PUBLICATION

T. Tran, B. Yebka, X. Song, G. Nazri, K. Kinoshita and D. Curtis, "Thermal and Electrochemical Studies of Carbons for Li-Ion Batteries. 2. Correlation of Active Sites and Irreversible Capacity Loss," *J. Power Sources*, **85**, 269 (2000).

Non-Carbonaceous Anode Materials

Michael M. Thackeray

Chemical Technology Division, Argonne National Laboratory, Argonne IL 60439

(630)-252-9183; fax: (630)-252-4176; email: thackeray@cmt.anl.gov

Objective

- Replace carbon with an alternative anode material that is inexpensive and that will improve the safety of Li-ion cells.

Approach

- Search for, characterize, and develop inexpensive intermetallic electrodes that provide an electrochemical potential a few hundred millivolts above that of metallic Li with capacities >400 mAh/g and 1000 mAh/ml.
- Focus on nickel-arsenide and zinc-blende-type structures, and study their structural and electrochemical behavior during discharge and charge in Li cells.

Accomplishments

- Improved the performance of copper-tin electrodes by the use of metal-substituted compounds $Cu_{6-x}M_xSn_5$ (M=Fe, Ni, Zn); achieved a rechargeable capacity in excess of 300 mAh/g for the early cycles.
- Studied InSb electrodes in detail and established the importance of invariant face-centered-cubic (fcc) intermetallic electrode structures.

Future Directions

- Improve the processing and optimize the compositions of intermetallic electrodes, particularly those containing copper and/or tin.
- Interact with industry to evaluate the intermetallic electrodes in customized cells.
- Continue to explore intermetallic compounds in which there is a strong crystallographic relationship between parent and lithiated structures.

Considerable progress was made during the past calendar year in understanding the electrochemical behavior of intermetallic electrodes and the structural changes that occur upon reaction with Li. Progress has also been made in improving the electrochemical properties of these materials, with major focus on NiAs-type and zinc-blende-type structures. In particular, our research was directed toward the exploitation of the Cu-Sn system by investigating the substituted derivative structures $Cu_{6-x}M_xSn_5$, in which M=Mn, Fe, Co, Ni, and Zn. We demonstrated that electrodes with substituted compositions, such as Cu_5NiSn_5 and Cu_5FeSn_5, showed superior capacities and cycling stability compared to the unsubstituted parent electrode Cu_6Sn_5, when cycled between 1.2 and 0.2 V *vs.* metallic Li. For example, a rechargeable capacity >350 mAh/g was obtained during the early cycling of Cu_5FeSn_5 electrodes between 1.2 and 0.01 V *vs.* Li. When we restricted the lower voltage of $Li/Cu_{6-x}M_xSn_5$ cells to 0.2 V, the structure of the lithiated product (lithiated zinc-blende-type) exhibited a strong crystallographic relationship to that of the parent electrode (nickel arsenide-type). This relationship is believed to contribute to the good electrochemical cycling of these cells.

The realization that the zinc-blende framework of a lithiated copper-tin electrode (Li_2CuSn) provided a three-dimensional interstitial space for Li led to a detailed investigation of the family of III-V semiconductors, MSb (M=Al, Ga, In), as possible negative electrodes for Li-ion batteries. Preliminary investigations showed that InSb attains significantly superior electrochemical behavior over AlSb and GaSb. Our research has thus focused on the InSb system, which can deliver a rechargeable capacity of ~300 mAh/g at a C/18 rate.

Two ternary phases in the Li-In-Sb system were identified previously at 400°C by Sitte and Weppner; they lie on the InSb-Li_3Sb tie line [$Li_zIn_{1-z/3}Sb$ ($0 \le z \le 3$)] in the Li-In-Sb phase diagram (Fig. 5) and have compositions close to $Li_{1.5}In_{0.5}Sb$ (z=1.5) and $Li_2In_{0.33}Sb$ (z=2).

The electrochemical reaction of Li with InSb is analogous to the reversible high-temperature reaction of Li with Fe_3O_4 (spinel-type structure) during which Li is inserted into, and iron extruded from, an invariant fcc oxygen array to generate a series of ternary Li-Fe-O compounds. InSb has a zinc-blende structure in which both the In and Sb atoms are arranged in independent fcc arrays that are interlinked to form a diamond-like lattice, each In atom being tetrahedrally coordinated to a Sb atom, and vice versa. There are two crystallographically independent interstitial tetrahedral sites for Li: one site is coordinated to four Sb atoms, and the second to four In atoms. During the discharge of Li/InSb cells, *in situ* X-ray absorption fine structure data showed that 1) the reaction occurs by Li insertion into, and In extrusion from, InSb to yield electrode compositions $Li_xIn_{1-y}Sb$ ($0 < x \le 3$, $0 < y \le 1$), and 2) not all the Li is reincorporated back into the fcc Sb array during charge. In the Li_3Sb structure, the Li atoms occupy the In sites and all the tetrahedral interstitial sites of the InSb structure. Therefore, a strong structural relationship exists between the parent InSb electrode and its fully lithiated product, *i.e.,* the Li_3Sb structure can be regarded as having a lithiated zinc-blende structure $Li_2(LiSb)$ in which (LiSb) refers to the zinc-blende framework. What is remarkable about this structural relationship is that the unit cell parameter of pure Li_3Sb (Fm3m, *a*=6.572 Å) is only 1.4% larger than that of InSb (Fd3m, *a*=6.478 Å), reflecting only a 4.4% increase in the volume of the fcc Sb lattice, thereby contributing to the reversibility of the electrode. When the volume of the extruded In is taken into account, the Li_3Sb/In electrode is 46.5% larger in volume than InSb. Lithiation of the extruded In metal occurs below ~0.55 V to yield a series of Li_xIn compounds ($0 < x \le 4$).

The approach we adopted to identify intermetallic electrodes by considering structural relationships between parent and lithiated compounds has opened up new avenues for our research, and it became the underlying theme of our project in 2000; it will continue to be so during 2001.

PUBLICATIONS

J.T. Vaughey, J. O'Hara and M.M. Thackeray, "Intermetallic Insertion Electrodes with a Zinc-Blende-Type Structure for Li Batteries: A Study of Li_xInSb ($0 \le x \le 3$)," *Electrochem. and Solid State Lett.*, **3**(1) 13 (2000).

J.T. Vaughey, K.D. Kepler, C.S. Johnson, T.Sarakonsri, R. Benedek, J.O. O'Hara, S. Hackney and M.M. Thackeray, "Intermetallic Insertion Electrodes for Lithium Batteries," *The Electrochem. Soc. Inc., Proc*. **99-24**, 280 (2000).

M.M. Thackeray, J.O. Thomas and M.S. Whittingham, "Science and Applications of Mixed Conductors for Lithium Batteries," *Materials Research Society Bulletin*, 39 (March, 2000).

C.S. Johnson, J.T. Vaughey, M.M. Thackeray, T. Sarakonsri, S.A. Hackney, L. Fransson, K.K. Edström and J.O. Thomas, "Electrochemistry and In-Situ X-ray Diffraction of InSb in Lithium Batteries," *Electrochem. Comm.*, **2** (8), 595 (2000).

C.H. Chen, J.T. Vaughey, A.N. Jansen, D.W. Dees, A.J. Kahaian, T. Goacher and M.M. Thackeray, "Studies of Mg-substituted $Li_{4+x}Mg_xTi_5O_{12}$ Spinel Electrodes ($0 \le x \le 1$) for Lithium Batteries," *J. Electrochem. Soc*., **148**, A102 (2001).

PRESENTATIONS

C.S. Johnson, J.T. Vaughey and M.M. Thackeray, "Cycling Performance of Intermetallic Insertion Electrodes in Lithium Batteries," *4th Chicago*

Battery Workshop, Illinois Institute of Technology, Chicago, IL, April 13-14, 2000.

J.T. Vaughey, C.S. Johnson, A.J. Kropf, R. Benedek, M.M. Thackeray, H. Tostmann, T. Sarakonsri, S. Hackney, L. Fransson, K. Edström and J.O. Thomas, "Structural and Mechanistic Features of Intermetallic Materials for Lithium Batteries," *10th International Meeting on Lithium Batteries*, Lake Como, Italy, 28 May - 2 June, 2000.

C.S. Johnson, J.T. Vaughey, D.W. Dees, A.N. Jansen, M.M. Thackeray, T. Sarakonsri and S.A. Hackney, "Electrochemistry and Impedance Analysis of Intermetallic Electrodes for Lithium Batteries," *10th International Meeting on Lithium Batteries*, Lake Como, Italy, 28 May - 2 June, 2000.

J.T. Vaughey, C.S. Johnson, R. Benedek, M.M. Thackeray, A.J. Kropf, H. Tostmann, L. Fransson, K. Edström, J.O. Thomas, T. Sarakonsri and S.A. Hackney, "A New Class of Intermetallic Anodes for Lithium Batteries," *Gordon Conference on Solid State Chemistry*, NH, July 31-August 4, 2000.

J.T. Vaughey, C.S. Johnson, R. Benedek, M.M. Thackeray, L. Fransson, K. Edström and J. Thomas, "Mechanistic and In-situ X-ray Studies of Intermetallic Electrodes for Lithium-Ion Batteries," *198th Meeting of the Electrochemical Society*, Phoenix, AZ, October 22-27, 2000.

M.M. Thackeray, J.T. Vaughey and C.S. Johnson, "Recent Developments in Anode and Cathode Materials for Lithium-Ion Electrochemical Cells,", *Materials Research Society Meeting*, Boston, MA, November 27-December 1, 2000.

M.M. Thackeray, J.T. Vaughey and C.S. Johnson, "Intermetallic Electrodes for Lithium Batteries,", *DOE Workshop on Interfaces, Phenomena and Nanostructures, in Lithium Batteries,* Argonne, IL, December 11-13, 2000.

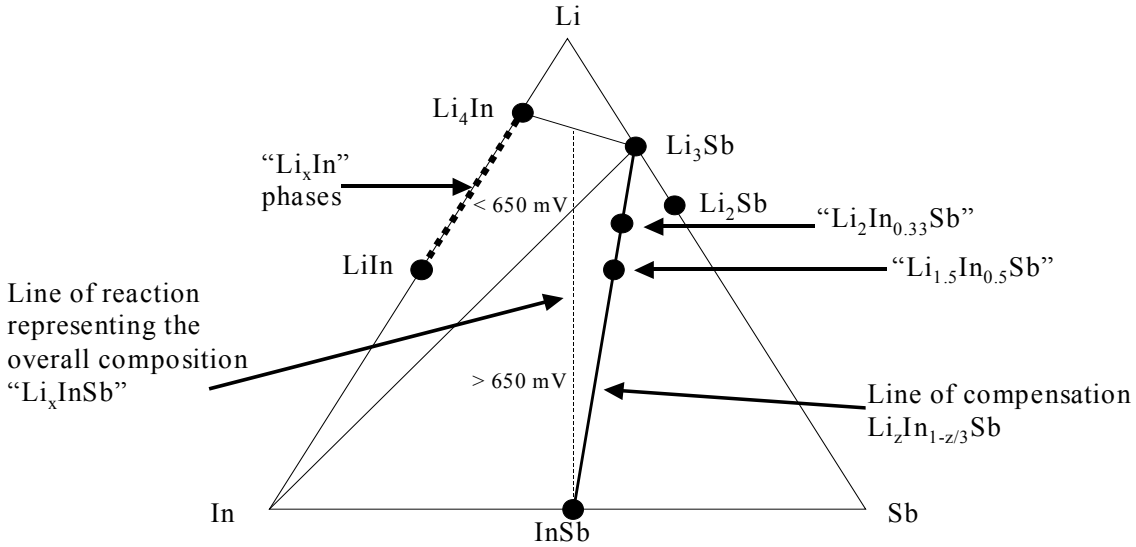

Figure 5. The Li-In-Sb phase diagram.

Materials: Novel Anodes

M. Stanley Whittingham

Chemistry and Materials Research Center, State University of New York at Binghamton, Binghamton, NY 13902-6000

(607) 777-4623, fax: (607) 777-4623; e-mail; stanwhit@binghamton.edu

Objective

- Replace the presently used carbon anodes with safer materials that will be compatible with manganese oxide cathodes and associated electrolytes.

Approach

- Explore, synthesize, characterize, and develop inexpensive materials that have a potential ~500 mV above that of pure Li and higher volumetric energy densities than carbon.
- Evaluate all materials electrochemically in a variety of cell configurations, and for thermal and kinetic stability.

Accomplishments

- Determined that vanadium and manganese oxides, in their highest oxidation states, are not prime candidates for anode materials, despite reports from France and Japan.
- Found pure aluminum to have a high capacity and to react readily with Li, but its capacity faded rapidly upon cycling.
- Identified some simple binary alloys of Al and of Sn.

Future Directions

- Improve the electrochemical performance of the materials identified, and complete a survey of all Al-based binary systems and their reactivity with Li.
- Identify several additional non-Al binary alloys.
- Evaluate Mn-containing alloys, as they should be immune from poisoning by Mn migration from the cathode.

The goal of this project is to identify low-cost, low-weight anode materials that are safer than the presently used carbonaceous materials and are compatible with next-generation cathode materials. Although carbonaceous materials are being successfully used in Sony Li-ion cells, there are safety issues as the capacity increases. This project is taking two approaches: use of oxides giving essentially a simple symmetric cell:

$$Li_{1+y}MnO_2 \text{ |electrolyte| } Li_{1-y}MnO_2$$

or use of simple metal alloys, such as those based on Al:

$$LiAlM_y \text{ |electrolyte| } Li_{1-y}MnO_2$$

We studied several manganese oxides including the spinel and layered phases. In each case the material could be reduced to Li_2O and Mn based on the Li utilization. However, little capacity was retained after recharge to 1 V *vs.* Li, so the effort was switched to mixed manganese-vanadium oxides and to vanadium oxides. French and Japanese workers (*Solid State Ionics* **139**, 57, 2001) have studied MnV_2O_6 and found positive results but with a relatively low storage capacity, 400Ah/kg, in the 0 to 1.0 V range. MnV_2O_5, a material first synthesized by us, was expected to have a higher storage capacity because of its lower oxygen content. However, we found very little capacity even after extensive mechanical grinding. This low capacity combined with the need to find a means of initially charging the material without wasting the active cathode material makes such oxides unattractive as

anodes. We are therefore discontinuing work on these manganese-vanadium oxides as anodes. However, in the process of this work, a new low-temperature route for the synthesis of $LiMn_2O_4$ was found. We can now prepare both the spinels and layered phases of Li_xMnO_2 below 200°C.

Aluminum is the ideal anode material, being low cost, readily available, and forming a simple alloy with lithium, LiAl. This reaction occurs at about 0.3 V above pure Li on an essentially flat plateau as shown in Fig. 6. However, the material expands significantly upon Li incorporation causing break-up of the anode. This combined with the brittleness of the LiAl causes contact problems during cycling, resulting in relatively poor cycling behavior as shown in Fig. 7. Even so it was the first anode used in rechargeable Li batteries, being coupled with TiS_2 (Exxon-1978).

The data shown in Fig. 6 were obtained in a clamped Swagelok™ design cell wherein pressure is applied continuously to the electrodes. When a higher-capacity flooded-electrolyte bag cell is used the capacity falls even more rapidly. Clearly cell construction is critical for the behavior of anode materials. This is due to the need to maintain pressure on the particulate matter so that optimum contact is maintained as the volume changes. We have obtained a button cell set-up, which will allow for more reproducible cell systems.

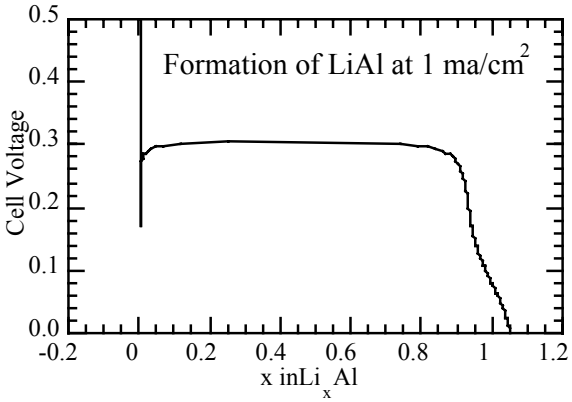

Figure 6. Incorporation of Li into Al at 1 mA/cm^2 in the cell Li ||electrolyte| Al.

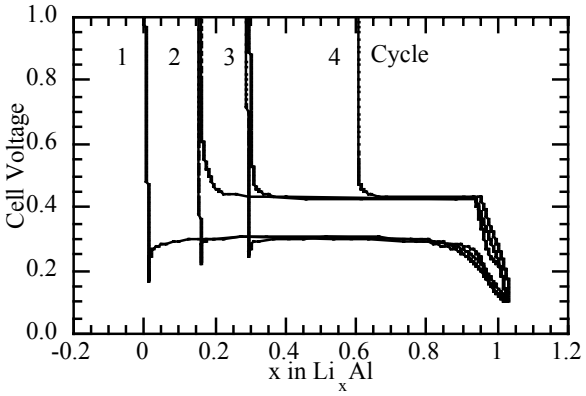

Figure 7. Cycling of Al metal in a clamped Swagelok cell.

A number of Al alloys were prepared and their ability to take up Li is being evaluated. Preliminary data for two Ni and Si samples are shown in Fig. 8. Both show some capacity above 1 V suggesting reaction with oxide films or possible electrolyte reaction. Such reactions are not observed with Al itself. The Ni reduced the capacity of Li at room temperature and therefore did not merit further study. The capacity of the Si-containing sample was not significantly better than Al itself and its rechargeability was worse. The addition of Cu or Mg to Al also resulted in lower capacities.

We investigated two other binary Al compounds, aluminum carbide Al_4C_3 and aluminum boride AlB_2, for their ability to react with Li. We hope that by investigating such compounds the large volumetric changes occurring during the reaction between pure Al and Li can be ameliorated.

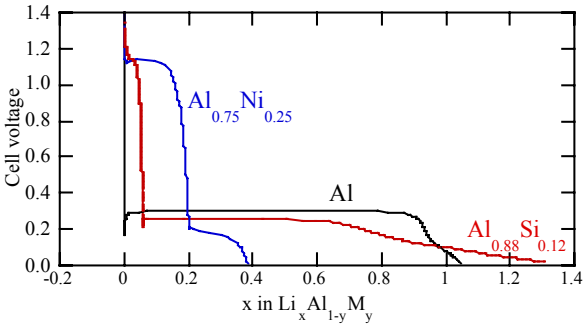

Figure 8. Electrochemical insertion of Li into Al, $Al_{1-y}Si_y$, and $Al_{1-y}Ni_y$.

Figure 9 shows the behavior of aluminum carbide, Al_4C_3, a combination of two known anode-active materials. The reaction potential of 1 V is

higher than either single component. The carbide reacts with 3 Li per formula unit during discharge between 0.8 and 0.05 V *vs.* pure Li giving an initial capacity significantly higher than that of graphitic carbon, but slightly less than that of pure Al. The rechargeability of this material was poor with less than 1 Li recovered upon charge, just as for the aluminum silicon 'alloy'. We will test in the button cell configuration so these cells can be kept under compression.

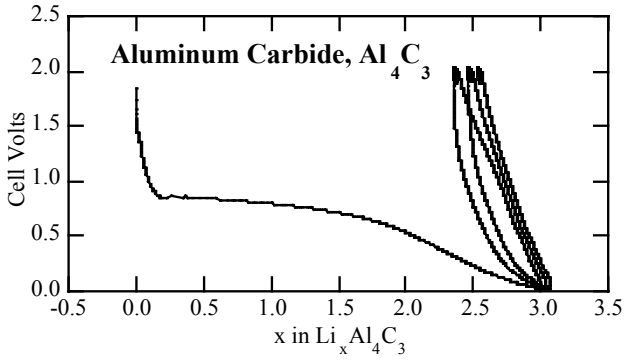

Figure 9. Electrochemical insertion of Li into Al_4C_3.

Figure 10 shows the behavior of aluminum boride, AlB_2, in a low-capacity Swagelok™ cell. It reacts with 0.8 Li per formula unit, and up to half of this could be recovered when charging the cell. The initial capacity translates to 430 Ah/kg, *i.e.,* slightly higher than that of graphite, 340 Ah/kg. We will evaluate this system in a button cell. Little change in the XRD diffraction pattern was observed after reaction.

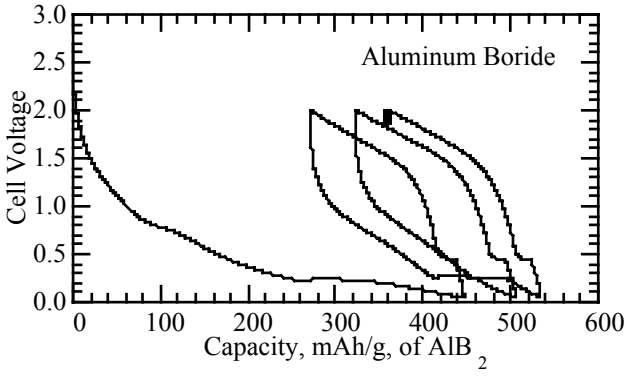

Figure 10. Electrochemical insertion of Li into aluminum boride.

We began an investigation of some simple Sn-based materials, and we are confirming the much better behavior of Sn_2Mn over at least the initial cycles. Such a material is particularly attractive as it should not be poisoned by Mn transported from the cathode.

PUBLICATION

S. Yang, P.Y. Zavalij and M.S. Whittingham, "Synthesis and Crystal Structure of $Li_2Sn(OH)_6$," *Acta Cryst*., **C57**, 228-229 (2001).

PRESENTATION

S. Yang and M.S. Whittingham, "Aluminum Based Anode Materials for Lithium Batteries," *Materials Research Society Meeting*, Boston MA, November 27-30, 2000.

TASK AREA 3: ELECTROLYTES

Electrolytes: R&D for Advanced Lithium Batteries

John B. Kerr

Lawrence Berkeley National Laboratory, 62-203, Berkeley, CA 94720

(510)-486-6279, fax (510)-486-4995; email: jbkerr@lbl.gov

Objectives

- Determine the feasibility of the Li metal electrode with organic electrolytes and provide operating conditions that prevent dendrite growth.
- Determine the limitations on Li-ion transport in polymer electrolytes and composite electrodes and develop new materials capable of ambient-temperature operation with Li metal electrodes.
- Determine the limits of stability of organic electrolytes at high-voltage cathode materials (4 V) and develop materials and methods to increase stability.
- Provide cross-linkable polymers for use in the Li/polymer and gel polymer test systems and scale up synthesis and processing to 100 cm^2 pouch cells.

Approach

- Apply a combination of synthesis, analysis, modeling and testing, *i.e.,* a physical organic chemistry approach to electrolyte design, thereby ensuring that not only are the sources of poor performance and failure pinpointed but the problem can be corrected through as-developed materials design and synthesis capabilities.

Accomplishments

- Conducted experiments which demonstrated that the mechanical properties of the electrolyte play a significant role in dendrite growth at Li metal electrodes.
- Developed methods to separate the mechanical properties from the ion-transport properties to provide high-rate Li/polymer batteries.
- Prepared polymer electrolytes that contain ion-solvating ether groups which are different from the commonly used ethylene oxide units, and observed significant increases in conductivity, that show promise for room-temperature performance of Li/polymer batteries.

Future Directions

- Carry out detailed quantitative measurements of the transport and mechanical properties of polymer electrolytes to optimize transport *vs*. interfacial behaviors to minimize dendrite growth.
- Prepare and optimize polymers with new ion-solvating groups and appropriate architectures to achieve ambient-temperature operation with solid polymer electrolytes.
- Develop polymer electrolyte systems capable of operation with 4-V cathodes and Li metal electrodes.
- Develop quantitative measures to characterize electrolyte side reactions.
- Develop synthetic capabilities to provide materials and processing for larger-scale Li/polymer and polymer gel test systems.

Links between dendrite growth and mechanical and transport properties. Lithium cycling experiments in symmetrical cells with linear polymer electrolytes based on PEO have clearly demonstrated that dendrites are formed rapidly if the limiting current is exceeded, as expected for electrode position of metals. The limiting current for the Li electrode is calculated from knowledge of the transport properties of the electrolyte (diffusion coefficient, transference number) and the dimensions of the cell (area, thickness). However, even with current densities well below the calculated limiting current, rapid dendrite growth is observed with linear polymer electrolytes. These polymers are essentially viscous liquids with a linear chain structure. Cross-linked linear and comb-branch polymer structures have been shown to possess properties of solids (see 1999 Annual Report). Significant improvements in the cycling behavior were observed with increasing cross-link density and hence higher elastic moduli. Figure 11 shows the behavior of a comb-branch polyepoxide ether electrolyte which has been cross-linked with a 10% density. Cycling is continued for over 100 cycles and a total of 150 coulombs of charge is passed before the cell suddenly fails due to a short-circuit arising from a dendrite. With a polymer that has a cross-link density of only 5% the cycle life is only 15 cycles (22 coulombs). Without cross-linking, dendrite growth is observed very quickly. Quantitative study of these effects in addition to study of side reactions is under way in order to allow prediction of safe operating conditions that prevent growth of dendrites.

Polymers with improved ion-transport properties. New polymer structures have been prepared with conductivity that is superior to what has been achieved to date with PEO-based polymers. In collaboration with modeling groups (M. Ratner, L. Curtis and J. Halley), who provided theoretical guidance, the polymer structures have evolved from linear PEO-like materials to comb-branch or dendritic polymers with side chains that contain ether side groups that are more labile than those based on ethylene oxide units. Among these groups are 1,3-propanediol units. The effect of incorporating this unit into the polymers is shown in Fig. 12. These results show that the theoretical understanding of ion transport through the polymer hosts has advanced greatly in recent years and that room-temperature solid polymer electrolytes are within reach.

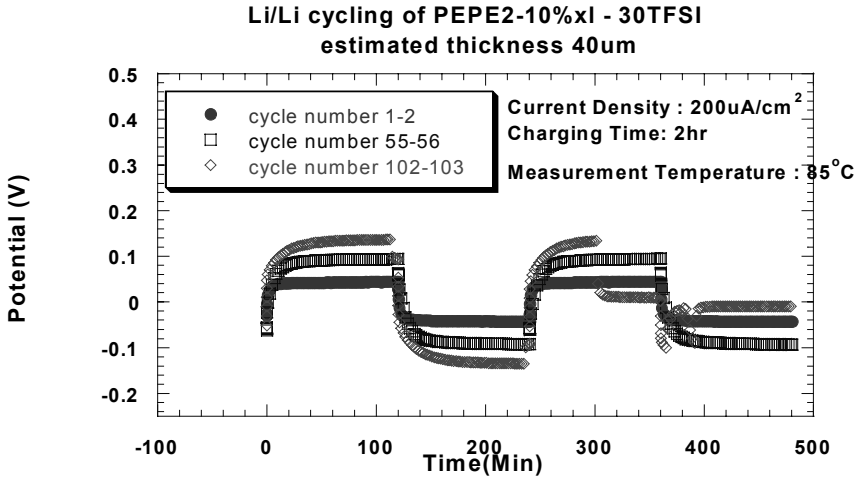

Figure 11. Dendrite growth during cycling of symmetrical Li/Li cells.

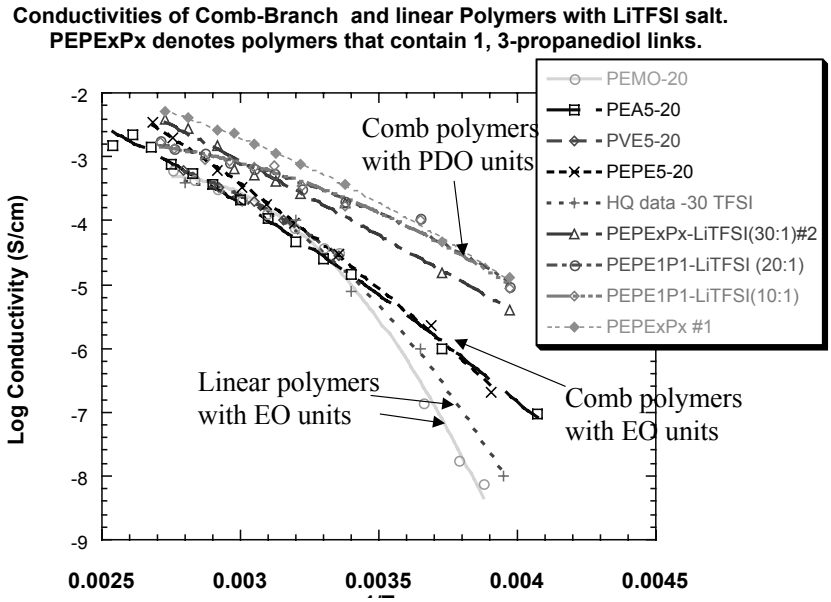

Figure 12. Conductivity measurements for linear and comb branch polymers based on ether solvating groups.

PUBLICATIONS

L. Edman, A. Ferry and M.M. Doeff, "Slow Recrystallization in the Polymer Electrolyte System $P(EO)_nLiTFSI$," *J. Mater. Res.,* **15**, 1950 (2000).

L. Edman, M.M. Doeff, A. Ferry, J. Kerr and L.C. De Jonghe, "Transport Properties of the Solid Polymer Electrolyte System $P(EO)_nLiTFSI$," *J. Phys. Chem. B.*, **104**, 3476 (2000).

M.M. Doeff, L. Edman, S.E. Sloop, J. Kerr and L.C. De Jonghe, "Transport Properties of Binary Salt Polymer Electrolytes," *J. Power Sources,* **89**, 227 (2000).

K.E. Thomas, S.E. Sloop, J.B. Kerr and J. Newman, "Comparison of Lithium-Polymer Cell Performance with Unity and Nonunity Transference Numbers," *J. Power Sources*, **89**, 132-138 (2000).

O. Buriez, Y.B. Han, J. Hou, J.B. Kerr, J. Qiao, S.E. Sloop, M.M. Tian and S.G. Wang, "Performance Limitations of Polymer Electrolytes Based on Ethylene Oxide Polymers," *J. Power Sources*, **89**, 149-155 (2000).

Composite Polymer Electrolytes for Use in Lithium and Lithium-Ion Batteries

Saad A. Khan, Peter S. Fedkiw and Gregory L. Baker*[+]

Department of Chemical Engineering, North Carolina State University, P.O. Box 7905, Raleigh NC 27695-7905; [+]*Department of Chemistry, Michigan State University, East Lansing, MI 48824-1322*

**Phone: (919) 515-4519; Fax: (919) 515-3465; e-mail: khan@eos.ncsu.edu*

Objective

- Develop composite polymer electrolytes (CPEs) that are low-cost, have high conductivities, impart electrode-electrolyte interfacial stability, and yield long cycle life.

Approach

- Use surface-functionalized fumed silica fillers in BATT-baseline systems to determine the effects of filler type and concentration on interfacial stability and cell cycling.
- Utilize a combination of electrochemical characterization, rheological techniques, and chemical syntheses to correlate electrochemical characteristics with mechanical properties and materials chemistry (*e.g.,* silica-type or PEO-type).

Accomplishments

- Determined that the presence of fumed silica in CPEs increases cell capacity and decreases capacity fading in full-cell cycling of Li/Li_xCoO_2 and $Li/Li_xMn_2O_4$ couples.
- Established effects of fumed silica surface groups on Li/Li_xCoO_2 cell capacity and cycling.
- Synthesized and measured the conductivity of fumed silica with dual functionalities containing different ratios of alkyl to cross-linkable groups.
- Studied the effects of cross-linkable CPE constituents on the interfacial resistance between Li and CPE.

Future Directions

- Determine how fumed silicas (hydrophobic R805 and hydrophilic A200) affect full-cell cycling using vanadium-based, 3-V cathodes and baseline PEO-type materials in coin cells.
- Establish the relationships between interfacial stability and mechanical properties.

The objective of this research is to develop a new range of CPEs for use in rechargeable Li and Li-ion batteries. In particular, our goal is to develop highly conductive electrolytes that exhibit good mechanical properties, and at the same time show good compatibility with typical electrode materials. The unique feature of our approach is the use of surface-functionalized fumed silica fillers to control the mechanical properties of the electrolytes and enhance electrode-electrolyte interfacial stability.

Full-cell cycling studies of Li/Li_xCoO_2. We have previously reported that fumed silica-based CPEs with low-molecular-weight PEOs exhibit conductivities exceeding 10^{-3} S/cm at 25°C, have electrochemical properties (Li transference number, conductivity) decoupled from mechanical properties, and thus provide a range of mechanical moduli (as high as 10^6 Pa). Furthermore, the presence of fumed silica enhances Li-electrolyte interfacial stability. Beside the above-mentioned electrochemical and mechanical properties, a long cycle life with a high capacity is also crucial for the electrolytes of rechargeable batteries. Full-cell cycling with fumed silica-based CPEs using Li anodes and metal oxide cathodes has been carried out.

The effect of fumed silica and its surface chemistry on full-cell cycling was studied using a standard $LiCoO_2$ composition (91 wt% $LiCoO_2$, 6 wt% graphite SFG15, and 3 wt% PVDF), shown in Fig. 13. Three types of fumed silica were used: native fumed silica A200 with hydroxyl groups, octyl-modified R805, and PEO-modified FS-EG3. Cell capacity quickly fades after the first few cycles in the absence of fumed silica, but the addition of 10 wt% particulates diminishes the capacity fade, with the effect dependent upon the silica surface chemistry. The native fumed silica (A200) exhibited the best improvement of capacity fading, whereas the PEO-modified fumed silica (FS-EG3) showed the least improvement.

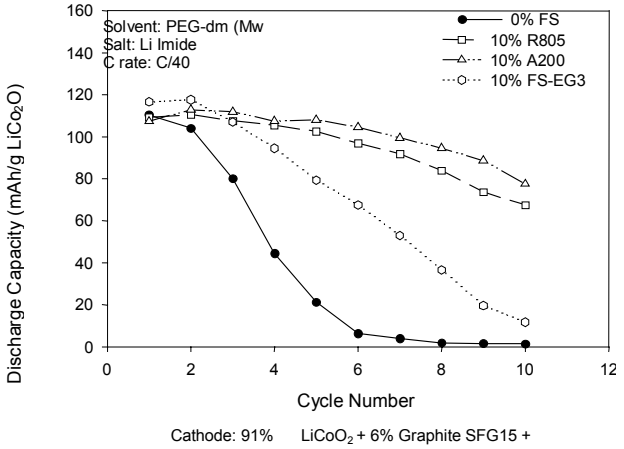

Figure 13. Effect of fumed silica and its surface chemistry on cell capacity of Li/electrolyte/$LiCoO_2$ cycling.

Full-cell cycling studies of Li/$Li_xMn_2O_4$. Figure 14 shows the effect of octyl-modified fumed silica on the discharge capacity of Li/$Li_xMn_2O_4$ cycling. The beneficial effect of fumed silica is independent of cathode materials; as with Li_xCoO_2, fumed silica increases the discharge capacity and lowers capacity fading relative to the base electrolyte. Such independence gives us the flexibility to extend the application of our composites to a variety of rechargeable Li and Li-ion batteries with diverse cathode materials.

Conductivity of cross-linkable CPEs. The conductivities of crosslinked and uncrosslinked CPEs with trichlorosilyl octyl methacrylate (TOM) 1:1, TOM 4:1, and TOM 1:4 fumed silica [X:Y refers to X moles of methacrylate groups and Y moles of octyl group in Fig. 15] are shown as a function of temperature and fumed silica surface group. The conductivity of the cross-linked CPEs is independent of the fumed silica surface group and decreases by a factor of two after cross-linking. This suggests that the crosslinking occurs between adjacent fumed silica particles and does not affect the bulk electrochemical properties of the electrolyte. Consequently, the selection of salt and polymer matrix can be varied to tune the electrochemical properties. Finally, the room-temperature conductivity of the PEGdm(250) CPEs is close to 10^{-3} S/cm.

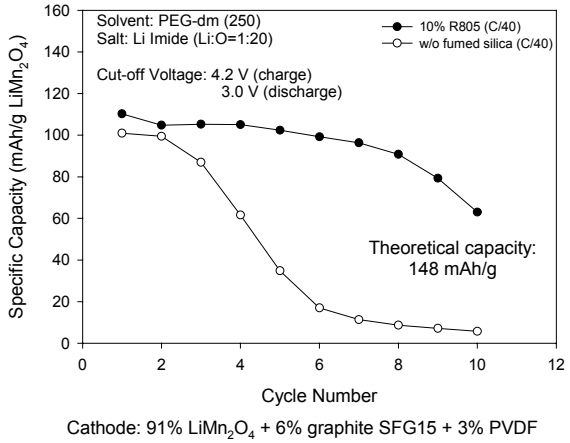

Figure 14. Effect of octyl-modified fumed silica (R805) on Li/$Li_xMn_2O_4$ full-cell cycling.

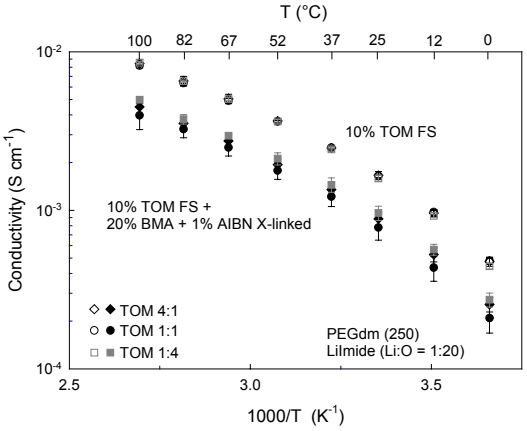

Figure 15. Conductivity of cross-linkable CPEs containing PEGdm(250) and various dual-functionalized fumed silicas (TOM 1:1, TOM 4:1, and TOM 1:4).

Interfacial stability studies of Li/CPE interface for cross-linkable CPE components. An important concern in CPE development is the formation of a stable interface with Li. One of our

concerns is the possible interaction of the monomer and initiator with Li metal and developing possible avenues for mitigating this problem. We have previously reported the remarkable success of interface stabilization by addition of fumed silica to the polyethylene glycol-dimethy ether (PEG-dme)-based electrolytes. However, the presence of reactive species such as butyl methacrylate (BMA) and the initiator azo-bis-isobutyronitrile (AIBN) may pose a problem. Figure 16 shows the effect of the cross-linkable CPE constituents on interfacial resistance. The addition of TOM 1:1 stabilizes the interface. The interfacial stabilizing effect of TOM 1:1 is less than that of R805 FS (data not shown). Recall that TOM 1:1 has 25% of its surface covered with methacrylates. Although the TOM 1:1 is less able to stabilize the interface, the interfacial resistance is still better than that of the base electrolyte. The addition of BMA significantly increases the interfacial resistance. AIBN did not statistically increase the interfacial resistance relative to the base electrolyte. This issue of constituents affecting the interface merits further study along with development of techniques to mitigate the unfavorable interaction of BMA with Li.

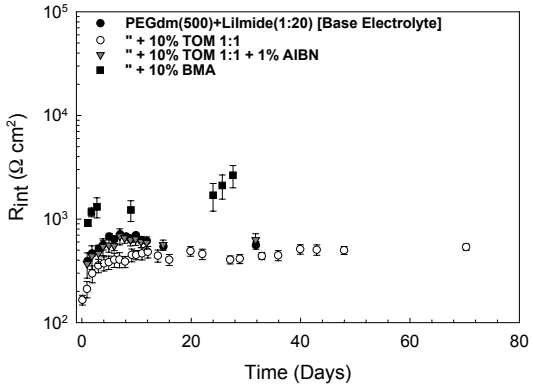

Figure 16. Time-dependent stability of Li/CPE interface for various uncross-linked CPE compositions.

Current Research Focus. We have been in a transition period since October 2000, and we are now focusing on the BATT-baseline system. We have initiated our research on full-cell cycling using vanadium-based, 3-V cathodes. V_6O_{13} from Kerr-McGee, graphite SFG15 from Timcal, and PVDF binder from Kynar are used as our cathode materials. We have been working on establishing a standard procedure and optimizing compositions of vanadium oxide cathodes. We initiated full-cell cycling at 0.08 mA/cm^2 using vanadium oxide cathodes with liquid electrolyte, 10 wt% R805, and 10 wt% A200 composites.

The mechanism of ion transport and how to tune the electrochemistry of an electrolyte remains an area rich in opportunity and poor in consensus among researchers. We continued our study of the fundamentals of ion transport using techniques in nuclear magnetic resonance (NMR), rheology, and electrochemistry. Our research agrees with the overall view that the more motion a polymer chain has the better the total charge transport. However, at extremely high concentrations (those corresponding to about one polymer chain per LiTFSI) the charge transport is not optimum but the Li transference number approaches 0.5 due to a restriction of anion mobility. The lower conductivity may be acceptable under certain conditions given the higher Li transference number.

PUBLICATIONS

S.R. Raghavan, J. Hou, G.L. Baker and S.A. Khan, "Colloidal Interactions between Particles with Tethered Nonpolar Chains Dispersed in Polar Media: Direct Correlation between Dynamic Rheology and Interaction Parameters," *Langmuir,* **16(3),** 1066-1077 (2000).

S.R. Raghavan, H.J. Walls and S.A. Khan, "Silica Dispersions in Organic Liquids: Evidence of Solvation Forces Dictated by Hydrogen-bonding," *Langmuir*, **16 (21),** 7920-7930 (2000).

H.J. Walls, J. Zhou, J.A. Yerian, P.S. Fedkiw, S.A. Khan, M.K. Stowe and G.L. Baker, "Fumed Silica-Based Composite Polymer Electrolytes: Synthesis, Rheology, and Electrochemistry," *J. Power Sources,* **89**, 156-162 (2000).

H.J. Walls and T.A. Zawodzinski, Jr, "Anion and Cation Transference Numbers Determined by Electrophoretic NMR of Polymer Electrolytes Sum to Unity," *Electrochem. Solid-State Lett*., **3(7),** 321-324 (2000).

J.A. Yerian, S.A. Khan and P.S. Fedkiw, "Cross-linkable Fumed Silica-Based Composite Electrolytes for Rechargeable Lithium," *Proc.*

198th Meeting of the Electrochem. Soc., Phoenix, AZ, October 2000.

J. Zhou, P.S. Fedkiw and S.A. Khan, "Interfacial Stability of Fumed-Silica Based Composite Polymer Electrolytes for Rechargeable Lithium Batteries," *Proc. 198th Mtg. of the Electrochem. Soc.*, Phoenix, AZ, October 2000.

M.K. Stowe, J.Hou and G.L. Baker, "Crosslinkable Composite Polymer Electrolytes: Ionic Conductivity and Polymerization Behavior Using Methacrylate Monomers," *Proc. 198th Mtg. of the Electrochem. Soc.*, Phoenix, AZ, October 2000.

Highly Conductive Polyelectrolyte-Containing Rigid Polymers

Duward F. Shriver and Semyon Vaynman***

**Chemistry Department, Northwestern University, Evanston, IL 60208*

***Department of Materials Science and Engineering, Northwestern University, Evanston, IL 60208*

(847) 491-4475; fax: (847) 491-1022; e-mail: svaynman@northwestern.edu

Objectives

- Synthesize a new class of rigid polymer electrolytes.
- Test rigid polymer electrolytes in rechargeable Li batteries.

Approach

- Synthesize new types of polymer electrolytes that contain a rigid polymer rather than the flexible low-T_g polymers used in conventional polymer electrolytes.
- Fabricate electrochemical cells with these electrolytes and evaluate their performance.
- Correlate the performance of electrolytes in the cells with their chemical structure and their reactivity toward components of the electrochemical cell.

Accomplishments

- Synthesized highly conductive rigid polymer electrolytes that contain functional groups such as carboxy and sulfone, and discovered complexes containing carboxy groups have higher ionic conductivity than a similar polymer-salt complex containing sulfone (~10^{-4} S/cm *vs.* $5x10^{-6}$ S/cm at room temperature).
- Conducted tests on symmetrical Li/polymer electrolyte/Li cells that indicated the formation of a very resistive interface when a carboxy-containing rigid polymer electrolyte was used, but a much less resistive layer was formed between Li metal and sulfone-containing rigid polymer electrolyte.
- Incorporated rigid polymer electrolytes into Li cells, and found that the capacity of the cell with carboxy-containing rigid polymer electrolyte was not satisfactory; the capacity of the cell with sulfone-containing rigid polymer electrolyte was more than 100 mAh per gram of active cathode material at current density of 15 $\mu A/cm^2$, but the capacity of the cell was reduced significantly with an increase in current density due to high resistance of that electrolyte.
- Synthesized new sulfone-containing rigid polymer electrolytes with a higher density of cation-coordinating sites.

Future Directions

- Modify rigid polymer electrolyte to increase its ionic conductivity and to reduce its reaction with anode.
- Test modified electrolyte in Li cells.

During 1999 two rigid polymer systems that contain carboxy groups were developed in our laboratory: poly(vinylene carbonate) (PVIC) and poly(1,3-dioxolan-2-one-4,5-diyl oxalate) (PVICOX), which displayed both favorable conductivity and mechanical properties. These polymers contain a high density of coordinating sites, which is necessary to dissolve salts. Also, the high density of polar groups reduces the activation energy for ion hopping from one polar site to the next. These properties lead to high ionic conductivity of the salt-polymer system. PVICOX has ionic conductivity of 10^{-4} S/cm at room temperature. A polymer electrolyte containing PVICOX was incorporated into Li cells. The capacity of the cell was low due to the formation of a very resistive interface between the Li anode and electrolyte.

Because PVICOX reacted with the Li anode, we synthesized polymers that contain sulfone groups.

Sulfone or sulfoxide-functionalized organic molecules have some of the highest dipole moments and dielectric constants known and display very good cation-complexing properties. Therefore, it was expected that polymers containing sulfur-oxygen bonds should readily dissolve significant amounts of Li salts and provide rapid ion transport. Furthermore, due to the strongly electron-withdrawing character of these groups, their polymers should have very good anodic stability.

The synthesis of the polyarylsulfone (a) was carried out by poly-condensation of Na-4,4'-sulfonyldiphenoxide with 3,4-dichlorosulfolane (Fig. 17).

A phase transfer catalysis (PTC) which involves a two-phase system of mutually insoluble aqueous and organic layers (liquid-liquid PTC) was employed. The transport of the ionic reactant from the aqueous layer into the organic phase takes place *via* a lipophilic transfer agent, tetrabutyl ammonium bromide.

The synthesized polymer was mixed with lithium triflate in 1:1 and 4:1 molar ratios. The mixtures were dried for 72 h in vacuum ($6x10^{-6}$ Torr) and the ionic conductivity was measured. The results presented in Fig. 18 indicate lower ionic conductivity than we expected by analogy with our highly conductive rigid polymer electrolyte PVICOX. As with PVICOX, a higher lithium triflate concentration leads to higher conductivity. This trend in conductivity is opposite of that for conventional polymer-salt complex electrolytes. Unlike typical polymer electrolytes these new materials are rigid at room temperature.

As reported previously, PVICOX is not chemically stable when in contact with Li metal; the resistance of the cell increases by a couple of orders of magnitude in the first few hours due to formation of a layer between PVICOX and Li. According to Fig. 19, a polysulfone (a)-containing polymer electrolyte is more stable toward Li metal than PVICOX. After 64 h, the resistance of the cell only triples.

Cells that contained Li metal, cathode material, and the rigid polymer electrolyte polysulfone (a) mixed with lithium triflate (1:1), were assembled and tested. The cathode consisted of 55% $LiMn_2O_4$ (from Kerr-McGee), 35% polymer electrolyte (MEEP-lithium triflate (4:1)), and 10% carbon (from Superior Graphite). A capacity of up to 100 mAh/g of active cathode material was achieved at current density of 15 $\mu A/cm^2$ (Fig. 20). However, the capacity dropped significantly with an increase in current density to 40 $\mu A/cm^2$, due to high cell resistance.

Another sulfone-containing polymer (polysulfone (b)) is being synthesized in our laboratory at the present time using 1,4-dithiane-2,5-diol and dibromosulfolane as starting materials. We explore different synthetic routes to this polymer with emphasis on high yield. We anticipate that when doped with salt, this polysulfone (b) will display higher ionic conductivity than that of polysulfone (a), because the polymer (b) has a higher density of cation-coordinating sites than (a). We also expect high stability of polymer (b) toward Li.

The synthesis of this polymer as shown in Fig. 21 is underway now.

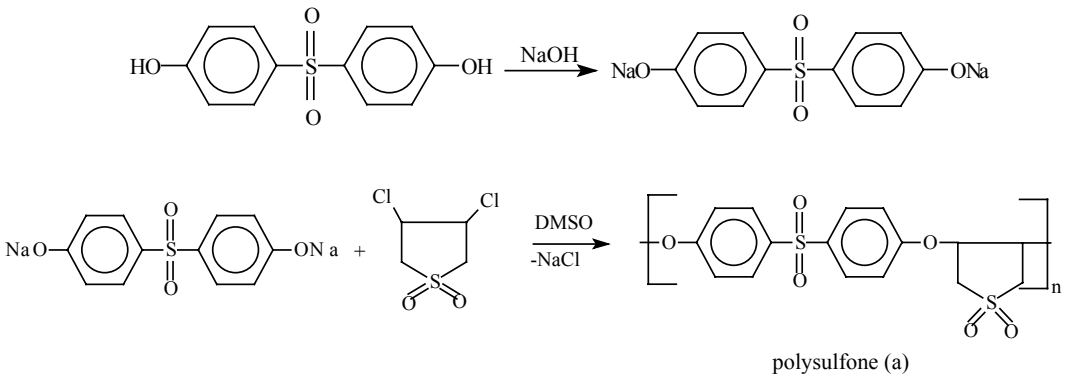

Figure 17. Synthesis of polysulfone (a).

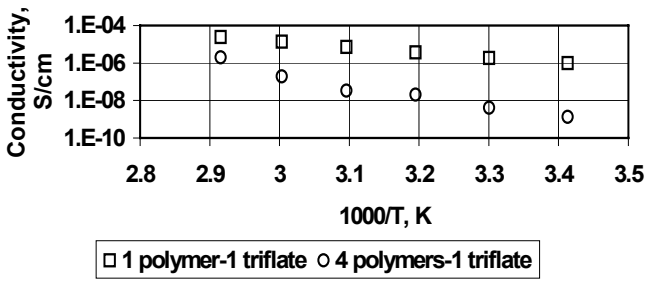

Figure 18. Ionic conductivity of the polysulfone (a) - containing electrolyte.

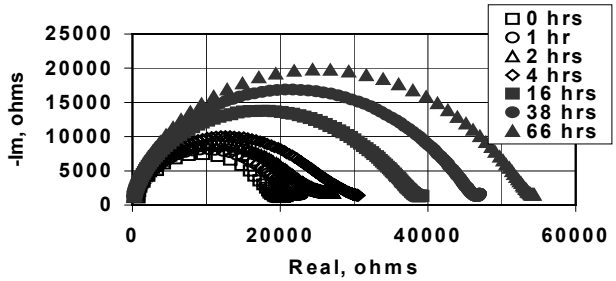

Figure 19. The impedance of Li/polysulfone (a) electrolyte system.

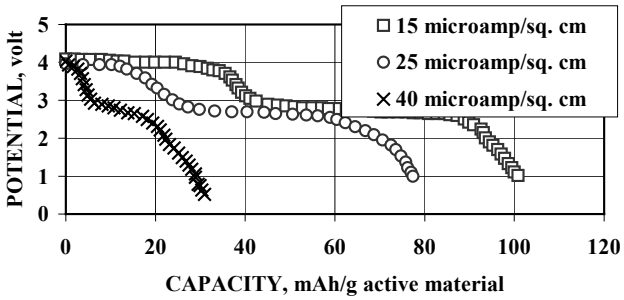

Figure 20. Discharge of of Li/(PVICOX)/ $LiMn_2O_4$;C; MEEP-lithium triflate cell at 25˚C.

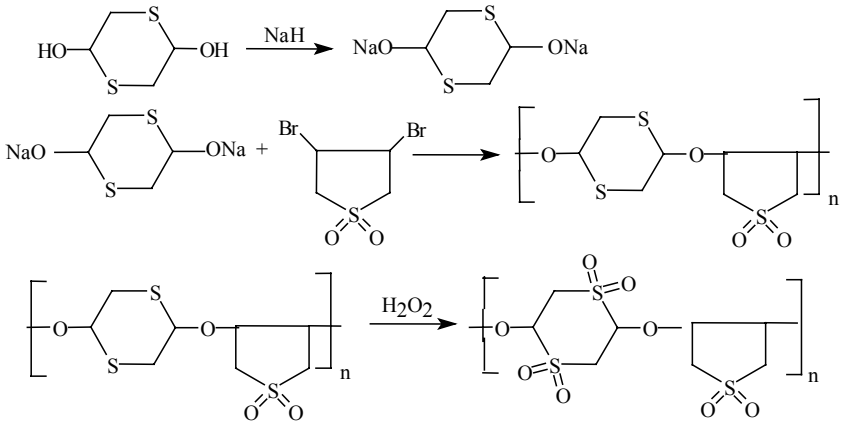

polysulfone (b)

Figure 21. Synthesis of polysulfone (b).

Nonflammable Electrolytes

K. Kinoshita

Lawrence Berkeley National Laboratory, 90-1142, Berkeley CA 94720

(510) 486-7389, fax: (510) 486-4260; email: k_kinoshita@lbl.gov

Objective

- Identify chemical additives that improve the safety of nonaqueous electrolytes for Li-ion batteries by stabilizing the SEI layer on carbon.

Approach

- Identify species that are incorporated in the SEI layer to improve its stability.
- Conduct electrochemical evaluation of additives to determine the reversible and irreversible capacity loss using the baseline liquid or gel electrolytes.

Accomplishment

- Studied the reaction of PF_5 gas and EC/DMC suggesting that decomposition of $LiPF_6$ to PF_5 facilitates the thermal decomposition of EC/DMC containing $LiPF_6$.

Future Direction

- Evaluate a chemical additive that enhances the thermal stability of the SEI layer on carbon in a liquid electrolyte to determine its electrochemical performance compared to baseline systems.

Our experimental effort focused on the thermal stability of electrolytes and additives, including flame retardants such as those identified by the Illinois Institute of Technology (IIT). The thermal decomposition of 1 M $LiPF_6$ in 1:1 mol ratio EC/DMC at 85ºC was compared to the reaction between EC/DMC and PF_5 gas. Both produce a brown solution and gaseous products. The decomposition products from PF_5 + EC/DMC and 1 M $LiPF_6$ in 1:1 EC/DMC, which were detected by gas chromatography (GC), are similar. Proton NMR provided evidence for the presence of oligoether carbonates in the reaction products. The reaction of PF_5 gas and EC/DMC suggests that decomposition of $LiPF_6$ to PF_5 facilitates thermal decomposition of EC/DMC containing $LiPF_6$. Limiting the decomposition of $LiPF_6$ should improve the safety of Li-ion batteries. Based on our studies and the results obtained by IIT, decomposition products from the electrolyte and flame retardants may improve the thermal stability of the SEI layer on carbon anodes.

A sample of hexa-methoxy-tri-aza-phosphazene (HMTAP) was received from IIT, and thermal stability tests were conducted by heating a baseline electrolyte [1 M $LiPF_6$ in a mixture of 1:1 EC/DMC] containing 3% HMTAP at 85ºC. After three days at 85ºC, the electrolyte remained relatively clear (slight brown coloration) and no gas was evolved when the sample vial was opened. In contrast, the baseline electrolyte without HMTAP showed a visible change to a dark brown color, and gas evolution was observed under the same experimental conditions.

The GC results obtained for the thermal decomposition of the baseline electrolyte (LP30) is compared with the electrolyte containing 3 wt% HMTAP (LP30 + HMTAP) in Fig. 22. The plot shows the GC peak ratios for the reaction product detected at 14.5 min to that for EC *vs.* the time at

which the samples were held at 85ºC. Without HMTAP in the electrolyte (LP30), a significant increase is observed in the amount of reaction product detected by GC. On the other hand, when HMTAP is present (LP30 + HMTAP), EC decomposition is inhibited. This is due to the increased basicity of HMTAP over EC; HMTAP will react preferentially with PF_5, which is a Lewis acid. HMTAP reacts through ring-opening polymerization (HMTAP-ROP), and the products are believed to be associated with the GC peak at 33 min. The increase in the concentration of the decomposition product with time is also shown in Fig. 22. This analysis suggests that HMTAP inhibits EC decomposition in LP30 at 85ºC. The similar decomposition rates of HMTAP and EC in LP30+HMTAP imply that the reaction is limited by generation of PF_5 in the electrolyte; the additive does not change this rate.

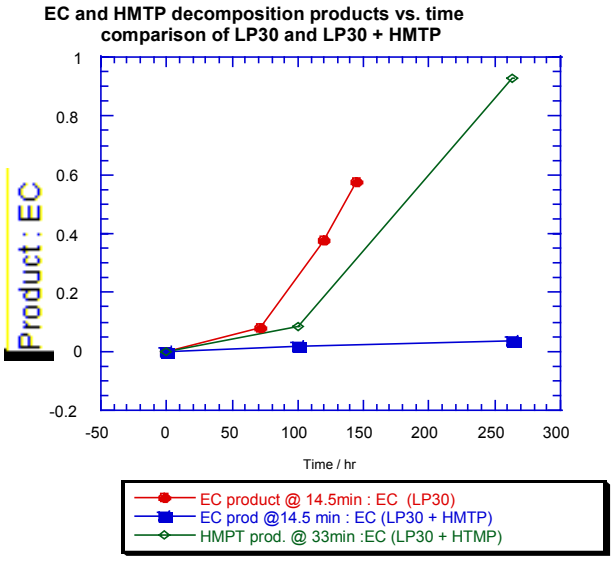

Figure 22. The concentration of reaction products as a function of time for LP30 and LP30+HMTAP at 85ºC.

Proton NMR studies of the thermal reaction products from EC/DMC/$LiPF_6$ showed peaks due to DMC, EC and polyether carbonates $(CH_2CH_2O)_mCOO)_n$ as reported in the literature ["The polymerization of ethylene carbonate" L. Vogdanis & W. Heitz *Macromol. Chem., Rapid Commun.* **1986**, *7*, 543]. It appears that PF_5 causes polymerization reactions in the electrolyte. Based on this result, a sample of PE_3C (a polyethercarbonate) is proposed for evaluation as an additive for Li-ion cells. This material should simulate the end product that may be produced during the formation of the SEI layer (electrolyte decomposition) at the anode. Upon electron transfer to cyclic carbonates, rearrangement and loss of CO_2 can occur, thereby forming a lithium alkoxide. The alkoxide can react with the carbonyl group and lead to polyethercarbonate (PEC) products.

A sample of PE_3C was given to IIT and evaluated at IIT as an additive in 2016 coin cells (Li/carbon) containing 1 M $LiPF_6$ and EC+DEC. A Gen-1 ATD Program anode (MCMB+ 6% SFG) was used. The charge (Li^+-ion de-intercalation)/discharge (Li^+-ion intercalation) cycles of two cells (K2 and K3) that contained 7% PE_3C are compared to a cell that contained no PE_3C (Fig. 23). Charge/discharge were carried out at the C/20 rate, and the first-cycle irreversible capacity loss of the cell without additive was 44 mAh/g and those for K2 and K3 were slightly higher, 57 mAh/g and 55 mAh/g, respectively. The corresponding first-cycle reversible capacities were 314, 312 and 315 mAh/g, respectively. Based on these data, it appears that the presence of the additive in the electrolyte has a very small effect on the reversible capacity but produces a higher irreversible capacity loss. The specific capacity is slightly higher in the cells with additives after several cycles but this result is not conclusive. Additional data are being collected. The role of PE_3C in enhancing the thermal stability of the SEI layer has not been substantiated.

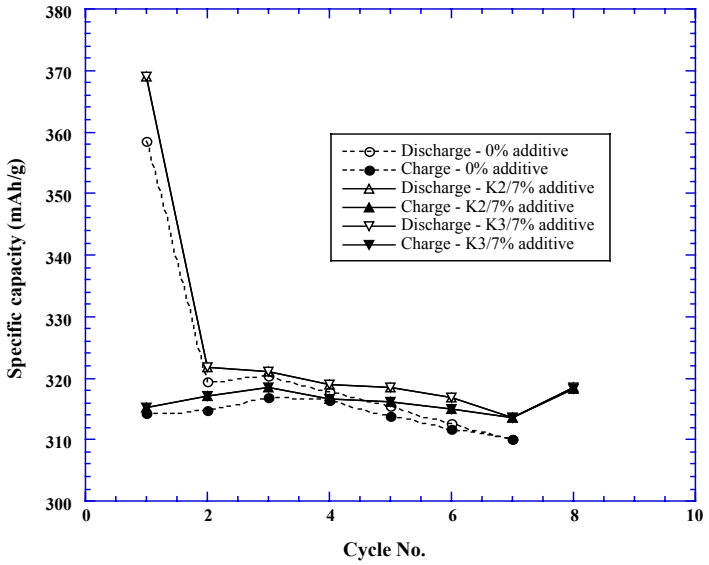

Figure 23. Charge/discharge cycling of 2016 coin cell containing baseline electrolyte and PE_3C additive.

Development of Nonflammable Electrolytes

J. Prakash

Illinois Institute of Technology, Department of Chemical and Environmental Engineering,

10 W 33rd Street, Chicago, IL 60616

(312) 567-3639, fax: (312) 567-8874; e-mail: prakash@iit.edu

Objective

- Develop NFEs with high flash point (>100°C), high ionic conductivity (10^{-3} S/cm), and wider voltage window (0-5 V *vs*. Li) in an effort to provide better thermal stability and fire safety.

Approach

- Modify existing electrolytes by using novel flame-retardant (FR) additives that are compatible with active electrode materials and the environment.
- Use chemical, electrochemical, and thermal techniques to investigate the stability and performance of electrolytes modified with FR additives

Accomplishments

- Completed an extensive study on the thermal and electrochemical characterization of the FR additive, HMTAP $N_3P_3[OCH_3]_6$, in Li-ion cells.
- Completed the scale-up synthesis of the flame retardant HMTAP.

- Supplied the HMTAP material to the ATD Program (ANL, PolyStor and LBNL) and Mitsubishi Chemical Company, Japan, for further testing.
- Demonstrated the feasibility of using this material as a FR additive in PNGV Li-ion cells.

Future Directions

- Develop new FR additives hexa-ethoxy-tri-aza-phosphazene (HETAP) and urea-diphosphonate (UDP) and new Li-salts with high conductivity and high thermal stability to reduce self-heat rate (SHR) especially at higher temperatures during thermal runaway.
- Perform thermal diagnostic studies of BATT Program baseline Li-polymer and low-cost Li-ion cells with and without FR additive in order to understand the degradation, failure, and safety mechanisms.

Investigation of $N_3P_3[OCH_3]_6$ FR additive in Li-ion cells. In 2000, we successfully demonstrated the scale-up synthesis of the FR additive ($N_3P_3[OCH_3]_6$) with improved yield and purity. We synthesized 10 to 15 g batches of high-purity FR additive $N_3P_3[OCH_3]_6$, characterized it for chemical and electrochemical stability, and supplied samples to the ATD group (ANL, LBNL and Polystor Co.) for further investigations.

Optimization of the amount of FR additive in Li-ion cells. The thermal properties of the HMTAP in Li-ion cells were investigated in collaboration with ANL using differential scanning calorimetry (DSC) and Accelerated Rate Calorimetry (ARC) methods. Figure 24 shows a typical self-heat rate profile of the electrolyte with and without the FR additive in the ARC in presence of metallic Li. It is evident that the addition of 5-10 wt% FR additive to the electrolyte shifts the exothermic peaks beyond 260°C. The shift of the exothermic peak with 5-10 wt% FR additive in comparison with those for electrolyte without FR may be attributed to a passivation layer that is formed on the surface of the Li metal. In addition, investigations of the pressure development within an ARC bomb also showed that 5-10 wt% FR additives significantly reduce the pressure buildup in the bomb compared with those for electrolyte without FR under similar conditions.

The effect of FR additive on the thermal behavior of the fully charged Li-ion cell electrodes was also investigated. Pre-cycling was carried out in sealed graphite/$LiNi_{0.8}Co_{0.2}$ 32 cm^2 cells. $LiPF_6$ in 50:50 wt% EC-DMC was used as electrolyte. These cells were galvanostatically cycled at a C/10 charge-discharge rate. After a few cycles, the cells were charged at C/10 rate to 4.15 V and held at 4.15 V. These charged cells were then opened in a dry glove box filled under Ar atmosphere and the electrode materials were recovered. The recovered materials were sealed in ANL-made ARC bombs for the ARC studies. A typical thermal profile of a fully charged anode is shown in Fig. 25. It is clear that the presence of the FR additive in these electrodes shifts the onset of the exothermic peak to higher temperature. Thermal investigations suggest that 5-10 wt% HMTAP additive is necessary to reduce the SHR and internal pressure.

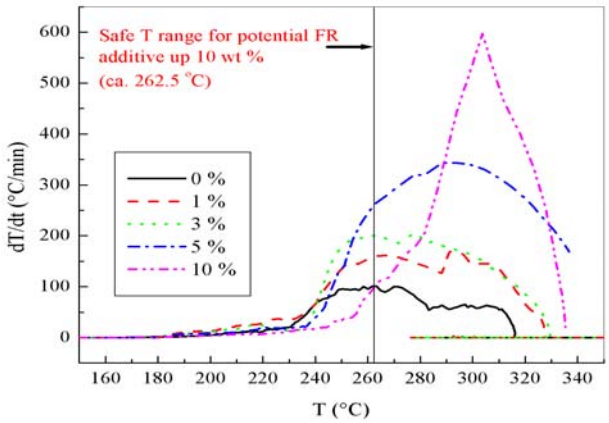

Figure 24. Temperature profile of the Li-ion electrolyte with and without HMTAP FR additive.

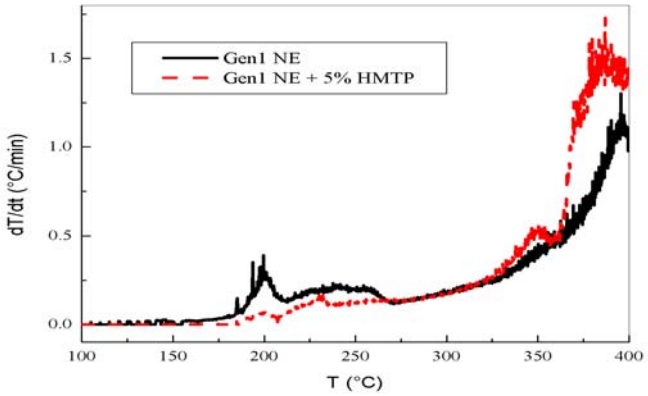

Figure 25. Effect of the FR additive on the ARC profiles of the fully charged graphite anode.

In order to investigate the effect of HMTAP concentration on the performance of the Li-ion cells, we cycled the sealed Li-ion cells with PNGV Gen-1 chemistry containing 1-10 w% HMTAP. The results of 5-wt% FR on the cell performance are shown in Fig. 26 and indicate there is no detrimental effect of the amount of the FR additive on the Li-ion cell performance. The results of the present investigations show that the HMTAP ($N_3P_3[OCH_3]_6$) is a viable FR for Li-ion cells and the optimum amount of the FR additive is in the range 5-10 wt% of the electrolyte weight.

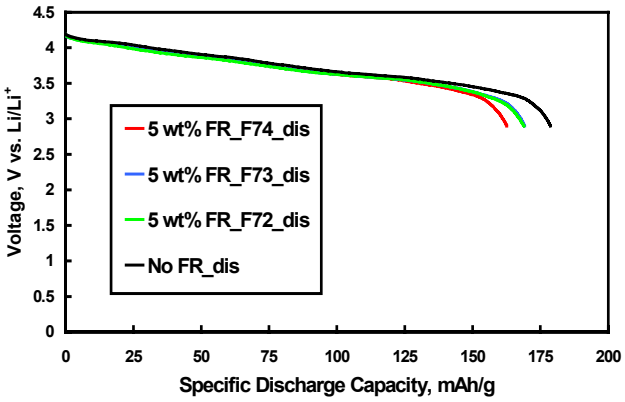

Figure 26. Electrochemical performances of a PNGV Li-ion cell with 5-wt% HMTAP in 1 M $LiPF_6$ with EC:DEC(1:1).

The shift of about 25°C in the onset temperature of the thermal runaway (Figs. 24 and 25) is very encouraging for the safety of Li-ion cells. However, the SHR at temperatures above 265°C was found to increase in presence of HMTAP. In order to address the issue of SHR at higher temperatures and to meet the milestone (FR additives for Li-ion batteries), we also initiated studies on other FR additives such as HETAP and UDP with reduced SHR at higher temperatures as a possible replacement for HMTAP.

HETAP ($N_3P_3[OCH_2CH_3]_6$). We also successfully synthesized HETAP and characterized its electrochemical stability in Li-ion electrolyte using cyclic voltammetry (CV) in the voltage window of 0-5 V. The new FR additive HETAP showed good electrochemical stability up to 5 V *vs.* Li. Further electrochemical and thermal studies on this material are currently underway.

PUBLICATIONS

J. Prakash, C. Lee and K. Amine, "A Novel Flame-Retardant Additive for Li-ion Batteries," *U.S. patent application* filed 2000.

C. Lee, R. Venkatachalapathy and J. Prakash, "Development of Non-flammable Electrolytes for Li-ion Batteries," *Electrochem. and Solid-State Letters*, **3**, 63 (2000).

C.W. Lee, R. Venkatachalapathy and J. Prakash, "Flame-Retardant Materials for Lithium Batteries," *197th Meeting of the Electrochemical Society*, Toronto, Canada, Abst. No.120, May 2000.

C.W. Lee, H. Joachin and J. Prakash, "Studies on Electrochemical and Thermal Properties of Lithium-Ion Battery Electrolytes with Different Salts," *198th Meeting of the Electrochemical Society*, Phoenix, AZ, Abst. No 143, October 2000.

J. Prakash, "Investigations of Nonflammable Phosphozene Based Compounds for Li-ion Batteries," *10th International Meeting on Lithium Batteries*, Como, Italy, Abstr. 347, June 2000.

K. Kinoshita and J. Prakash, "Prospects for Nonflammable Electrolytes in Li-ion Batteries," *Proceedings of the 4th Chicago Battery Workshop*, Illinois Institute of Technology, Chicago, IL, April 2000.

Nonflammable Electrolytes for Li-Ion Batteries

Alan B. McEwen

Covalent Associates, Inc., 10 State Street, Woburn, MA 01801

(781) 938-1140; fax: (781) 938-1364; e-mail: mcewen@covalentassociates.com

Objectives

- Develop nonflammable electrolytes for Li-ion batteries.
- Optimize the electrolytes for BATT Program objectives regarding liquid electrolytes and to meet DOE safety goals.

Approach

- Investigate ionic liquids as nonflammable and nonvolatile electrolyte solvents.
- Synthesize new ionic liquids and formulate these into Li-ion electrolytes.
- Determine flammability and flashpoint of the electrolytes.
- Determine the performance characteristics of these new electrolytes by measuring conductivity, Li intercalation, and cycle life of half-cell and full-cell batteries.

Accomplishments

- Developed NFEs for Li-ion batteries using ionic liquids.
- Demonstrated reversible Li intercalation in anode and cathode materials.
- Constructed coin cell batteries demonstrating cycling performance.

Future Directions

- Synthesize new low-cost ionic liquids and formulate these into Li-ion electrolytes with the addition of Li salts and common organic solvents.
- Determine electrolyte performance with $LiFePO_4$ and $Li_{1.02}Al_{0.25}Mn_{1.75}O_{3.92}S_{0.03}$ positive electrodes and Sn-based negative electrodes.
- Assess the performance of the relatively inexpensive Li salt $LiBF_4$ and LiTFSI in the ionic liquid electrolyte formulations.

The application of fluorinated ethyl acetates as electrolyte solvents for nonflammable Li-ion electrolytes was the original task of this project. The suitability of these solvents as electrolyte solvents for Li-ion batteries was demonstrated. Good conductivity (7.5 mS/cm) and cycling performance on graphite and $LiCoO_2$ was observed. We have found, however, that the flashpoint of the fluorinated ethyl acetate solvents and electrolyte mixtures based on these solvents is below room temperature (Table 1). Because this fails the criteria of nonflammability we changed the focus of our research and development efforts.

We initiated an investigation into using Covalent's proprietary ionic liquids (*U.S. Patent 5,827,602*) as Li-ion electrolytes due to the inability of fluorinated esters to meet the nonflammable criteria. We shifted the focus of the project to investigate these novel materials that have a wide liquid range, high thermal stability, and lack a vapor pressure. In addition, they are nonflammable and non-corrosive, giving them a thermal application range from below room temperature to approaching 400°C.

Using a NFE, formulated with an ionic liquid, carbonate solvent, and 1 M $LiPF_6$ salt, we obtained

good cycling behavior (Fig. 27) in coin cells using graphite anodes and $LiCoO_2$ cathodes. We cycled between 3.0 and 4.3 V. These imidazolium based ionic liquid Li-ion electrolytes have good conductivity (10 mS/cm) and form stable SEIs on graphite with the small addition of carbonate solvents. Although by themselves carbonate solvents are flammable, in these ionic liquid formulations there is no flash point or burning in flammability tests.

Table 1. Flashpoint temperatures (°C) for fluorinated acetate electrolytes.

Solvent	1M $LiPF_6$	1M LiBeti	1M iMethide
Ethyl Acetate	< 26	< 26	< 26
TFEA[a]	< 27	< 27	< 27
EA:EC (1:1)	< 25	< 26	< 26
TFEA:EC(1:1)	< 28	< 27	< 27

TFEA: trifluoroethyl acetate

We demonstrated the reversible intercalation of Li into graphite (Fig. 28) using an ionic liquid formulated electrolyte. One can see the three stages of Li intercalation into graphite. Good reversibility was also demonstrated.

We also have obtained promising results with a Li metal/$LiCoO_2$ cell with the same ionic liquid electrolyte used previously in a Li-ion cell (Fig. 29).

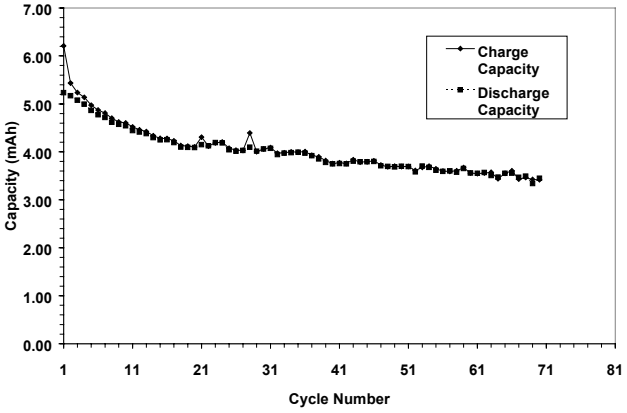

Figure 27. Cycling capacity for a coin cell with a nonflammable Li-ion electrolyte.

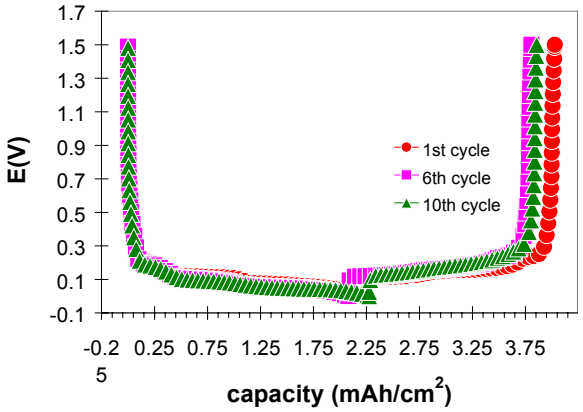

Figure 28. Cycling results for an ionic liquid based electrolyte in a Li/graphite cell.

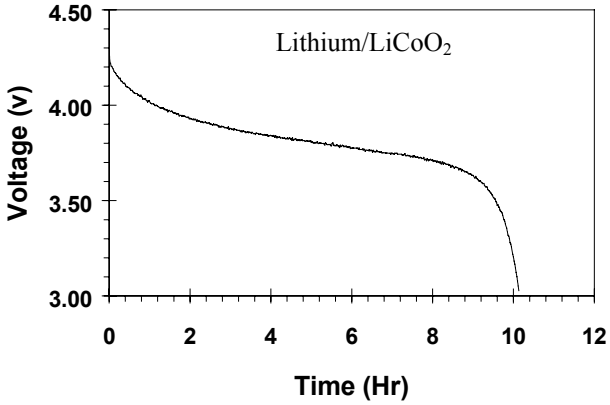

Figure 29. Voltage profile of a Li/$LiCoO_2$ cell using an ionic liquid electrolyte.

Excellent results were obtained in a graphite/$LiCoO_2$ coin cell using an ionic liquid based Li-ion electrolyte (Fig. 30). As depicted in Fig. 27 we continue to obtain good cycling efficiency for over 60 cycles.

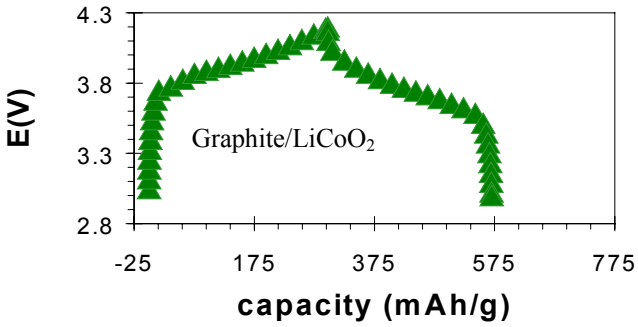

Figure 30. Performance of a coin cell battery with an ionic liquid electrolyte. First cycle.

Solvent additive study. The influence that electrolyte composition has on the capacity and cycle life in graphite/$LiCoO_2$ coin cells was studied. We focused on developing a stable SEI with these ionic liquid NFEs that have good cycle life and excellent high-temperature stability. At constant Li salt and ionic liquid composition a correlation between additive identity and performance was determined (Fig. 31).

Lithium salt study. We determined the influence Li salt identity (*e.g.*, LiBeti, LiImide, LiMethide, or $LiPF_6$) has on cell performance. We investigated using the LiBeti [$LiN(SO_2C_2F_5)_2$] salt due to its improved thermal stability relative to $LiPF_6$ and improved corrosion stability relative to the LiImide [$LiN(SO_2CF_3)_2$] salt. We have observed that the capacity and cycle life is dependent on Li salt composition (Fig. 32).

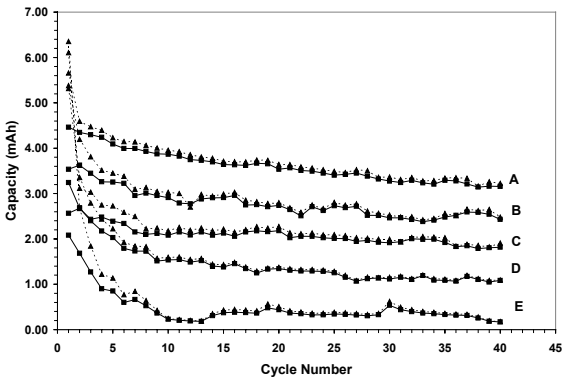

Figure 31. Ionic liquid electrolyte: graphite/$LiCoO_2$ coin cell cycling dependence on additive formulation.

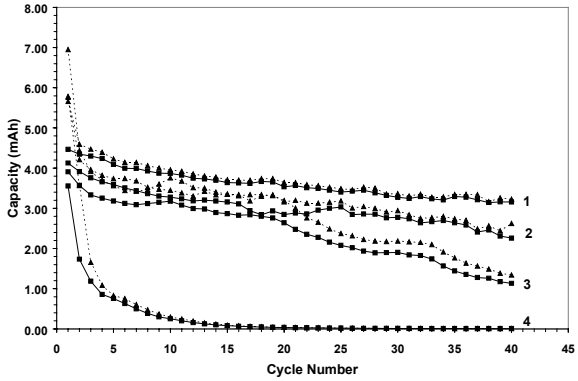

Figure 32. Ionic liquid electrolyte: graphite/$LiCoO_2$ coin cell cycling dependence on Li salt identity.

Development of Novel Electrolytes

Kraig A. Wheeler

Delaware State University, Department of Chemistry, Dover DE 19901

(302) 739-4934, fax: (302) 739-3979; e-mail: kwheeler@dsc.edu

Objectives

- Develop improved electrolytes for Li-ion batteries.
- Investigate the electrochemical and physical properties of polysulfone cross-linked polyethylene oxide (PEO) electrolytes.

Approach

- Prepare polysulfone cross-linked PEO's using preparative synthetic organic methods and a homologous series of polyethylene glycol (PEG) precursors (molecular weight (MW) 400, 2000, and 4600).
- Determine polymer structure and purity using spectroscopic techniques.
- Assess dissolution potential of Li-ion electrolytes with polysulfones.
- Evaluate electrochemical performance of sulfone electrolytes in Li-ion cell applications.

Accomplishments

- Prepared and characterized a homologous series of sulfone cross-linked PEO polymers.
- Achieved effective Li-ion dissolution of $LiN(CF_3SO_2)_2$ with polysulfone-chloroform mixtures.
- Detected onset of polymer decomposition at >4.0 V in Li-ion cell studies of polysulfones.

Future Direction

- Complete electrochemical characterization of sulfone materials.

The goals of this project center on developing polysulfone-based electrolytes for Li-ion cell applications. Essential components of this research contribution include the fabrication, characterization, and structure-property assessment of a homologous series of Li-ion polysulfone electrolytic materials. Understanding the influence of the polymeric skeletal framework and sulfone functionality to electrochemical stability is of primary importance to this project.

The fabrication of the target polymers (Fig. 33) followed a rational design that incorporates both anionic and radical initiated processes. Selective deprotonation of appropriate PEG precursors (MW 400, 2000, 4600) under mild basic conditions followed by subsequent treatment with 3-chloro-2-(chloromethyl)propene gave the expected polycondensates as confirmed by spectroscopic methods. Extended reaction times, elevated temperatures, and radical initiation processes resulted in unwanted cross-linking of the polyethers. The development of alternative methods using *in situ* reaction conditions provided highly viscous materials with minimal cross-linking for each PEG employed. The radical initiated reaction of divinylsulfone and these olefinic polyethers formed controlled cross-linked molecular frameworks that lack hydroxyl and olefinic functionalities characteristic of the PEG and dichloropropene starting materials. Purification of these functional materials gave a self-standing polymer support with excellent mechanical properties.

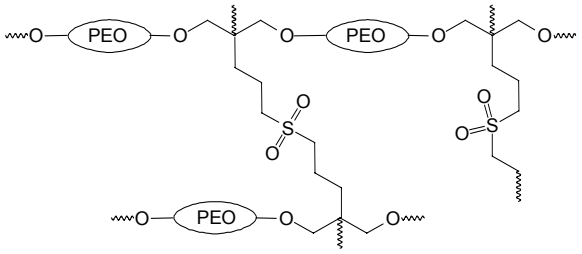

Figure 33. Structural topology of sulfone cross-linked PEO polymers.

Most polymer electrolytic systems with relatively high crystalline content are widely recognized as being restricted in the area of ion-transport process. Elevated temperatures and rational structure modifications provide, when effective, tools to fabricate amorphous polymeric substrates. The structural design criteria employed in this study produced polysulfone architectures void of any significant crystalline content at room temperature due to the construction of a random molecular framework produced from cross-linking the PEO polycondensates and divinyl sulfone.

Our efforts to understand the electrochemical stability of these sulfone cross-linked polymers build upon our prior CV studies of similar arylsulfone systems. CV's were performed at 25°C on each polysulfone sample using a Pt microdisc (working) and Li strip (reference and counter) electrodes. Electrolytic materials were prepared by either swelling the polycondensate in a 0.1 M bis(trifluorosulfonyl) imide (LiIm) solution or direct

solvation of LiIm with the polysulfone. Inspection of the voltammograms acquired from these studies revealed the onset of polymer decomposition at ~4.0 V *vs.* Li and showed stability under reversible electrochemical sweeps (Fig. 34). The electrochemical behavior of polysulfone/LiIm systems in Li-cells shows favorable responses supported by the lack of severe electrolytic degradation at elevated voltage potentials.

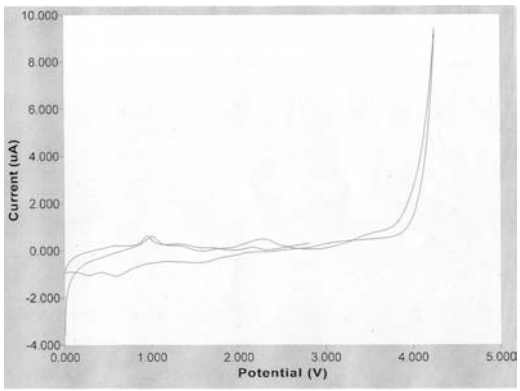

Figure 34. Voltammogram of MW 400 Polysulfone/LiIm.

PUBLICATION

J.-J. Lee, T. Bae, D.A. Scherson, B. Miller and K.A. Wheeler, "Underpotential Deposition of Aluminum and Alloy Formation on Polycrystalline Gold Electrodes from $AlCl_3$/MEIC Room-Temperature Molten Salts," *J. Electrochem. Soc.* **147**, 562 (2000).

TASK AREA 4: CATHODES

Novel Cathode Materials

Michael M. Thackeray

Argonne National Laboratory, Chemical Technology Division, Argonne IL 60439

(630)-252-9183; fax: (630)-252-4176; e-mail: thackeray@cmt.anl.gov

Objective

- Develop low-cost manganese oxide cathodes to replace vanadium oxide electrodes in Li-polymer cells and cobalt/nickel oxide electrodes in Li-ion cells.

Approach

- Search for, characterize, and develop low-cost manganese oxides for Li-ion and Li-polymer cells.
- Focus on layered lithium-manganese oxides derived from Li_2MnO_3 for Li-ion cells, and stabilized α-MnO_2 for Li-polymer cells.

Accomplishments

- Investigated the concept of exploiting a layered Li_2MnO_3 rock salt structure to stabilize layered $LiMO_2$ structures.
- Synthesized and evaluated "solid-solution" or composite electrodes having the general formula $[x(Li_2MnO_3)\bullet y(LiMO_2)]$; M = Mn, Ni and Co in Li half-cells.
- Developed optimized compositions which yielded specific capacities of ~150 mAh/g between 4.5 and 3.0 V in Li cells at 50°C, but for less than 100 cycles.
- Achieved a rechargeable capacity of more than 200 mAh/g for 40 cycles with stabilized α-MnO_2 electrodes in liquid-electrolyte Li cells.

Future Directions

- Investigate alternative (non-aqueous) processing routes to synthesize $[x(Li_2MnO_3)\bullet y(LiMO_2)]$ composite electrodes to improve their capacity and cycling stability with a performance target of 150 mAh/g for 100 cycles at 50°C in Li/$[x(Li_2MnO_3)\bullet y(LiMO_2)]$ cells.
- Stabilized α-MnO_2 electrodes in Li/polymer cells in collaboration with J. Kerr at LBNL.

A major focus of our research on novel or improved cathodes for Li-ion and Li-polymer cells has been the exploitation of a concept to use a layered Li_2MnO_3 (rock salt) component to stabilize a layered $LiMnO_2$ structure during electrochemical cycling of Li/$LiMnO_2$ cells. In this respect, it is well known that layered $LiMnO_2$ electrodes transform irreversibly to a spinel-type structure; the transformation leads to poor capacity retention and cycle life. Promising electrochemical behavior has been achieved with layered lithium manganese oxide electrodes derived by acid treatment of Li_2MnO_3. Such treatment removes lithia (Li_2O) from Li_2MnO_3 and yields a layered $Li_{2-2x}MnO_{3-x}$ phase that shows a resistance to the transformation to spinel. The $Li_{2-2x}MnO_{3-x}$ structure can be represented, alternatively, as $(1-x)Li_2MnO_3\bullet MnO_2$, in which the MnO_2 component retains a layered configuration. Electrochemical lithiation of this compound in a non-aqueous Li cell results in the formation of a

layered product, $(1\text{-}x)Li_2MnO_3 \bullet LiMnO_2$, in which the electrochemically inactive Li_2MnO_3 can be viewed as a stabilizing agent for the electrochemically active MnO_2 component. This finding has immediate implications for using Li_2MnO_3 to stabilize other layered $LiMO_2$ structures in order to improve electrode capacity and cycle life.

The approach outlined above has been used to evaluate the performance of layered $xLi_2MnO_3 \bullet yLiMO_2$ (M= Mn, Ni, Co, Cr) electrodes. In one example, an experiment was conducted to make $Li_2MnO_3 \bullet 4LiNi_{0.8}Co_{0.2}O_2$ in which the Li_2MnO_3 component comprises 20% of the composite structure. Figure 35 shows the voltage profile obtained from a $Li/Li_2MnO_3 \bullet 4LiNi_{0.8}Co_{0.2}O_2$ coin cell at 50°C; Fig. 36 shows the cycling stability of the cell over the first ten charge and discharge cycles. The voltage profile suggests that Li is inserted into, and extracted from, the metal oxide host structure during discharge in a single-phase process. Apart from an approximate 25% capacity loss during the first cycle, the capacity remains steadily above 150 mAh/g. The extent to which the Li_2MnO_3 component plays a role in stabilizing such layered electrodes, particularly at the top of charge, is unknown. It is speculated that the presence of the Li_2MnO_3 domains, which are structurally compatible with the $LiMO_2$ domains, are a contributing factor to electrode stability.

As part of the BATT program, we have recently initiated work on stabilized α-MnO_2 electrodes for Li-polymer cells. This development effort follows a DOE/BES-supported research project in which stabilized α-MnO_2 electrodes were identified. Our early electrochemical data obtained from liquid-electrolyte Li cells show that capacities in excess of 200 mAh/g can be obtained at an average voltage of 2.8 V *vs.* metallic Li and a C/12 rate.

PRESENTATIONS

C.S. Johnson and M.M. Thackeray, "Cycling Performance of Stabilized Alpha Manganese Dioxide Electrode Materials," *198th Meeting of the Electrochemical Society*, Phoenix, AZ, October 22-27, 2000.

C.S. Johnson and M.M. Thackeray, "Recent Developments and Prospects for Layered Manganese Oxide Electrodes for Lithium Batteries," *198th Meeting of the Electrochemical Society*, Phoenix, AZ, October 22-27, 2000.

C.S. Johnson and M.M. Thackeray, "Electrochemical Processes of Manganese Oxide Materials," *DOE Workshop on Interfaces, Phenomena and Nanostructures, in Lithium Batteries*, Argonne, IL, December 11-13 2000.

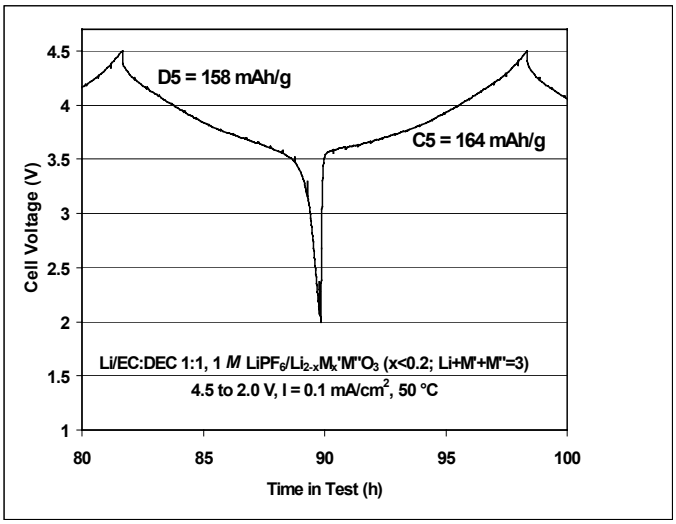

Figure 35. The voltage profile of a $Li/Li_2MnO_3 \bullet 4LiCo_{0.2}Ni_{0.8}O_2$ coin cell.

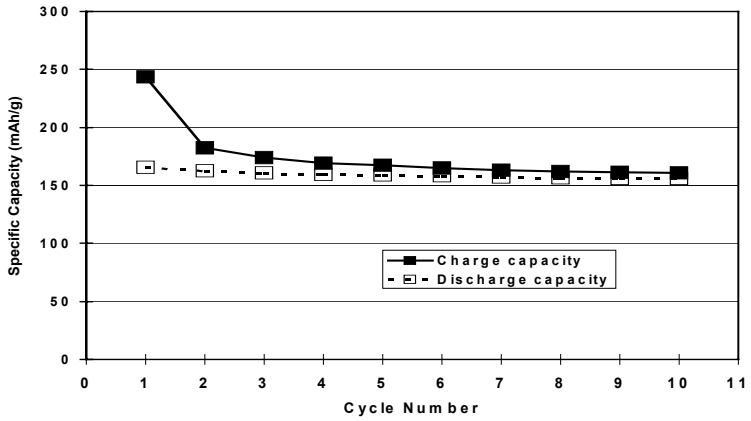

Figure 36. Specific capacities delivered by a $Li_2MnO_3 \bullet 4LiCo_{0.2}Ni_{0.8}O_2$ positive electrode in a Li coin cell over 10 cycles at 50°C (~C/8 rate).

New Cathode Materials Based on Layered Structures

M. Stanley Whittingham

State University of New York at Binghamton, Chemistry and Materials Research Center, Binghamton, NY 13902-6000

(607) 777-4623, fax: (607) 777-4623; e-mail: stanwhit@binghamton.edu

Objective

- Find lower-cost and higher-capacity cathodes, exceeding 200 Ah/kg, that are based on benign materials.

Approach

- Place emphasis on manganese dioxides, both pure and modified with other transition metals, using predominantly low-temperature synthesis approaches.
- Synthesize these materials and characterize them structurally for thermal and chemical stability.
- Evaluate stabilized vanadium oxides for Li/polymer cells.

Accomplishments

- Determined that layered manganese dioxides can be structurally stabilized, that their stability is a function of current density and/or cut-off voltages, that their electronic conductivity can be significantly enhanced, that their cell cycling can be substantially improved by addition of other transition metals, and that hydrothermally synthesized manganese oxides cycle as well as high-temperature materials.
- Showed that vanadium oxides can also be stabilized by the addition of Mn ions, and can achieve capacities over 220 Ah/kg.

Future Directions

- Identify changes in $LiMnO_2$ structure as a function of current density during cell cycling, determine the structure and composition of the vanadium-stabilized $LiMnO_2$, and increase its electrochemical capacity, to understand better the behavior of the $Li_{1.2}Mn_{0.4}Cr_{0.4}O_2$ cathode and to determine if there is an iron analog.
- Complete, for Li-polymer cells, the evaluation of the Mn-stabilized δ-vanadium oxides and compare them to the iron phosphates.

The goal of this project is to identify transition metal oxides with properties superior to $LiCoO_2$, including higher capacity, lower cost and being benign to the environment.

Stabilized manganese oxide cathodes. Layered $LiMnO_2$, which has the potential of cycling 1 Li per Mn ion, is unstable relative to the spinel $LiMn_2O_4$ during cycling. Two approaches were used to stabilize the layer structure of manganese dioxide: *i*) the incorporation of pinning ions to hold the layers apart thus minimizing the diffusion of Mn which is required for spinel formation, and *ii*) the partial substitution of some of the Mn ions by later transition metals such as Fe, Co or Ni.

We have completed a preliminary electrochemical evaluation of the use of alkali metals to pin the MnO_2 layers apart, combined with partial substitution of part of the Mn ions by Fe, Co, or Ni. Last year we reported the enhancement of the electronic conductivity of these materials by partial Mn substitution.

Surprisingly we found the stability of these layered manganese dioxides is strongly affected by the rate of cycling. Figure 37 shows the cycling of a hydrothermally formed potassium manganese oxide at 0.1 and 1 mA/cm^2. At the lower current density the expected behavior for the layered material is found. However, at 1 mA/cm^2 the 4 V plateau typical of spinel is observed even for the first charge. Thus, it appears that these alkali pillars are being removed during cycling at high rates/high potentials.

We formed the corresponding lithium manganese oxides and found the same spinel-like phase formation occurring upon the first charge as shown in Fig. 38.

However, we have shown that vanadium oxygen pillars can be incorporated between the manganese oxide layers [Pub. no. 5]. These pillars are expected to be relatively immobile at ambient temperatures. Figure 39 shows the corresponding cycling data for these pillared compounds. Clearly in this case the manganese oxide is maintaining its layered behavior and is not showing any of the 4-V behavior typical of spinel-like phases. Thus, the principle of pillaring to prevent Mn diffusion appears to be correct. The capacity of the vanadium-oxide pillared manganese oxide is 150 Ah/kg but drops below 100 Ah/kg upon increasing the discharge rate to 1 mA/cm^2. Future efforts will be targeted at improving the capacity of these pillared compounds at higher rates, comparing them with the recently reported high lithium chromium manganese compounds, and the Mn-stabilized V_2O_5.

Stabilized vanadium zxide and comparison to iron phosphate cathodes. We earlier reported, [Pub. no. 1], the high-capacity, 220 Ah/kg, of the double-sheet V_2O_5 structures, and their structure retention during cycling. Our original Mn-stabilized δ-V_2O_5 compound was a mixture of two phases. In an attempt to identify the electrochemically active phase(s) we have succeeded in preparing a pure phase of one of the two components. This material, $[(CH_3)_4N]_{0.2}Mn_yV_2O_5$, has a lattice repeat distance of 13Å, and contains only 0.06 Mn per V_2O_5; it is thermally stable to over 250°C with no structural changes. Its initial capacity is 220 Ah/kg with a mean discharge potential of 3 V and very little polarization. However, increasing the Mn content from 0.06 to 0.1 drops the capacity to 180 Ah/kg as shown in Fig. 37. Researchers at DuPont are also working on this class of material and have confirmed the high capacity (198^{th} ECS Meeting, Phoenix AZ, October 2000).

We initiated studies of the iron phosphate class of cathodes, which are being actively studied by Armand *et al* at the University of Montreal and HydroQuébec, following the initial discovery by the Goodenough group. We made the $Li_3Fe_2(PO_4)_3$ phase using a hydrothermal approach. Its electrochemical behavior is shown in Fig. 41, and although the capacity is not large it is retained well during cycling. We have also formed $LiFePO_4$ hydrothermally, and if coated with carbonaceous material will cycle well and at above 150 Ah/kg capacity (discussions with Armand). We will actively pursue the hydrothermal approach to evaluate this class of material as the base case for

comparison to our cathode materials. $LiFePO_4$ is reported to have a better rate capability and higher capacity than $LiCoO_2$, and to improve the performance of $LiCoO_2$ when admixed with it (Armand at IBA meeting, March 2001).

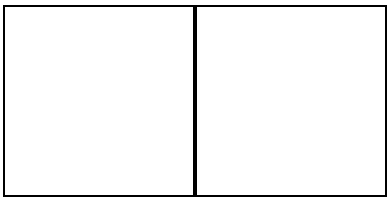

Figure 37. Cycling of $K_yMn_{0.9}Co_{0.1}MnO_2$ at 0.1 mA/cm^2 (left) and 1 mA/cm^2 (right).

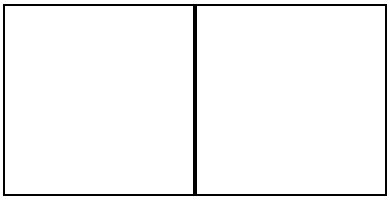

Figure 38. Electrochemical cycling of $Li_yMn_{0.9}Co_{0.1}MnO_2$ and $Li_yMn_{0.9}Ni_{0.1}MnO_2$ at 1 mA/cm^2.

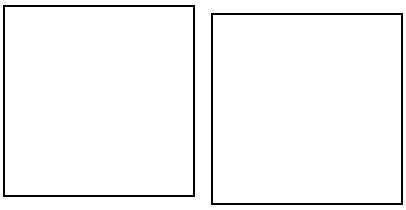

Figure 39. Electrochemical cycling of $(VO_z)_{0.1}MnO_2$ at 0.1 mA/cm^2 (left) and 1 mA/cm^2 (right).

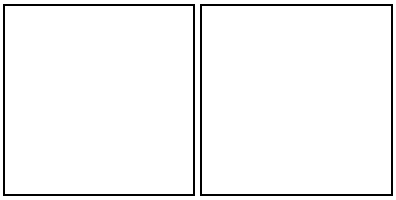

Figure 40. Capacity of Mn-stabilized vanadium oxides, (left) Mn=0.06, and (right) Mn=0.10.

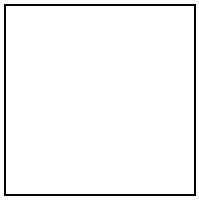

Figure 41. Electrochemical cycling of lithium iron phosphate, $Li_3Fe_2(PO_4)_3$ (contains Fe_2O_3 impurity).

PUBLICATIONS

F. Zhang and M.S. Whittingham, "Hydrothermal Synthesis and Electrochemistry of a δ-Type Manganese Vanadium Oxide," *Electrochem Commun.,* **2**, 69-71 (2000).

M.S. Whittingham. P. Zavalij, F. Zhang, P. Sharma and G. Moore, "The Stabilization of Layered Manganese Oxides for Use in Rechargeable Lithium Batteries," *Proc. Mater. Res. Soc*., **575**, 77-82 (2000).

M.M. Thackeray, J.O. Thomas and M.S. Whittingham, "Science and Applications of Mixed Conductors for Lithium Batteries," *Mater. Res. Soc. Bulletin*, 39-46 (2000).

M.S. Whittingham, "25 Years of Intercalation Chemistry for Battery Materials," *Electrochem. Soc. Proc.,* **99-24**, 7 (2000).

F. Zhang, K. Ngala and M.S. Whittingham, "Synthesis and Electrochemistry of a Vanadium-Pillared Manganese Oxide, *Electrochem Commun.*, **2**, 445-447 (2000).

F. Zhang and M.S. Whittingham, "Electrochemistry of the Layered Manganese Dioxides $M_xMn_{1-y}(Co,Fe,Ni)_yO_2$, M= Li, K," *Electrochem. and Solid-State Lett.*, **3**, 309-311 (2000).

M.S. Whittingham and P.Y. Zavalij, "Manganese Dioxides as Cathodes for Lithium Rechargeable Cells: The Stability Challenge," *Solid State Ionics*, **131**, 109-115 (2000).

M.S. Whittingham, "Insertion Electrodes as SMART Materials: The First 25 Years and Future Promises, *Solid State Ionics*, **134**, 169-178 (2000).

PRESENTATIONS

M.S. Whittingham, "Lithium Intercalation into Vanadium and Manganese Oxides," *Max-Planck Worshop*, Schloß Ringberg, Germany, March 17, 2000, .

M.S. Whittingham, "Soft Chemistry Synthesis of Vanadium and Manganese Oxide Hosts for Intercalation Reactions, Chemistry Department, University of Michigan, Ann Arbor, MI, March 21, 2000,

M.S. Whittingham, "Hydrothermal Synthesis of Manganese Vanadium Oxides," *American Chemical Society*, San Francisco, CA, March 26, 2000.

M.S. Whittingham, "The Stabilization of Layered MnO_2 Relative to Spinel Formation," *IBA 2000*, Argonne National Laboratory, Argonne, IL, May 11, 2000.

M.S. Whittingham, "The Control of Structure and Properties of Vanadium and Manganese Oxides through Tailored Soft Synthesis," *European Materials Research Society*, Strasbourg, France, June 1, 2000,

M.S. Whittingham, "Cathode Materials: Manganese Oxides – Overview and Results," DOE/LBNL Review, Berkeley, CA, June 6, 2000.

K. Ngala and M.S. Whittingham, "Synthesis and Characterization of Manganese Vanadium Oxides," *Gordon Research Conference*, New London, NH, July 2000.

P.Y. Zavalij and M.S. Whittingham, "Vanadium Oxide Framework Structures," *Intl. Symposium on the Reactivity of Solids*, Budapest, Hungary, August 28, 2000.

M.S. Whittingham, "Soft Chemistry Synthesis of Vanadium and Manganese Oxide Hosts for Intercalation Reactions," *Solid State Chemistry 2000*, Prague, Czech, September 4-8, 2000.

K. Ngala, P. Y. Zavalij and M. S. Whittingham, "Pillared Oxides of Manganese and Vanadium for Lithium Batteries - Geometric and Electronic Factors," *198th Electrochemical Society Meeting,* Phoenix, AZ, October 24, 2000.

M.S. Whittingham, "Manganese Dioxides for Lithium Batteries: The Stability Challenge," *Japan National Battery Meeting*, Nagoya, Japan, November 20–22, 2000.

P.Y. Zavalij and M.S. Whittingham, "Vanadium Oxide Frameworks Modified with Transition Metals," *Materials Research Society*, Boston, MA, November 27-30, 2000.

K. Ngala and M.S. Whittingham, "Synthesis and Characterization of Manganese Vanadium

Oxides," *Materials Research Society*, Boston, MA, November 27-30, 2000.

M.S. Whittingham, "The Control of Structure and Properties of Vanadium and Manganese Oxides through Tailored Soft Synthesis," *Intl. Symposium on Soft Solution-Processing*, Tokyo, Japan, December 8-11, 2000.

M.S. Whittingham, "Manganese and Vanadium Oxides as Battery Cathodes," NTT Research Labs., Ibaraki, Japan, December 12, 2000.

Synthesis and Characterization of Cathode Materials

Marca M. Doeff
Lawrence Berkeley National Laboratory, 62-203, Berkeley CA 94720
(510) 486-5821, fax: (510) 486-4881; e-mail: mmdoeff@lbl.gov

Objective

- Develop low-cost cathodes based on benign materials (*e.g.*, manganese oxides, lithium iron phosphate) having electrochemical characteristics (cycle life, energy, and power densities) consistent with the goals of the USABC and/or PNGV.

Approach

- Use novel synthesis methods to produce pure materials with optimum particle size and morphology.
- Carry out systematic substitutions to improve electrochemical properties.
- Test materials in several different cell configurations under a variety of conditions, including normal cycling and high-rate discharge at both room and elevated temperatures.

Accomplishments

- Demonstrated that Li/1 M $LiPF_6$ EC-DMC/tunnel-Li_xMnO_2 cells can be cycled over 250 times with no capacity fading, and can be discharged at up to the 5C rate repeatedly without damage.
- demonstrated excellent cycling behavior at 85°C for polymer cells containing tunnel-Li_xMnO_2 (less than 0.02% average capacity loss per cycle over 140 discharges at the 1.5 C rate).
- Increased reversible capacity 20% by substitution of 22% of the Mn in tunnel-MnO_2 with Ti.

Future Directions

- Investigate $LiFePO_4$ as electrode material; overcome rate limitations caused by poor electronic conductivity by using sub-micron particles and coating with carbon during synthesis.
- Expand investigation of the effects of substitution on the electrochemical behavior of tunnel-containing manganese oxides.

We have identified a remarkably stable manganese oxide phase with an unusual double-tunnel structure ($Na_{0.44}MnO_2$). The theoretical capacity is estimated to be at least 200 mAh/g. It undergoes ion-exchange and reductive intercalation processes readily and reversibly and does not convert to spinel below about 400°C. Over-charge/over-discharge studies have also indicated that this structure is highly resistant to damage from abuse.

In 2000, we showed that the rate behavior and cycling characteristics of Li_xMnO_2 made from $Na_{0.44}MnO_2$ depended strongly on the particle morphology. Best results were obtained when $Na_{0.44}MnO_2$ made by a glycine-nitrate process (GNP) was used as the precursor. This combustion synthesis method results in a drastic reduction in the particle dimension along which ion diffusion takes place. Lithium cells containing GNP-Li_xMnO_2 electrodes show excellent rate capability (Fig. 42) and cycle without fading. This material also performs well in a polymer cell configuration at elevated temperatures (Fig. 43), in sharp contrast to spinel materials, which lose capacity rapidly.

These characteristics indicate that Li_xMnO_2 with the $Na_{0.44}MnO_2$ structure should perform well in HEV batteries, where high power, abuse-tolerance, and long cycle life are necessary, but high energy

density is not required. For EV applications, however, higher capacity is needed. At present, it is not possible to extract all of the Li ions from Li_xMnO_2 without oxidizing the electrolyte and compromising cycle life. This limits the practical capacity to about half of theoretical.

Partial substitution of Mn with other metals changes the electrochemical characteristics, and, in some cases, flattens the voltage profile, allowing more capacity to be delivered. For example, $Li_xTi_{0.22}Mn_{0.78}O_2$ delivers 20% more capacity than Li_xMnO_2 in the same cell configuration.Substitution of >22-at% level does not result in further improvement, however, because too much electro-active Mn is replaced with inert Ti.

Although higher capacity is obtained for Li cells with $Li_xTi_{0.22}Mn_{0.78}O_2$ electrodes, the rate capability and cycling behavior are inferior to those with GNP-Li_xMnO_2, negating the advantage except at low current densities (Fig. 44). A sol-gel synthesized product had very small average particle size, but had markedly inferior electrochemical properties, because the distribution of Ti differed from that of the solid-state synthesized material.

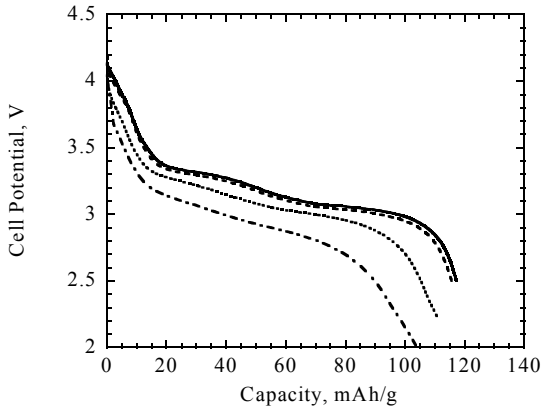

Figure 42. Discharge number 118 of a Li/1 M $LiPF_6$ EC-DMC/GNP-Li_xMnO_2 cell at 25 μA/cm^2 (—), discharge number 98 at 0.14 mA/cm^2 (-----), discharge number 121 at 0.5 mA/cm^2 (·····), and discharge number 108 at 2.5 mA/cm^2 (– · – · –) or 5C rate.

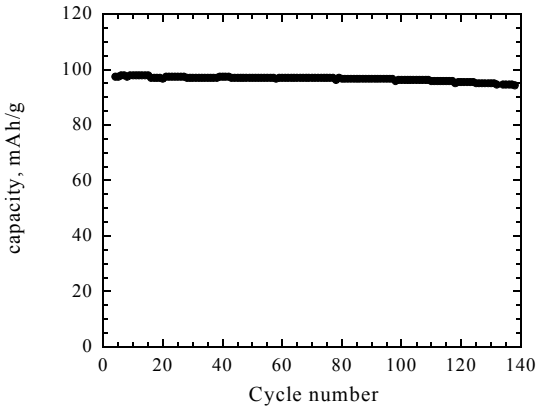

Figure 43. Cycling data for a Li/P(EO)$_8$LiTFSI/GNP-Li_xMnO_2 cell discharged at 0.5 mA/cm^2 or 1.5 C rate between 3.6 and 2.5 V at 85°C.

We have also been successful in preparing $Li_xCu_{0.11}Mn_{0.89}O_2$ with the tunnel structure, but its electrochemical characteristics appear to be inferior to those of Li_xMnO_2. Also, attempts to substitute Mn with V, Fe, Co, Ni, Zr, or 22-at% Cu result in layered compounds or mixtures of phases rather than the desired tunnel compound.

Future work will continue on the promising tunnel manganese oxide compounds. Our goal is to increase reversible capacity without sacrificing the power capability, and excellent stability demonstrated by GNP-Li_xMnO_2. To do this, a better understanding of intercalation into these materials is necessary, as well as knowledge about the substitution behavior and chemistry. We will also begin investigating $LiFePO_4$, another promising electrode material. At present, $LiFePO_4$ shows severe rate limitations due to its poor electronic conductivity. To ameliorate this, we will optimize particle size and coat particles with carbon.

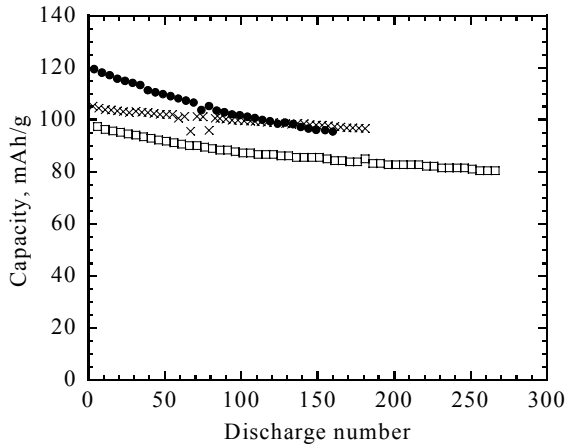

Figure 44. Cycling data for Li/P(EO)$_8$LiTFSI/ $Li_xTi_{0.22}Mn_{0.78}O_2$ cells at 85°C, discharged at 0.1 mA/cm^2 between 3.6 and 2.5 V (x), 0.1 mA/cm^2 between 3.6 and 2.4 V (●), and 0.5 mA/cm^2 between 3.6 and 2.5 V (□).

PUBLICATIONS

L. Edman, A. Ferry and M.M. Doeff, "Slow Recrystallization in the Polymer Electrolyte System P(EO)$_n$LiTFSI," *J. Mater. Res.,* **15**, 1950-4 (2000).

L. Edman, M.M. Doeff, A. Ferry, J. Kerr and L.C. De Jonghe, "Transport Properties of the Solid Polymer Electrolyte System P(EO)$_n$LiTFSI," *J. Phys. Chem. B.*, **104**, 3476 (2000).

M.M. Doeff, L. Edman, S.E. Sloop, J. Kerr and L.C. De Jonghe, "Transport Properties of Binary Salt Polymer Electrolytes," *J. Power Sources,* **89**, 227 (2000).

M.M. Doeff, T.J. Richardson, K.T. Hwang and A. Anapolsky, "Factors Influencing the Discharge Characteristics of $Na_{0.44}MnO_2$-based Positive Electrode Materials for Rechargeable Lithium Batteries," in *Proceedings of the International Meeting of The Electrochemical Society*, Honolulu, HI, October 1999, G-A. Nazri, M.M. Thackeray, and T. Ohzuku, eds., The Electrochemical Society, Inc., **99-24**, 48 (2000).

PRESENTATIONS

M.M. Doeff, "Novel Tunnel-containing Manganese Oxides with Excellent Reversibility," *DOE Workshop on Interfaces, Phenomena, and Nanostructures in Lithium Batteries*, Argonne, IL, December 11-13, 2000.

M.M. Doeff, T.J. Richardson, A. Anapolsky and M. Gonzales, "Stable Manganese Oxides for Lithium Battery Applications," invited lecture presented by M.M. Doeff at the *Pacific Conference on Ceramic Materials*, San Francisco, CA September, 2000.

M.M. Doeff, "Synthesis and Electrochemical Characterization of Tunnel-containing Doped Manganese Oxides," *Solid State Chemistry I Gordon Conference*, New London, NH, July 2000.

M.M. Doeff, T.J. Richardson, K.-T. Hwang and A. Anapolsky, "Improved Discharge Characteristics of Tunnel-containing Manganese Oxide Electrodes for Rechargeable Lithium Battery Applications," presented by M.M. Doeff at the *IBA-2000 Manganese Oxide Symposium*, Chicago, IL, May, 2000.

M.M. Doeff, "Lithium-Polymer Batteries on a Laboratory Scale," invited lecture, *Nordic Energy Research Program Workshop*, Lund, Sweden, May 2000.

M.M. Doeff, "Electrochemical Characterization of Li-Polymer Batteries," invited lecture, *Nordic Energy Research Program Workshop*, Lund, Sweden, May 2000.

TASK AREA 5: DIAGNOSTICS

Diagnostics: Electrode Surface Layers

Frank R. McLarnon

Lawrence Berkeley National Laboratory, 90-1142, Berkeley CA 94720

(510) 486-4636; fax: (510) 486-4260; e-mail: frmclarnon@lbl.gov

Objectives

- Apply advanced *in situ* and *ex situ* techniques to characterize the structure, composition, formation, and growth of surface layers on BATT Program electrodes.
- Establish direct correlations between electrode surface changes, interfacial phenomena, and cell capacity decline.

Approach

- Use ellipsometry, Raman spectroscopy, and advanced microscopic techniques to characterize electrodes taken from baseline BATT Program cells, as well as thin-film electrodes in model cells.
- Measure changes in electrode surface morphology, electrode surface chemistry, and SEI thickness and composition that accompany cell cycling.

Accomplishments

- Determined how the storage of model thin-film $LiMn_2O_4$ electrodes in pure DMC solvent and in $LiPF_6$-EC-DMC electrolyte at elevated temperatures changes the electrode structure, morphology, SEI layer, and surface chemistry.
- Measured the thickness and composition of SEI layers formed during cycling of model thin-film carbon electrodes in $LiClO_4$-EC-DMC electrolyte.

Future Directions

- Identify changes in $LiAl_{0.05}Ni_{0.80}Co_{0.15}O_2$ and $Li_{1.02}Al_{0.25}Mn_{1.75}O_{3.92}S_{0.03}$ cathode surface morphology and chemistry which accompany cycling in $LiPF_6$-EC-EMC, $Li(CF_3SO_2)_2N$ +cross-linked PEO, and $LiBF_4$ + cross-linked gel electrolytes.
- Characterize SEI formation and growth on Li and carbonaceous anodes in $LiPF_6$-EC-EMC, $Li(CF_3SO_2)_2N$ +cross-linked PEO, and $LiBF_4$ + cross-linked gel electrolytes.

We extended our study of model thin-film spinel $LiMn_2O_4$ electrodes to determine the effects of elevated temperature on interfacial phenomena. We used XRD, atomic force microscopy (AFM), and Raman spectroscopy to characterize changes to the electrode structure, morphology, and surface chemistry caused by one-day exposure to pure DMC solvent or 1 M $LiPF_6$/EC-DMC electrolyte at 25, 60, and 70°C. A CV of a fresh $LiMn_2O_4$ electrode in $LiPF_6$-EC-DMC electrolyte displayed two sets of anodic and cathodic peaks, as expected for a spinel $LiMn_2O_4$ electrode, and 43 CVs at 25°C resulted in ~9% capacity decline.

The capacity of the electrode exposed to pure DMC at 70°C vanished completely, even though there were no accompanying changes in its XRD pattern, suggesting that the electrode capacity decline was caused by a surface process, rather than by changes in the bulk electrode structure. Current-sensing AFM (CSAFM) images of a fresh $LiMn_2O_4$ thin-film electrode revealed densely packed 100-250 nm particles with average surface roughness ~24 nm and non-uniform surface conductance, *i.e.*, the

conductance was lower on the upper surfaces of individual $LiMn_2O_4$ grains than on their sides or at grain boundaries. The surface morphology of the electrode exposed to DMC at 60°C was similar to that of a fresh electrode, however its surface conductance decreased significantly. CSAFM images of the electrode exposed to DMC at 70°C showed no surface electronic conductance and moderate changes of surface morphology. The electrode granular structure was preserved, but its average surface roughness dropped to ~9 nm. These observations suggest the formation of a thin SEI layer and/or surface chemical modification of $LiMn_2O_4$.

Our thin-film $LiMn_2O_4$ electrodes lost 3 and 4% of their capacities upon exposure to $LiPF_6$-EC-DMC electrolyte at 60 and 70°C, respectively, in sharp contrast to the complete loss of capacity upon exposure to pure DMC at 70°C. The XRD peaks of these electrodes shifted toward higher angles and their respective lattice parameters decreased to 8.13 and 8.10 Å, suggesting that Li was extracted to form $Li_xMn_2O_4$ with $x<1$. Also, the electrolyte became brown at 70°C, indicating Mn dissolution. AFM images revealed the formation of pits 150-250 nm deep, clearly indicating Mn dissolution. The surface conductance dropped significantly at 60°C and almost completely disappeared at 70°C. However, in this case SEI layer formation did not cause significant capacity loss, as was the case for electrodes exposed to pure DMC.

Both Raman and surface-enhanced Raman (SER) spectroscopies were used to determine the compositions of SEI layers formed at elevated temperatures. The ordinary Raman spectrum of a fresh $LiMn_2O_4$ electrode exhibited peaks at 624, 580, and 480 cm^{-1}, which are assigned to A_{1g}, T_{2g}, and T_{2g} phonons, respectively. Upon exposure to pure DMC at 60 or 70°C, a new peak appeared at 656 cm^{-1}, consistent with spectra of hausmanite Mn_3O_4 and bixbyite Mn_2O_3. Because the peak intensities at 624 and 580 cm^{-1} remained unchanged, the 556 cm^{-1} peak clearly reflects Mn_2O_3 character and may be a signature of surface conversion of $LiMn_2O_4$ into Mn(III) oxide in DMC at elevated temperatures. The Raman spectrum of the electrode stored in $LiPF_6$-EC-DMC electrolyte at 70°C showed even more dramatic changes: the peak at 624 cm^{-1} vanished, the peak at 580 cm^{-1} became prominent, and a strong resonance enhancement was observed at 514 nm excitation. These complex changes can be explained in terms of at least partial delithiation and conversion to λ-MnO_2, consistent with our XRD data. SER spectra showed new peaks at 240, 889, 918, and 985 cm^{-1}; broad multi-peak maxima at 1300 and 1600 cm^{-1}; and peaks between 2100 and 2160 cm^{-1}. These new peaks (except for that at 918 cm^{-1}) are invisible in the ordinary Raman and SER spectra of fresh electrodes, and therefore must be associated with the SEI layer. The breadth and poor definition of these peaks suggest a complex SEI containing multiple organic compounds, along with derivatives of carbonates and carboxylic acids of complicated molecular symmetry. The broad peak at 240 cm^{-1} can be assigned to the lithium-oxygen stretch in lithium alkoxides Li-O-R (R=alkyl) and/or Li coordinated to carboxylic Li-(CO_2)-R or carbonate $(Li\text{-}O)_2$-C=O groups. The broad maxima at 1300 and 1600 cm^{-1} correspond to symmetric and asymmetric vibrations, respectively, of carboxyl and carbonate groups. However, the features observed in reference Raman and SER spectra of $(COONa)_2$, HCOONa, and CH_3COOLi cannot account for all of the peaks we observed. The peaks at 918/889 and 985 cm^{-1} are probably C-C stretching and deformation vibrations of the carboxyl groups (-COO). None of the reference spectra showed intense bands in the 2100-2160 cm^{-1} region. These features often accompany SER spectra and may arise from adsorbed molecules on Ag, *i.e.*, so-called "impurity lines." These peaks are located above and below -C≡O (2135 cm^{-1}), which suggest the presence of polynuclear carbonyl complexes.

We began efforts to characterize in detail the surface phase segregation of $LiNi_{0.8}Co_{0.2}O_2$ cathodes taken from DOE-ATD Program Li-ion cells. This work serves three purposes: *(i)* to enhance our capabilities for the study of BATT Program electrodes, *e.g.,* identifying the role of sulfur additives on electrode surface chemistry; *(ii*) to provide better understanding of $LiNi_{0.8}Co_{0.2}O_2$ interfacial processes; and *(iii*) to support ATD Program diagnostics. A "reference library" was constructed by recording Raman spectra of $LiNi_{0.8}Co_{0.2}O_2$ powders and commercially available materials, and collecting literature data. Raman microscopy was used not only to determine the micron-scale chemical and structural uniformity of these materials, but also to compare their spectral characteristics to those of $LiNiO_2$ and $LiCoO_2$, which exhibit peak pairs at 468, 546 and 487, 597 cm^{-1}, respectively. In contrast, the micro-Raman spectrum of $LiNi_{0.8}Co_{0.2}O_2$ powder exhibits a broad

peak at ~520 cm^{-1} and a sharp peak at ~555 cm^{-1}, which indicate the presence of a solid solution of Co-substituted nickel oxides rather than a mixture of separate crystalline phases.

Micro-Raman spectra of $LiNi_{0.8}Co_{0.2}O_2$ cathodes taken from Li-ion cells stored or cycled at elevated temperatures (40°C) displayed significant spectral changes. The broad 520 cm^{-1} peak split into separate peaks at 479, 553, and 565 cm^{-1} and a weak shoulder at ~600 cm^{-1}, due to thermally induced surface phase segregation. Neither substitution of Co for Ni nor Li intercalation-deintercalation changed the $LiNi_yCo_{1-y}O_2$ R3m space group symmetry. However, the substitution of Co for Ni(III) oxides increased the crystal lattice parameter, as reflected by a 3-4 cm^{-1} shift of two characteristic 474/554 cm^{-1} NiO_2 peaks toward lower frequencies and an increased 474/554 peak ratio. Lithium intercalation into NiO_2 had the opposite effect: the peaks shifted toward higher frequencies and the 474/554 peak ratio decreased. The presence of separate peaks at both sides of the original NiO_2 peaks and strong relative peak intensity variations in the spectra of $LiNi_{0.8}Co_{0.2}O_2$ cathodes suggest the formation of stable crystalline phases of Ni(III) or Ni(IV) oxides with different amounts of Co and Li on the cathode surface.

In collaboration with the research group of J.W. Evans (p. 53), we carried out *in situ* spectroscopic ellipsometry (SE) and electrochemical quartz crystal microbalance (EQCM) experiments to characterize the formation and growth of SEI layers on carbon electrodes. We recorded ellipsometric spectra before and after cycling of an electron-beam-deposited thin-film carbon electrode between 0 and 3 V *vs*. Li/Li^+ at 2 mV/s in a half cell with 1 M $LiClO_4$/EC-DMC electrolyte. We considered two optical models to describe the electrode: (*i*) a compact and homogeneous carbon layer, and (*ii*) an effective-medium approximation of a rough, porous carbon layer. The latter model showed better fitting results and is consistent with the electrode surface roughness measured by AFM. We found that the SEI layer thickness was about 60 nm after the 1st cycle and increased to about 90 nm after the 20th cycle. The SEI refractive index varied from 1.41 to 1.52, and its extinction coefficient was close to zero, *i.e.*, the SEI layer was more optically compact than common polymers and exhibited almost no electronic conductivity. The EQCM frequency shift during long-term cycling correlated well with our SE results. Detailed analysis of our SE and EQCM data indicated that the SEI density was ~1.5 g/cm^3, which is larger than the densities (1.0-1.2 g/cm^3) of expected polymer-like products of alkyl carbonate reduction. We conclude that the SEI must contain denser inorganic Li compounds (*e.g.*, Li_2O, Li_2CO_3, $LiClO_4$) in addition to alkyl carbonates.

PUBLICATION

F. Kong and F. McLarnon, "Spectroscopic Ellipsometry of Lithium/Polymer-Electrolyte Interfaces," *J. Power Sources*., **89**, 180-89 (2000).

PRESENTATIONS

F. Kong, R. Kostecki, G. Nadeau, X. Song, K. Zaghib, K. Kinoshita and F. McLarnon, "*In Situ* Studies of SEI Formation," *10th International Meeting on Lithium Batteries*, Como, Italy, May-June 2000.

R. Kostecki, Y. Matsuo and F. McLarnon, "Interfacial Phenomena on selected Cathode Materials," *Workshop on Interfaces, Phenomena, and Nanostructures in Lithium Batteries*, Argonne, IL, December 2000.

Battery Materials: Structure and Characterization

James McBreen

Brookhaven National Laboratory, ES&T-Bldg. 555, P.O. Box 5000, Upton, NY 11973-5000

(631)344-4513, fax. (631)344-5815; email jmcbreen@bnl.gov

Objective

- Establish direct correlations between electrode material changes, interfacial phenomena, and cell capacity decline.

Approach

- Apply a combination of *in situ* and *ex situ* synchrotron techniques to characterize electrode materials and electrodes taken from baseline BATT Program cells.
- Develop and apply X-ray absorption spectroscopy (XAS) techniques that are sensitive to both surface and bulk processes in electrodes.

Accomplishments

- Completed an extensive study of the effect of Li and O stoichiometry on the phase behavior of spinel $LiMn_2O_4$ cathodes during cycling at ambient and low temperatures.
- Completed a study of the effects of electrode history on the phase behavior of $LiMn_2O_4$ cathodes.
- Completed *in situ* XAS studies of Li-Cr-Mn-O cathodes.
- Demonstrated the feasibility of collecting high-quality *in situ* XAS data on very dilute dopants in cathode materials.

Future Directions

- Develop a combination of electron yield and fluorescent XAS at transition metal K- and L-edges as a tool for identification of inorganic surface degradation products in cathodes. These will be used in conjunction with K-edge XAS of low Z elements such as C, O and F.
- Identify the changes in $LiNi_xMn_{2-x}O_2$ and $Li_{1.02}Al_{0.25}Mn_{1.75}O_{3.92}S_{0.03}$ when cycled in $LiPF_6$-EC-DMC electrolyte.

Our objectives are to develop and apply advanced diagnostic techniques to elucidate the molecular aspects of materials and electrode processes in Li-ion batteries, and to use this information to develop electrode and electrolyte structures with low cost, good performance, and long life. Work in 2000 was focused on *in situ* high-resolution XRD and XAS studies of lithium manganese oxide materials. Also methods were devised to collect high-quality *in situ* XAS data on very dilute dopants in cathode materials.

High-resolution XRD studies of $LiMn_2O_4$. $LiMn_2O_4$ compounds with various oxygen stoichiometries were prepared by heat treating $Li_{1.07}Mn_{1.93}O_4$ at 600°C under Ar. The O stoichiometry was determined from separate thermographic analysis (TGA) measurements. The DSC results in Fig. 45 show that the temperature for the phase transition and kinetics of the conversion from the cubic to the tetragonal phase increased with decreasing oxygen stoichiometry. In the case of stoichiometric materials the conversion occurs in the vicinity of 0°C. For the longer heat treatments the conversion occurred at ambient temperature or above.

Figure 46 shows that the O stoichiometry also had major effects on the phase transformations at low temperature. The results indicate that the existence of an oxygen deficiency in $LiMn_2O_4$ is a critical condition for formation of the low-temperature phase. Also, the greater the oxygen deficiency the higher the transition temperature. The XRD results at low temperature are more consistent with a mixture of a tetragonal and a cubic phase,

rather than a single phase with an orthorhombic structure. XRD results, at 300 K, showed a mixed phase composition for a sample treated at 600°C under Ar for 12 h. After treatment of the sample under O_2 at 700°C for 10 h only a single cubic phase was seen at 300 K. This strongly supports a mechanism based on oxygen deficiency.

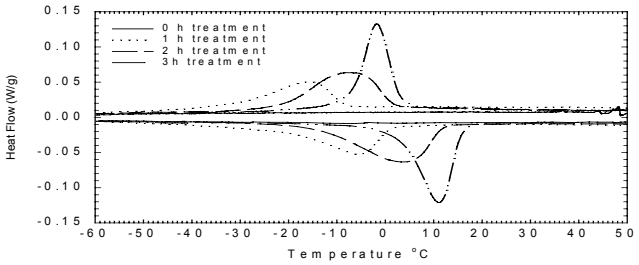

Figure 45. DSC trances between -60 and 50°C for the untreated (0h), 1 hour (1h), 2 hour (2h), and 3 hour (3h) heat treatment of $Li_{1.07}Mn_{1.93}O_4$ at 600°C under Ar.

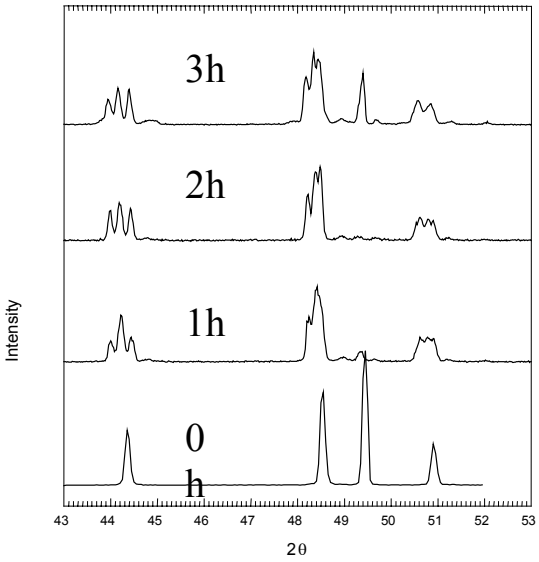

Figure 46. XRD patterns (λ=1.195Å) at 240 K for the untreated (0h), 1 hour (1h), 2 hour (2h), and 3 hour (3h) heat treatment of $Li_{1.07}Mn_{1.93}O_4$ at 600°C under Ar.

$LiMn_2O_4$ with a low oxygen stoichiometry clearly displayed three cubic phases during charge. Stoichiometric materials and materials with excess Li stoichiometry display pseudo single-phase behavior in the early stages of charge. This is followed by two-phase behavior toward the end of charge. Preliminary cycling studies indicate that the oxygen stoichiometry also affects capacity maintenance and phase behavior during cycling.

Effect of Al substitution in $LiMn_2O_4$. An Al-doped $Li_xMn_2O_4$ spinel material with the composition $Li_{1.02}Al_{0.09}Mn_{0.91}O_4$ was prepared from a γ-MnOOH precursor. This material had excellent stability when cycled over both the 4.1 and 3 V plateaus. After a few initial cycles the capacity stabilized at 200 mAh/g. *In situ* XRD scans were taken several times over the first fifty cycles. The tetragonal phase was present on the 20th cycle after discharge to 2.2 V. This indicates that Al substitution does not eliminate formation of the tetragonal phase on the 3 V plateau, but rather facilitates the process and mitigates the bad effects of tetragonal phase formation.

Li-Cr-Mn-O cathodes. *In situ* XAS and XRD studies were carried out on a new cathode material, $Li[Li_xCr_yMn_{1-x-y}]O_2$, developed at NRC, Canada. This is a layered material and replacement of ~20% of the transition metal atoms with Li improves the electrochemical characteristics of the material. A careful *in situ* XAS study at the Cr and Mn K-edges indicated that Mn was Mn(IV) and Cr was Cr(III) in the as-prepared material. During charge no further oxidation of the Mn occurs. Both the near edge data (XANES) and the extended X-ray absorption fine structure (EXAFS) at the Cr K-edge, during the first charge, indicate that about 40% of the Cr(III) is oxidized to Cr(VI) The data in Fig. 47 indicates that enormous changes occur in the Cr environment during charge. Analysis of the EXAFS shows that the oxidized Cr migrates from octahedral to tetrahederal sites. The reverse occurs during discharge, with a small fraction of the Cr(VI) remaining on tetrahedral sites. In subsequent cycles there is no further increase in the residual of Cr(VI) at the end of discharge. The results also indicate that Mn and Cr are not randomly distributed in the lattice, but exist in separate domains; and that the excess Li is associated with Mn vacancies around the Mn(IV).

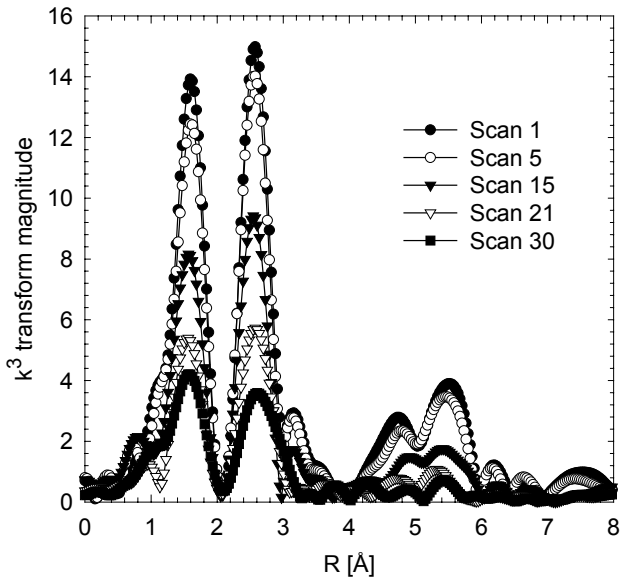

Figure 47. Fourier transforms of Cr K-edge EXAFS taken during the first charge from 3.5 to 4.5 V. 30 scans were taken during charge at the C/13 rate.

Ga XAS studies of $Li_{0.908}Co_{0.088}Ga_{0.003}O_2$: *In situ* Ga K-edge XAS was done on $Li_{0.908}Co_{0.088}Ga_{0.003}O_2$ in an effort to develop techniques to do XAS on dilute dopants. By doing the measurements in the fluorescence mode it was possible to get excellent data. As with the Cr in the previous section, enormous changes were seen in both the Ga K-edge XANES and EXAFS. The results indicate that during charge Ga migrates from octahederal to tetrahederal sites. Its efficacy as a dopant may be due to this migration preventing Ni from dropping into Ni sites. The Cr and Ga results demonstrate the ability of local probes such as XAS to deliver inportant structural information on complex systems.

PUBLICATIONS

A.N. Mansour, S. Mukerjee, X.Q. Yang and J. McBreen, "*In Situ* X-Ray Absorption and Diffraction Study of The Li Reaction With a Tin Composite Oxide Glass," *J. Electrochem. Soc.*, **147**, 869 (2000).

Y.J. Lee, F. Wang, S. Mukerjee J. McBreen and C.P. Grey, "^{6}Li and ^{7}Li Magic-Angle Spinning Nuclear Magnetic Resonance and *In Situ* X-Ray Diffraction Studies of the Charging and Disacharging of $Li_xMn_2O_4$ at 4 V," *J. Electrochem. Soc.,* **147**, 803 (2000).

X.Q. Yang, X. Sun and J. McBreen, "Structural Changes and Thermal Stability: *In Situ* X-Ray Diffraction Studies of a New Cathode Material $LiMg_{0.125}Ti_{0.125}Ni_{0.75}O_2$," *Electrochem. Commun.*, **2**, 733 (2000).

Diagnostics: Interfacial and Reactivity Studies

Philip N. Ross, Jr.

Lawrence Berkeley National Laboratory, 2-100, Berkeley CA 94720

(510) 486-6226, fax: (510) 486-5530; e-mail: pnross@lbl.gov

Objective

- Establish direct correlations between electrode surface changes, interfacial phenomena, and cell failure.

Approach

- Use Fourier transform infrared (FTIR) spectroscopy and X-ray photoelectron spectroscopy (XPS) to study model electrode/electrolyte combinations, *e.g.*, using glassy carbon electrodes and BATT Program electrolytes, to provide the basis to interpret more-complex spectra recorded for ATD Program cell materials.

Accomplishments

- Completed the experiments designed to determine the near-surface structure in lithiated highly ordered pyrolytic graphite (HOPG) and/or $LiC_6(0001)$.
- Completed experimental measurements of the electrochemical reduction potentials of all carbonate solvents of interest in Li-ion batteries.
- Completed computational studies of the electrochemical reduction and oxidation potentials of all organic solvents of interest in Li batteries.

Future Directions

- Establish thermal stability of the SEI layer on graphite anodes in ATD Program Gen 2 electrolyte.
- Identify some routes to improved stability *via* electrolyte additives and/or graphite pre-treatment.

We have completed experiments designed to determine the near-surface structure in lithiated HOPG and/or $LiC_6(0001)$, *i.e.*, which is the equilibrium surface plane, the graphene plane, or the Li-ion plane. We completed this determination by analysis of the take-off angle dependence of the Li 1s and C 1s photoelectron intensities and detailed modeling of the photoelectron emission/diffraction from the different surface terminations. The data clearly indicate termination in the graphene plane, in agreement with intuition.

The study of the reaction of diethyl carbonate (DEC) with lithiated C(0001) in ultra high vacuum (UHV) continues. The data is being compared in detail with that for DEC on metallic Li. Because we now know that the surface of lithiated C(0001) is terminated in the graphene plane, an interesting picture of the reaction with DEC emerges. The first step is electron transfer from the graphene sheet to the DEC molecule, which dissociates to form two anions, ethyl carbonate and ethyl carbanion. These anions are bound electrostatically to Li ions beneath the intervening graphene sheet. Since the binding is relatively weak, and no direct bonding to Li^+ occurs, for the most part the anions thermally decompose and/or recombine and desorb from the surface upon heating to 470 K. However, some Li^+ ions are also drawn out of the graphite lattice at 470 K to form an alkoxide-like species. This process is postulated to occur at step-edges in the HOPG, whose concentration can be varied by Ar-ion etching pre-treatment of the crystal. To date, CO_2 is the only gaseous reaction product clearly identified; the fate of the ethyl carbanion fragment from the initial dissociation is unclear.

FTIR analysis of the reduction product of EC on glassy carbon was conducted *ex situ*. The reduction potential was varied from 0.05 to 1.5 V (*vs.* Li/Li^+) at 0.25 V intervals. Unfortunately the results from these first experiments failed to show a systematic effect of reduction potential on the FTIR spectra. The only functional group observed, other than those of the bulk electrolyte, was the epoxy group, characterized by a strong, sharp C=O stretching band at 838 cm^{-1}, as shown in Fig. 48. This band has never been reported in other FTIR studies of Li or carbon anodes in any carbonate-based electrolytes. We also observed this band on some carbon anodes removed from Li-ion cells used in the ATD Program. In principle, ethylene oxide is the simple decomposition product of EC, according to

$$EC \rightarrow H_2COCH_2 + CO_2$$

But one rarely sees this reaction listed as a possibility in the literature.

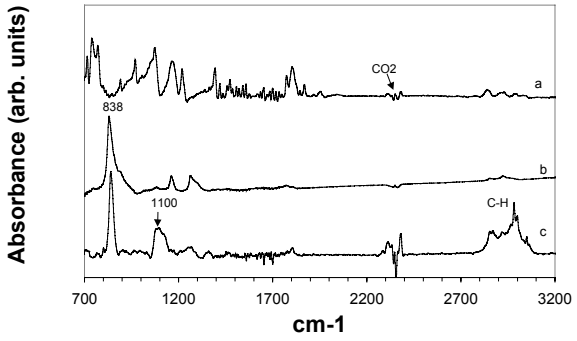

Figure 48. Diffuse reflectance mode FTIR spectra from: a) bulk electrolyte THF/$LiClO_4$ + 10 mM EC; b) glassy carbon electrode after reduction for 5 min. at 0.05 V (Li/Li^+); c) propylene oxide.

CV experiments were carried out to determine experimental values to compare against the calculated solvent reduction potential that we previously reported. The target solvent was dissolved in a tetrahydrofuran (THF)/$LiClO_4$ (0.1 M) electrolyte in a concentration of 1 vol%. A gold milli-electrode (1 mm radius) was employed with a slow scan rate of 2 mV/s. THF was selected because of its stability against reduction above Li metal potential (Fig. 49). The reduction at 1.8 V is generally ascribed to the reduction of H_2O, an impurity in the electrolyte. A summary of both calculated reduction potential and experimental results for four solvents is shown in the table.

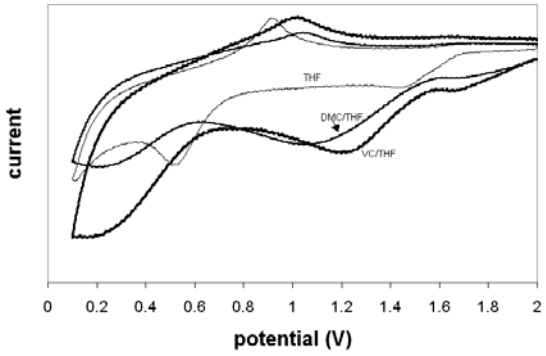

Figure 49. CV for THF-$LiClO_4$ electrolyte with 1 vol% solvent dissolved within.

Solvent	Calculated	Experimental
EC	1.46	1.36
DEC	1.33	1.24
DMC	0.86	1.32
VC	0.25	1.40

VC = vinylene carbonate

Both EC and DEC show good agreements between calculated and experimental results with the experimental values slightly lower by about 0.1 V. When calculating the reduction of linear carbonate solvents (DEC and DMC), it was assumed to be a two-electron-transfer process. An alkyl carbonate anion and alkyl radical were formed upon the first electron transfer while the 2nd electron was transferred to the alkyl radical to form an alkyl anion. This assumption seems to work well for DEC but not DMC. It is not energetically favorable for a methyl radical to accept an electron to form a methyl anion, which results in a lower calculated reduction potential of DMC. The experimental result, however, implies the reduction of DMC follows a different reaction pathway.

Vinylene carbonate (VC) was found to reduce at 1.40 V, much higher than the calculated value of 0.25 V, which suggests that the reduction process does not stop at a the non-bond-broken form of radical anion as we expected. Rather, a more energetically favorable product should be formed. Investigations were carried out to study the reduction products of VC. The relatively positive reduction potential for VC supports the postulated role of VC as an additive to propylene carbonate (PC)-based electrolyte for Li-ion cells. In the role, preferential reduction of VC forms an interfacial layer that prevents PC co-intercalation and graphite exfoliation.

A Li-ion battery composite carbon electrode (ATD Program Gen 1) electrode was used for the cycling experiments with VC as an additive to PC electrolyte. The composition of the anode was 75% MCMB carbon, 17% SFG-6 graphite, and 8% polyvinylidene difluoride (Kureha C) with a loading of 5.5 mg/cm^2 applied to both sides of a Cu foil current collector. Figure 50a shows constant-current (0.5 mA/cm^2) cycling of the composite carbon anode in PC electrolyte with 1 M $LiClO_4$. The long plateau around 0.4 V indicates significant solvent reduction. In consequence, the reversible capacity for the first

cycle was only 12%. Severe graphite exfoliation was observed in this electrolyte after just 10 cycles, and concurrent loss of capacity. Figure 50b shows the first constant-current charge and discharge of a nominally identical composite carbon anode in the same PC with addition of 5 vol% VC. The reversible capacity on the first cycle is significantly improved to 67%, and subsequent cycles had a cycling efficiency of 93–95%. The electrolyte turned slightly brown after 10 cycles. However, there was no observable exfoliation of the graphite. The effects of VC on PC reduction reported here are qualitatively consistent with those reported previously by Jehoulet *et al*.

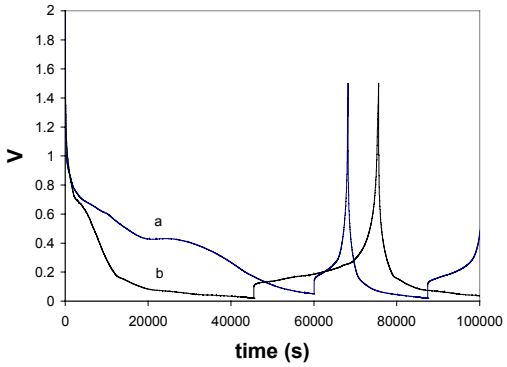

Figure 50. Constant-current (0.5 mA/cm^2) cycling of a composite carbon anode in (a) PC/$LiClO_4$ electrolyte, (b) PC/$LiClO_4$ electrolyte with 5% VC added.

The role of VC as additive was further investigated by *in situ* AFM. A solution with 1 vol% of VC in THF with 0.1 M $LiClO_4$ was used as the electrolyte. A polished glassy carbon (1.2 x 1.2 cm) was employed as the working electrode with Li metal as both the reference and counter electrodes. The potential was stepped down from the 2 to 0.5 V with 100 mV interval. Surface profiles were scanned at each step. The data indicate that a surface film was starting to develop on the electrode surface at 1.2 V. The AFM images at open circuit potential and 1.2 V are shown respectively in Figure 51 a and b. This finding is consistent with the reduction of VC in THF reported previously by our group (Fig. 49). The thickness of the surface film was measured to be ~10 nm. This observation confirms our previous conclusion that VC is forming a SEI layer at high potential before Li^+ intercalation into graphite and therefore prevents solvent co-intercalation.

We simulated the Li/PEO interface by deposition of Li onto a Pt electrode from the electrolyte THF/$LiClO_4$ + 35 mM PEGDME, with the PEGDME MW 400. After the electrochemical experiment, the electrode was removed from the cell, rinsed with THF and inserted into an airtight infrared cell fitted with a KBr window. *Ex situ* Infrared Reflection Absorption Spectroscopic (IRRAS) analysis of the interface was conducted and shown in Fig. 52b along with spectrum of the THF/PEGDME electrolyte on a Pt substrate (Fig. 52a). The two spectra are similar and no new feature is detected on the electrode interface, *i.e.,* no SEI is detected. IR is therefore, not useful in detecting SEI layer on the Li/PEO interface.

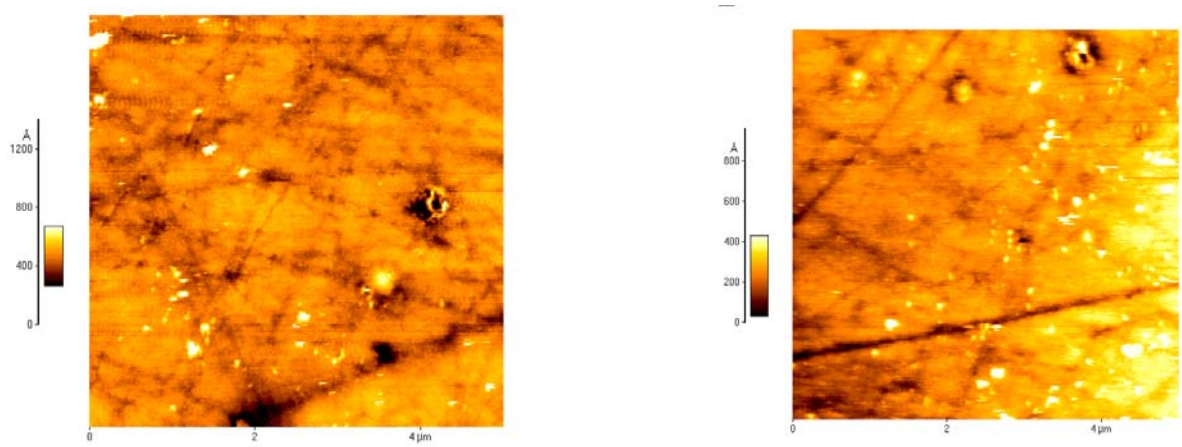

(a) (b)

Figure 51. AFM image of glassy carbon electrode surface at (a) open circuit potential 2.0 V, (b) 1.2 V.

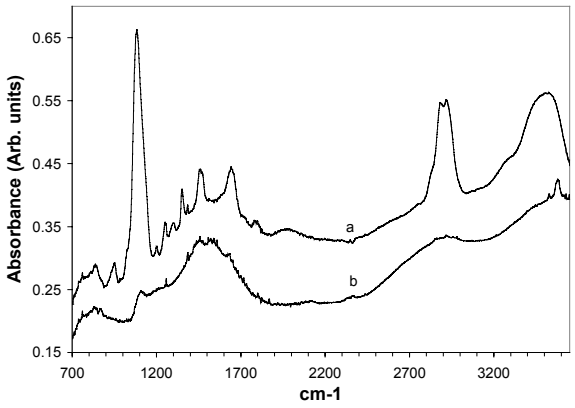

Figure 52. *Ex-situ* IR of Pt electrode surface in electrolyte THF/$LiClO_4$ + 35 mM PEGDME, a) before electrochemical reduction; b) after Li metal deposition.

Synthesis and Characterization of Electrodes

Elton J. Cairns

Lawrence Berkeley National Laboratory, 70-108B, Berkeley CA 94720

(510) 486-5028; fax (510) 486-7303; e-mail ejcairns@lbl.gov

Objectives

- Characterize the local atomic and electronic states of Li in BATT Program cathode materials, and determine how these states change during cell cycling.
- Develop intermetallic electrodes that have capacities higher than carbon electrodes and acceptable stability during cell cycling.

Approach

- Use ^{7}Li MAS-NMR to characterize BATT Program electrodes before and after cycling, and after being subjected to model failure processes.
- Determine the NMR isotropic chemical shift, linewidth, lineshape, and relaxation times for each Li species. Extend this to other important nuclei.
- Synthesize intermetallic electrodes for use as negative electrodes in BATT Program cells, and characterize the unique microstructures that result from synthesis methods such as high-energy milling.

Accomplishments

- Obtained preliminary ^{7}Li MAS-NMR spectra for several tunnel-structure lithium manganese oxides.
- Synthesized Mg-Si and Mg-Sn materials with various microstructures and demonstrated that their Li storage capacities exceed that of a typical carbon.

- Determined that conversion of Mg_2Sn and Mg_2Si into their constituent elements contributes to rapid capacity fade when cycled over a wide voltage window.

Future Directions

- Continue NMR work using a 100 MHz magnet to improve resolution.
- Compare results for tunnel-structure cathodes at different field strengths to assign isotropic peaks.
- Determine NMR linewidths and relaxation times for tunnel-structure cathodes.
- Obtain spectra for fresh and cycled BATT Program cathodes.
- Determine effects of intermetallic electrode microstructure on electrochemical performance by correlating cycling results with material properties.
- Use ^{119}Sn NMR to study the local environment of the Mg-Sn intermetallic electrodes.
- Use ^{7}Li NMR to determine sites for Li occupancy in intermetallic electrodes.

Cathodes. Several BATT Program tunnel-structure lithium manganese oxides were obtained from M. Doeff (p. 38 of this report), including Cu- and Ti-substituted manganese oxides. Representative spectra are shown in Fig. 53. These spectra were obtained using a 181 MHz magnet with MAS at 11 kHz. Although this is a rapid spinning rate, many MAS sidebands are observed to each side of the isotropic peaks. The resulting MAS envelopes are quite wide due to coupling between the ^{7}Li nucleus and unpaired electrons in the Mn d-orbitals. Even so, several chemically distinct types of Li are indicated. The Ti-substituted sample gives rise to significant spectral overlap of the isotropic peaks arising from a wide variety of Li sites. It is expected that future work conducted using a 100 MHz magnet will show greatly improved resolution of the peaks arising from chemically distinct Li sites due to the reduction of the bulk magnetization of the Mn d-electrons.

Intermetallic electrodes. There is a strong incentive to develop and characterize non-carbonaceous materials for use as negative electrodes that have higher capacities than carbon and that retain high capacities during cycling. We have shown that the Mg-Si and Mg-Sn alloys can store Li with capacities well in excess of typical carbonaceous electrodes, but more work is needed to characterize these materials and prevent rapid capacity decline during cycling.

Electrode materials were synthesized by mechanically alloying elemental powders in a planetary ball mill. Mechanical alloying is a useful method for producing battery materials because the products have a fine particle size, the product microstructure can be controlled by the milling conditions and heat treatments, and interesting metastable phases can be produced in large quantities. Mg_2Si, which is difficult to prepare by casting because of the large disparity in melting points between Mg and Si, was synthesized directly by mechanical alloying. In the Mg-Sn system, the stable, cubic Mg_2Sn phase could be converted to a metastable, rhombohedral phase with further milling, as shown in Fig. 54.

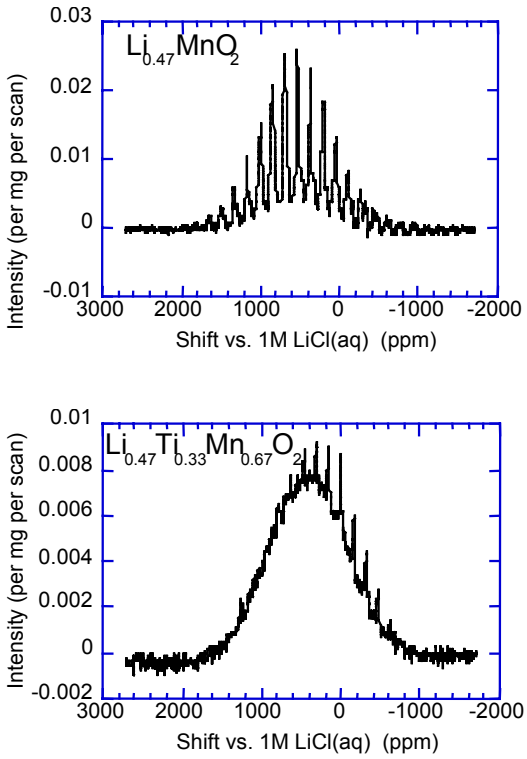

Figure 53. ^{7}Li MAS NMR spectra of tunnel-structure lithium manganese oxides. Spinning speed was 11 kHz.

Cycling these materials over a wide voltage window from 0 to 1 V *vs*. Li/Li^+ produced maximum discharge capacities greater than 600 mAh/g and 800 mAh/g for cubic Mg_2Sn and Mg_2Si, respectively. A typical charge and discharge curve for Mg_2Si is shown in Fig. 55, however cycling over this wide window led to a rapid capacity fade to capacities >100 mAh/g within 10 cycles. XRD measurements showed that this capacity fade was at least partly due to conversion of the alloys into their elemental starting materials, which presented the opportunity for reaction of Li with Si and Sn. The separation of intermetallic alloys into their constituents during Li cycling is a commonly-observed phenomenon that we wish to suppress.

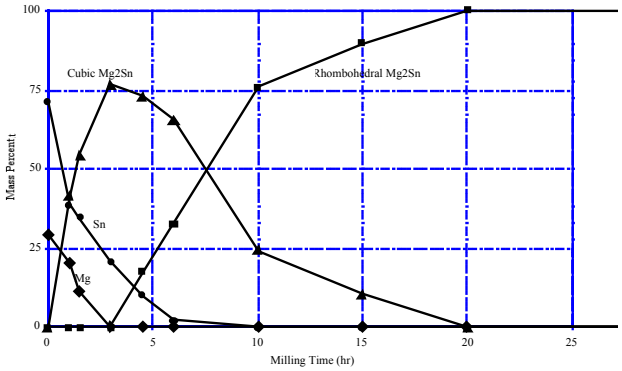

Figure 54. Batch composition *vs.* milling time at 2.1 W.

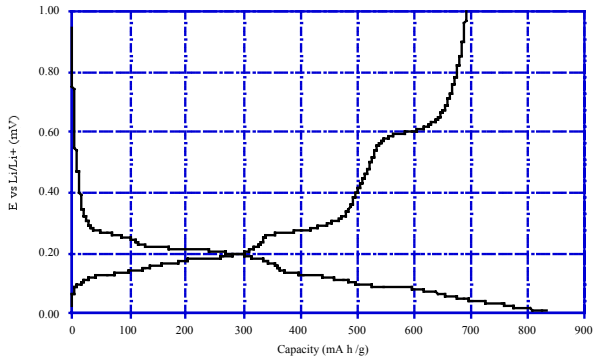

Figure 55. Charge/discharge cycle for Mg_2Si.

Lithium/sulfur cells. Our work on Li/S cells was completed in 2000, and included an investigation of the behavior of thin sulfur cathodes containing 70 wt% elemental sulfur, 20 wt% carbon black, and 10 wt% PEO (M.W. 5,000,000). These materials were mixed in acetonitrile for several days, and then cast onto a stainless-steel disk current collector. As-prepared electrodes were dried at 60°C for 24 h in vacuum before introduction into a glove box where cell assembly was carried out. The electrolyte was LiTFSI in PEGDME (MW 500), and the separator was Celgard 2400. Cell cycling was carried out at room temperature. Figure 56 shows that the cell discharge capacity increased for the first 20 cycles, a phenomenon that is probably related to slow permeation of the high-viscosity electrolyte into the electrode. The capacity slowly decreased over almost 400 cycles, with a capacity loss rate of 0.46 mAh/g per cycle. At 0.02 mA/cm^2, the specific capacity of the sulfur electrode was about 470 mAh/g, which corresponds to almost 30% utilization of active material. The capacity decreased to only 20 mAh/g of electrode at high rate (0.5 mA/cm^2), but it fully recovered when the current density was returned to 0.05 or 0.02 mA/cm^2.

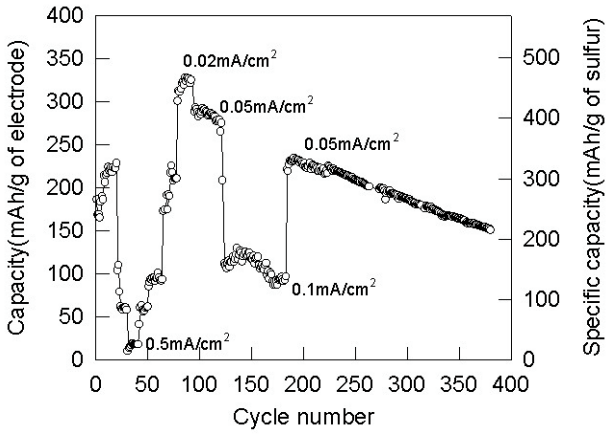

Figure 56. Capacity of sulfur electrode during cycling. Cut-off 1.5-3.0 V *vs.* Li/Li^+. Electrode area 1 cm^2. Electrode weight 1.6 mg/cm^2. Charge/discharge current 0.02-0.5 mA/cm^2. Electrolyte LiTFSI in PEGDME 500.

These results show good promise for the continuing development of the Li/S cell as an inexpensive, environmentally-benign cell with high specific energy. Modifications to the structure of the sulfur electrode should yield even higher sulfur utilization.

PUBLICATION

D. Marmorstein, T.H. Yu, K.A. Striebel, F.R. McLarnon, J. Hou and E.J. Cairns, "Electrochemical Performance of Lithium/Sulfur Cells with Three Different Polymer Electrolytes," *J. Power Sources*, **89**, 219 (2000).

Diagnostics: Electrochemical Quartz Crystal Microbalance (EQCM) Studies of the SEI on Carbon Anodes

James W. Evans (Lawrence Berkeley National Laboratory)
University of California, 585 Evans Hall, MC 1760, Berkeley CA 94720
(510) 642-3807, fax: (510) 642-9164; e-mail: evans@socrates.berkeley.edu

Objective

- Apply EQCM to characterize the SEI at the carbon/electrolyte interface in Li-ion batteries.

Approach

- Use *in situ* EQCM with combined CV to understand SEI formation and growth in Li-ion half cells.
- Characterize the system with other supplementary techniques such as ellipsometry (joint work with McLarnon group).
- Develop a model for SEI formation and growth on carbon anodes.

Accomplishments

- Estimated the SEI density on disordered carbon thin-film electrodes in 1 M $LiClO_4$/EC+DMC electrolyte.
- Observed mass changes corresponding to Li de-intercalation in CV with EQCM.
- Developed a model for interpreting measured EQCM data on a theoretical basis.

Future Directions

- Correlate SEI formation and growth with $LiPF_6$ or LiTFSI/EC+DMC electrolyte and impurities (*e.g.,* H_2O).
- Complete modeling of EQCM data according to each electrolyte and develop a general model for SEI formation and growth.

This program focuses on the characterization of the SEI on carbon electrodes in secondary Li-ion batteries. Along with Li de-intercalation in secondary Li batteries, other electrochemical/ chemical reactions are known to occur during the first few cycles and form an electrode surface layer, often referred to as the SEI. These reactions involving in SEI formation are associated with so-called irreversible capacity loss.

Because EQCM enables us to simultaneously measure, with high sensitivity, the mass change of the carbon electrode and the charge transfer associated with electrochemical reactions occurring on the carbon electrode, this technique is our major experimental tool for this study. Further, it allows us to determine the mass change per mole of electron transfer (mpe) for the species formed on the carbon electrode.

To fabricate a thin-film carbon electrode, a 100-nm thick carbon film was deposited by an electron-beam deposition technique onto one side of a smooth quartz substrate with two transition layers (500-nm Cu and 100-nm Cr), and Raman spectroscopy was carried out to characterize the thin-film carbon electrode. There is no visible dominant peak which is characteristic of graphite, diamond, glassy carbon, or any other form of ordered carbon but rather the superposition of all possible vibrations of various carbon structures. This is typical for a highly disordered/amorphous phase.

A galvanostatic cycling test was conducted with a constant current density of 10 μA/cm^2. There is a large irreversible capacity in the first cycle and the reversible capacity drops to about half of the theoretical value of graphite at later cycles. As expected from the fact that our carbon sample is disordered/amorphous, there is no distinct plateau that would imply staging phenomena in the graphitic structure.

CV and EQCM were applied simultaneously to a carbon electrode in 1 M $LiClO_4$/EC+DMC electrolyte. The measured quantities (current density, i, and resonant frequency change, Δf) for both techniques are plotted in Fig. 57. Because the mass increase corresponds to a decrease in the resonant frequency, the negative of Δf is plotted *vs.* potential to facilitate direct interpretation. Both the current density and frequency changes for the first cycle are larger than those of subsequent cycles. From the second to the 20th cycle, the shapes of the cyclic voltammograms and electrogravimetric curves are preserved. An irreversible peak appears at about 0.8 V in the first cathodic scan, and Li intercalation prevails as the potential approaches 0 V. For the anodic scan, Li de-intercalation is significant in the potential range above 0.5 V. This Li de-intercalation behavior was also reported in papers dealing with disordered carbon. The frequency change displays a trend similar to the CV. That is, the frequency shows a monotonic decrease, which implies accumulating mass on the working electrode, during the first cathodic scan. Furthermore, the frequency increases with increasing anodic current and decreases with increasing cathodic current.

Although this frequency response coincides qualitatively with the current behavior, there exists a quantitative discrepancy between them. While the charge stabilizes in later cycles, becoming almost reversible, the frequency continues to decrease with a decreasing amplitude of oscillation if we plot frequency and charge as a function of time during CV. In order to identify the source of the continuous frequency decrease, the transient frequency change at OCV was measured. The frequency decreases with the square root of time, and this dependency is the same regardless of the kind of electrodes (carbon, Al, and Ni tested) and solvents (EC+DMC and PC tested).

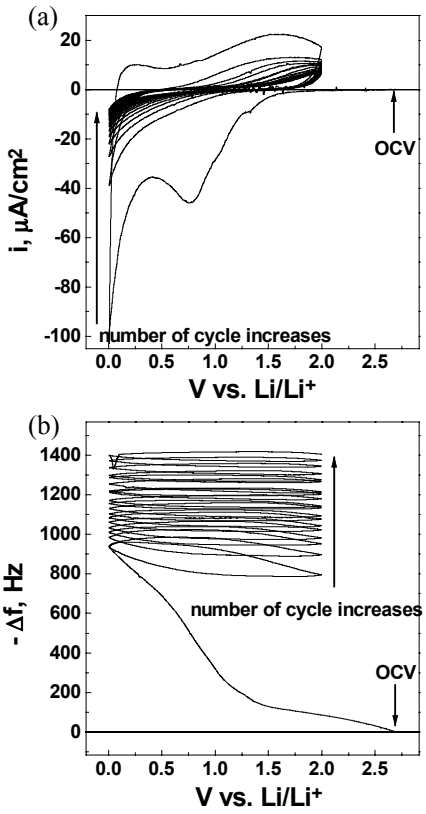

Figure 57. (a) CV and (b) resonant frequency change of the carbon electrode during the first 20 cycles in 1 M $LiClO_4$/EC+DMC (scan rate = 1mV/s).

With the correction using this frequency change at OCV as a base-line, mpe values were obtained for the first cathodic scan. The mpe values can be classified into three parts. The first region corresponds to the potential range from OCV to 1.1 V where mpe values are the highest (more than 30). The second region coincides with the irreversible peak at about 0.8 V, and the corresponding mpe is about 21. The last region could be termed an intercalation region where mpe values gradually approach 7, the theoretical value for Li intercalation. These results imply that organic species whose molecular weights are higher than those of inorganic species and Li ions form first and then inorganic species form. However, we cannot exclude the possibility of each formation potential being overlapped over the tested potential range.

Because most irreversible mass gain occurs in the first cathodic scan, ellipsometry was conducted to estimate the density of the SEI formed after the first cathodic scan under conditions identical to the EQCM experiment. The SEI density is estimated to

be about 1.3 g/cm^3 using the SEI thickness of about 60 nm as determined by ellipsometry. However, if the frequency change at OCV is also due to electrochemical/chemical reactions participating in film formation, the density would then be 1.6 g/cm^3. The estimated density of 1.3 to 1.6 g/cm^3 lies between those of inorganic and polymeric species proposed to be SEI components by several researchers. This supports the current understanding that the SEI is a composite of organic and inorganic species.

The resonant frequency is plotted with time during CV to investigate the SEI growth beyond the first cycle in Fig. 58. The measured frequency can be resolved into three parts based on a model that the total frequency change is due to Li de-intercalation, SEI formation, and a time-dependent term. The time-dependent term is estimated from the frequency change at OCV and is assumed not to entail charge transfer. The frequency change for SEI formation is separated by subtracting that for Li de-intercalation, which is estimated from the charge change, and the time-dependent term from the total measured frequency. This process is displayed in Fig. 58. The remaining SEI term shows that the SEI growth is arrested after 60000 s (equivalent to the 15th cycle under our experimental condition).

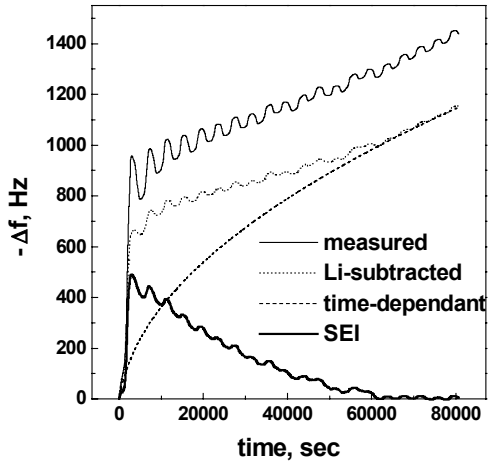

Figure 58. Resonant frequency changes (measured, Li de-intercalation-removed, time-dependent, and SEI-related) with time during CV for the first 20 cycles in 1 M $LiClO_4$/EC+DMC.

PUBLICATION

H. Yang, K. Kwon, T.M. Devine and J.W. Evans, "Aluminum Corrosion in Lithium Batteries – An Investigation Using the Electrochemical Quartz Crystal Microbalance," *J. Electrochem. Soc.,* **147**, 4399 (2000).

TASK AREA 6: MODELING

Improved Electrochemical Models

John Newman (Lawrence Berkeley National Laboratory)
University of California, Department of Chemical Engineering, 201 Gilman Hall, MC 1462, Berkeley CA 94720
(510) 642-4063, fax: (510) 642-4778; e-mail: newman@newman.cchem.berkeley.edu

Objectives

- Develop experimental and computational methods for measuring and predicting transport, kinetic, and thermodynamic properties.
- Model the behavior of electrochemical systems to optimize performance, identify limiting factors, and mitigate failure mechanisms.

Approach

- Refine the galvanostatic polarization technique to measure transport properties.
- Develop a molecular dynamics program to predict diffusion coefficients in multicomponent solutions.
- Develop a thermal model that accounts for concentration effects in insertion electrodes.
- Use potentiometric techniques to measure entropy.
- Develop a model of factors affecting dendrite formation on Li metal.
- Use Raman spectroscopy to measure *in situ* concentration profile and dendrite growth.

Accomplishments

- Completed measurement of the transference number and diffusion coefficient of polyethylene-methylene oxide (PEMO)-LiTFSI at 85°C and compared to transition-time experiments.
- Calculated the uncertainty in the molecular dynamics simulations of diffusivities in aqueous electrolytes.
- Measured entropy of reaction in $LiMn_2O_4$, $LiAl_{0.2}Mn_{1.8}O_4F_{0.2,}$ $LiNi_{0.8}Co_{0.2}O_2$, and graphite MCMB 25-28, and compared Monte Carlo simulations of entropy to measurements.
- Derived equations for determining the heat of mixing in electrochemical systems, and compared simulations of heat generation with calorimetry experiments.
- Developed a model of the effect of surface tension on dendrite growth.

Future Directions

- Develop a model of how side reactions affect measurement of transport properties.
- Complete molecular dynamics simulation of diffusion in multicomponent nonaqueous electrolytes.
- Measure the entropy of reaction of tunnel $Li_{0.44}MnO_2$ and $LiFePO_4$.
- Develop a model and conduct experiments to determine the influence of the SEI layer and of an elastic conducting matrix on the rate of capacity fade in lithium-tin electrodes.
- Conduct *in situ* confocal Raman spectroscopy to measure concentration profiles across polymer electrolytes and observe dendrite growth on Li electrodes.
- Simulate the effect of side reactions on the performance of "rocking chair" dual-insertion cells.

In order to develop improved polymer electrolytes, one must be able to measure the transport properties that one seeks to improve. We have developed and refined the galvanostatic polarization method for measuring a complete set of transport properties in polymer electrolytes, and, in

collaboration with John Kerr (LBNL), have completed measurements for LiTFSI in oxymethylene-linked PEMO at 85˚C and concentrations ranging from 0.03 to 3.1 molar. Unlike previous reports, negative values of the transference number were calculated at low concentrations, possibly due to side reactions and/or ion association. Transition-time experiments, which measure the time until depletion of salt at the cathode during passage of a current density higher than the limiting current, also showed evidence of side reactions. A model is being developed to understand how the occurrence of side reactions would affect galvanostatic polarization and transition-time measurements.

Measurement of the complete set of transport properties in multicomponent solutions is extremely difficult experimentally. We are developing a molecular dynamics simulation program to predict diffusion coefficients. The program has been validated for aqueous salt solutions, and is now being modified to simulate the nonaqueous liquid electrolytes of interest for Li batteries. Difficulties with the simulation algorithm have been encountered due to the planar structure of many of the carbonates.

Understanding heat generation is important both for designing thermal management systems to prevent overheating and for understanding calorimetry experiments. Our thermal research has three parts: derivation of an energy balance, measurement, and prediction of thermodynamic properties. An energy balance has been derived that includes heat of mixing within the electrolyte and the electrodes. The heat of mixing will be small for electrolytes and electrodes that possess transport properties high enough to be considered for commercial batteries. That heat which goes into formation of concentration gradients during passage of current will be released during relaxation of gradients after the current is interrupted.

Simulating heat generation requires knowledge of thermodynamic, transport, and kinetic properties. Measurements of entropy have been published in the literature for only a few electrodes. Assuming that the entropy of reaction is either constant or negligible is inappropriate for insertion compounds in which Li undergoes ordering on the lattice. Our calorimetry experiments for $LiAl_{0.2}Mn_{1.8}O_4F_{0.2}$ have demonstrated that entropic heat generation can be of the same order of magnitude as resistive heat generation, and that the entropic heat generation can vary in sign and magnitude with state of charge. Therefore, we have developed an experimental method for measuring the entropy of reaction as a function of state of charge, using LabVIEW to automatically control a water bath, potentiostat, and voltmeter. We plan to measure the entropy of reaction for all of the electrodes being considered for the BATT program. In addition, we have developed a Monte Carlo simulation of $LiMn_2O_4$ spinel to predict the entropy of reaction. The simulations closely match the measured values.

Alloy electrodes are being considered as alternatives to carbon or Li metal. We have conducted a literature review to determine which design options appear to successfully address the issue of loss of contact in alloy electrodes. We have learned that there are three simultaneous factors contributing to loss of contact: alloy expansion and contraction leading to cracking and particle contraction away from a continuous electrical path to the current collector, SEI formation around freshly exposed surface area, and particle agglomeration causing increased stresses during lithiation and delithiation. Therefore any design option must *i*) either involve no volume change or create a driving force to push particles together during contraction, *ii*) prevent resistive compounds from forming between particles during volume change, or *iii*) prevent particle agglomeration.

Lithium metal has the highest energy density of any electrode. However, it will never be safe to use commercially until one can figure out how to prevent the risk of dendrites shorting the cell. We are examining the effects of different physical properties, such as surface energy, transport properties in the electrolyte, and mechanical properties of the electrolyte and Li metal, on the growth rate of dendrites. A preliminary model of the effects of surface energy has been completed. A preliminary analysis using elasticity theory has shown that the mechanical properties of the polymer separator affect dendrite growth more significantly than surface forces; furthermore, the plasticity of the Li surface needs to be accounted for in the mechanical analysis.

In situ confocal Raman spectroscopy can be used to measure concentration gradients with high spatial resolution across the electrolyte and to observe dendrite growth. These experiments, to be performed in collaboration with Robert Kostecki

(LBNL), will allow measurement of transport properties as well as analysis of the effect of concentration gradients on dendrite growth. Work is still underway to construct a cell container that is airtight, inert, transparent, can be thermostated, and fits inside the confocal Raman microscope.

PUBLICATIONS

M. Doyle, J.P. Meyers and J. Newman, "Computer Simulations of the Impedance Response of Lithium Rechargeable Batteries," *J. Electrochem. Soc.*, **147**, 99 (2000).

H. Hafezi and J. Newman, "Verification and Analysis of Transference Number Measurements by the Galvanostatic Polarization Method," *J. Electrochem. Soc.*, **147**, 3036-3042 (2000).

C. Fellner and J. Newman, "High-Power Batteries for Use in Hybrid Vehicles," *J. Power Sources*, **85**, 229 (2000).

K.E. Thomas, S.E. Sloop, J.B. Kerr and J. Newman, "Comparison of Lithium-Polymer Cell Performance with Unity and Nonunity Transference Numbers, *J. Power Sources*, **89**, 132 (2000).

PRESENTATION

H. Hafezi, S.E. Sloop, J.B. Kerr and J. Newman, "Measurement and Analysis of the Transport Properties of Lithium Trifluoro-methane sulfonylimide (LiTFSI) in Oxymethylene-linked Poly(ethylene oxide) (PEMO)," *198th Meeting of the Electrochemical Society*, Phoenix, AZ, October 22-27, 2000.

Microstructural Modeling of Highly Porous Fibrous and Particulate Electrodes

Ann Marie Sastry

The University of Michigan, Department of Mechanical Engineering and Applied Mechanics, Ann Arbor, MI 48109-2125

(313) 764-3061; fax: (313) 747-3170; e-mail: amsastry@engin.umich.edu

Objectives

- Perform AFM imaging of Li-ion electrodes to better define simulation parameters for carbon morphologies and connectivities.
- Refine and expand simulations on conduction and mechanical load transfer in particle networks, and couple modeling of damage and mechanics phenomena.
- Elucidate the effects of small-scale particle-particle interconnects in materials.
- Develop common platforms for numerical implementation, suitable for use in analyzing a wide range of materials of high interest to DOE and industry.

Approach

- Develop 3D techniques for representation of particulate/fibrous networks, including models for intersections.
- Develop closed-form approximations for materials behavior dependence upon particle/fiber junctions.
- Characterize damage progression through continued simulations, and test the validity of numerical approaches.
- Expand experimental investigations to include testing of Li-ion cells.

Accomplishments

- Solved mechanics problems of closed-form small-scale composite particles (fiber-fiber).
- Investigated particulate geometries; developed algorithms for defining particle junctions.
- Completed 3D→2D correlations for small-scale mechanics problems.
- Continued development of techniques for coupled transport/mechanics for fibrous/spheroidal morphologies.

Future Directions

- Develop 3D→2D simplifications for particle/fiber morphologies.
- Continue full-scale cell testing of Li-ion cells to benchmark theoretical results from damage analysis.
- Package codes and combination with electrochemical modeling.

Degradation of Li-ion anode materials is currently a persistent problem, with damage presenting as blistering and/or delamination. The loads involved in these complex networks are multiaxial, and degradation affects not only the networks' ability to withstand subsequent loads, but also negatively affects conductivity. A range of methods for representing the arrays of particles within these materials have been explored, as shown in Fig. 59.

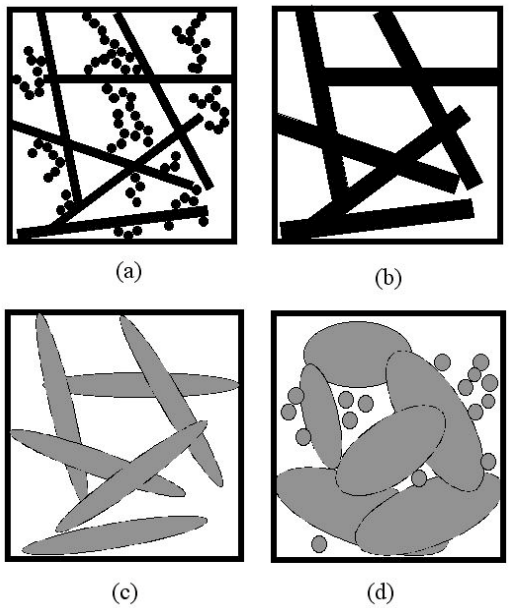

Figure 59. Four possible representations for porous materials comprised of fibers and particles, including (a) beams representing fibers, with spherical particles, (b) 2D beams representing fibers, (c) 2D ellipses representing fibers and (d) ellipsoidal particles of varying aspect ratio, representing both fibers and particles.

The connectivity of the network and the bond densities play a key role in assessing scale effects in simulation. Moreover, anode materials are heterogeneous mixtures of particles which are imperfectly bonded and non-straight. In light of the significance of bond type, we have concentrated on modeling the 3D interconnects in fiber/particle networks. We characterized the interpenetration of fibers or particles as degree of intersect (d.o.i.), as shown in Fig. 60.

Normalized effective moduli and peak stresses have been generated over several orders of magnitude in torsion spring constant representing bond stiffness, and for a wide range representative cell sizes. The reduction in both modulus and strength are more dramatic for compliant, rather than stiff bonds, as the scale of simulation size increases, in all cases. For the range of simulation sizes studied, there were no plateaux in these values, suggesting that unlike the conductivity problem, the mechanics problem requires a statistical approach detailed enough to quantify bond effects. For rigid bonds, the effect of on moduli and strengths over three orders of magnitude of simulation lengthscale were moderately small; few networks studied, however, appeared from image analysis to contain well-defined fiber-fiber bonds. These results suggest that for multiphase networks, the statistics of connectivity of even unpercolated phases are warranted.

(a)

(b)

Figure 60. 3D modeling with fillet. Detail of the joint of a finite element model of two intersecting fibers with (a) d.o.i.=0.571 and (b) d.o.i.=0.667.

Conduction modeling has similarly been focused on heterogeneous arrays, and the importance of non-percolated phases embedded within a percolated phase (Fig. 61, with material parameters chosen to be consistent with commonly used geometries of particles in Li-ion anodes) has been established, mirroring results for the mechanical simulations.

The implications of our findings include the importance of consideration of all phases in the material, concentration of efforts on representation of junctures rather than further attempts at resolving individual particle shape, and the importance of connective phases (*e.g.*, binders) in Li-ion cells in assuring connectivity and mechanical and conductive performance.

PUBLICATIONS

A.M. Sastry, C.W. Wang and L. Berhan, "Deformation and Failure in Stochastic Fibrous Networks: Scale, Dimension and Application," *Probabilistic Approaches to Fracture and Fatigue*, W. Soboyejo, Ed., Trans Tech Publications, Ltd. (2000).

C.W. Wang, L. Berhan and A.M. Sastry, "Structure, Mechanics and Failure of Stochastic Fibrous Networks: Part I. Microscale Considerations," *ASME J. Eng. Mater. Technol.*, **122**, 450-459 (2000).

C.W. Wang and A.M. Sastry, "Structure, Mechanics and Failure of Stochastic Fibrous Networks: Part II. Network Simulation and Application," *ASME J. Eng. Mater. Technol.*, **122**, 460-468 (2000).

PRESENTATIONS

A.M. Sastry, C.W. Wang and L. Berhan, "Localized Strain and Damage in Fiber/Particulate Networks: Damage Mechanisms in Li-ion Carbonaceous Substrates," *Workshop on Interfaces, Phenomena, and Nanostructures in Lithium Batteries,* Argonne National Laboratory, Chicago IL, December 2000.

A.M. Sastry, C.W. Wang and L. Berhan, "Deformation and Failure in Stochastic Fibrous Networks: Scale Dimension and Application," *The 2000 ASME International Mechanical Engineering Congress & Exposition*, Orlando, FL, November 2000.

C.W. Wang, L. Berhan and A.M. Sastry, "Damage Tolerance of Fiber-Particle Networks with Imperfect Bonding: Applications for Battery Technologies," *The 2000 ASME International Mechanical Engineering Congress & Exposition*, Orlando, FL, November 2000.

A.M. Sastry, Invited Presentation, "Stochastic Materials: Design and Selectivity," *ONR/DARPA Synthetic Multifunctional Materials Workshop,* Sedona, AZ, September 2000.

A.M. Sastry, Invited Presentation, "Integration of Battery Power Supply in Ultralight Metal Structures," *Ultralight Metals Workshop, ONR Ultralight MURI*, Brewster, MA, August 2000.

A.M. Sastry, Invited Seminar, Princeton Materials Institute, Princeton University, Princeton, N.J., April 2000.

A.M. Sastry, Invited Seminar, Department of Mechanical Engineering, Rutgers University, Piscataway, N.J., April 2000.

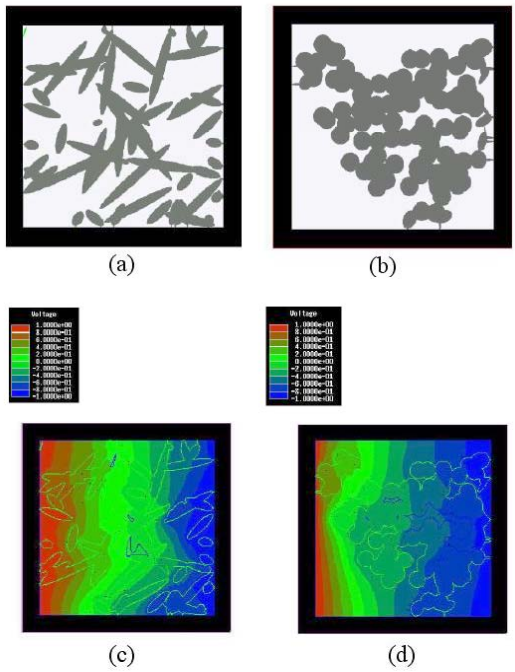

Figure 61. Networks in a unit cell (original volume fraction ≈ 50%) comprised of (a) ellipse, and (b) circles. Images (c) and (d) are voltage contours for fields (a) and (b). Resulting normalized effective conductivities for there arrays arrays, $K_{effective}/K_{fiber}$ are (a) 0.0708, and (b) 0.0 236, respectively

Thermal Modeling/Thermal Management

James W. Evans (Lawrence Berkeley National Laboratory)

University of California, Department of Materials Science and Mineral Engineering, 585 Evans Hall, MC 1760, Berkeley CA 94720

(510) 642-3807, fax: (510) 642-9164; e-mail: evans@socrates.berkeley.edu

Objective

- Study heat generation, heat transfer, and thermal management of large-scale batteries for EV applications.

Approach

- Develop simulation to express the heat generation rate based upon electrical and thermal state of battery.
- Experimental investigation of heat generation rates in small laboratory sized batteries.

Accomplishments

- Prepared calorimeter for measurements.
- Prepared galvanostat program for cyclic discharge.
- Compared 2D coupled results to original "thermal-only" model.

Future Directions

- Continue work to expand simulation to 3D.
- Measure thermal properties of Li/polymer batteries as a function of cyclic discharge.
- Reanalyze previous perturbation comparisons.

The primary focus of this research, for 2000, has been the development of the coupled model, and the extension of the model from 2D into 3D. Part and parcel of this modeling is a comparison of the coupled model to results predicted by the previous "thermal only" model and the perturbation analysis presented by Song and Evans.[1]

In previous, "thermal-only" models, classical thermal conductivity was used to determine the thermal distribution. The heat generation was taken from the electrochemical parameters *via* simplified relations, such as the Shepherd equations.[2] However, it is well known that there is a direct relationship between the local temperature inside a battery stack and the local conductivity. In fact it is this relationship which provides the opportunity for thermal run-away of a battery system. A coupled model was developed by Song and Evans to relate the local thermal parameters of a stack to the ionic conductivity.[3]

A comparison was made of the older "thermal-only" model and the coupled model. Figures 62 and 63 show a comparison of these two models for a perturbation simulation. In these figures it is seen that upon perturbation the coupled model returns to thermal stability much slower than the thermal-only model. This demonstrates that the coupled model behaves as expected as an increase in conductivity (hence heat generation) is induced locally at the site of the perturbation, therefore return to equilibrium is delayed.

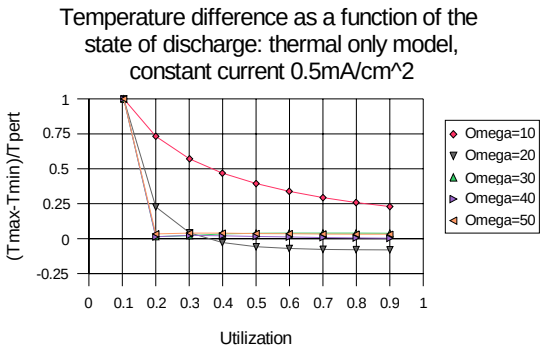

Figure 62.

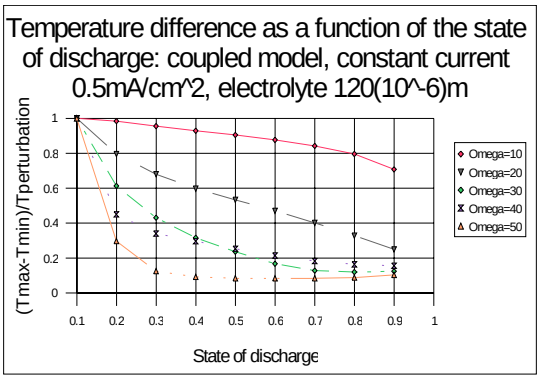

Figure 63.

During the course of this comparative study several questions were raised regarding the methods used in previous studies on perturbation analysis (using the thermal-only model). A startling discovery was that the parameters selected for the analytic solution showed the model becoming unstable only when the perturbations were the same size as the cell itself, which is a violation of the assumptions of perturbation theory. Figure 64 shows a plot of the system's response for a perturbation in the limit of stability as given by Song and Evans. For each data set there was no change in

the system, except the amplitude of the perturbation. According to an analytic solution, the response should be independent of the amplitude, and depend only upon the wavenumber. This indicates that there was a violation of the assumptions and the resulting numerical comparison, in the high wave number limit, is invalid.

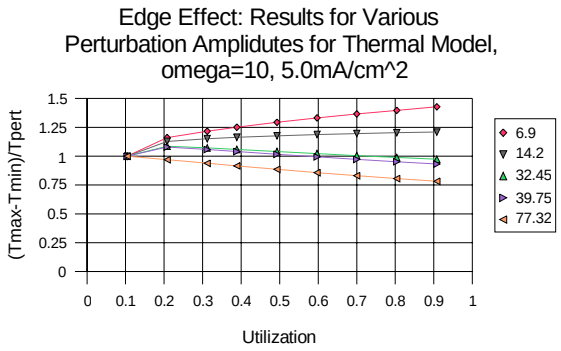

Figure 64.

FY 2001 will include a reanalysis of the previous 2D perturbation analysis within appropriate limits and with accurate thermal and electrochemical parameters.

Also in FY 2000 work began to expand the 2D coupled model to 3D. This is important as in a prismatic cell, there are two directions of easy conductivity, and one direction of hard thermal conductivity, as shown in Fig. 65. The current 2D model only uses one of the easy direction the hard direction. Expanding the cell into 3D will give a more accurate interpretation of the battery. It is hoped that results from this 3D model will be available by the end of FY2001.

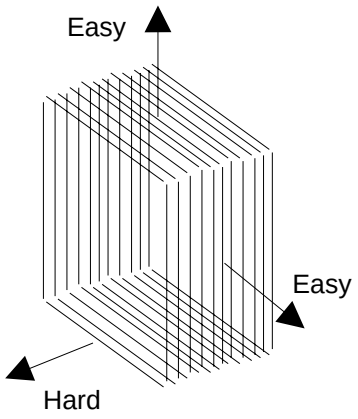

Figure 65.

REFERENCES

1. Song and Evans, *J. Electrochem. Soc.* **145**, 2328 (1998).
2. Chen and Evans, *J. Electrochem. Soc.* **141**, 2947 (1994).
3. Song and Evans, *J. Electrochem. Soc.* **147**, 2086 (2000).

LIST OF ACRONYMS

AFM	atomic force microscopy
AIBN	azo-bis-isobutyronitrile
ANL	Argonne National Laboratory
ARC	accelerating rate calorimeter
ATD	Advanced Technology Development
BATT	Batteries for Advanced Transportation Technologies
BES	Basic Energy Sciences
BMA	butyl methacrylate
BNL	Brookhaven National Laboratory
CB	comb-branch
ccp	cubic close packed
CPE	composite polymer electrolyte
CSAFM	current-sensing atomic force microscopy
CV	cyclic voltammetry
DEC	diethyl carbonate
DMC	dimethylcarbonate
DME	dimethoxyethane
DoD	depth of discharge
DOE	Department of Energy
d.o.i.	degree of intersect
DSC	differential scanning calorimetry
EC	ethylene carbonate
EMC	ethyl methyl carbonate
EQCM	electrochemical quartz crystal microbalance
ETR	Exploratory Technology Research
EV	electric vehicle
EXAFS	extended X-ray absorption fine structure
fcc	face-centered-cubic
FR	flame retardant
FTIR	Fourier transform infrared
GC	gas chromatography
GNP	glycine-nitrate process
HETAP	hexa-ethoxy-tri-aza-phosphazene
HEV	hybrid electric vehicle
HMTAP	hexa-methoxy-tri-aza-phosphazene
HOPG	highly oriented pyrolytic graphite
ICL	irreversible capacity loss
IIT	Illinois Institute of Technology
IRRAS	infrared reflection absorption spectroscopy
LBNL	Lawrence Berkeley National Laboratory

LiTFSI	Lithium bis(trifluoromethane-sulfonyl)imide
MAS	Magic Angle Spinning
MCMB	mesocarbon microbead
MEEP	methoxyethoxyethoxide phosphazene
mpe	mass change per mole of electron transfer
MSA	Mine Safety Appliances
MW	molecular weight
NFE	nonflammable electrolyte
NMP	1-methyl-2-pyrrolidinone
NMR	nuclear magnetic resonance
NRC	National Research Council
OAAT	Office of Advanced Automotive Technologies
OCV	open circuit voltage
PC	propylene carbonate
PEC	polyethercarbonate
PEG-DME	polyethylene glycol - dimethyl ether
PEMO	polyethylene-methylene oxide
PEO	poly(ethylene oxide)
PNGV	Partnership for a New Generation of Vehicles
PTC	phase transfer catalysis
PVDF	poly(vinylidene fluoride)
PVIC	poly(vinylene carbonate)
PVICOX	poly(1,3-dioxolan-2-one-4,5-diyl oxalate)
ROP	ring-opening polymerization
SE	spectroscopic ellipsometry
SEI	solid electrolyte interphase
SERS	surface-enhanced Raman spectroscopy
SHR	self heat rate
TFEA	trifluoroethyl acetate
TGA	thermogravimetric analysis
THF	tetrahydrofuran
TOM	trichlorosilyl octyl methacrylate
UDP	urea-diphosphonate
UHV	ultra high vacuum
USABC	United States Advanced Battery Consortium
VC	vinylene carbonate
XANES	X-ray absorption near-edge spectroscopy
XAS	X-ray absorption spectroscopy
XPS	X-ray photoelectron spectroscopy
XRD	X-ray diffraction
XRDA	X-ray diffraction analysis

ANNUAL REPORTS

1. Exploratory Technology Research Program for Electrochemical Energy Storage – Annual Report for 1999, LBNL-45767 (May 2000).

2. Exploratory Technology Research Program for Electrochemical Energy Storage – Annual Report for 1998, LBNL-42694 (June 1999).

3. Exploratory Technology Research Program for Electrochemical Energy Storage – Annual Report for 1997, LBNL-41950 (June 1998).

4. Exploratory Technology Research Program for Electrochemical Energy Storage – Annual Report for 1996, LBNL-40267 (June 1997).

5. Exploratory Technology Research Program for Electrochemical Energy Storage – Annual Report for 1995, LBNL-338842 (June 1996).

6. Exploratory Technology Research Program for Electrochemical Energy Storage – Annual Report for 1994, LBL-37665 (September 1995).

7. Exploratory Technology Research Program for Electrochemical Energy Storage – Annual Report for 1993, LBL-35567 (September 1994).

8. Exploratory Technology Research Program for Electrochemical Energy Storage – Annual Report for 1992, LBL-34081 (October 1993).

9. Exploratory Technology Research Program for Electrochemical Energy Storage – Annual Report for 1991, LBL-32212 (June 1992).

10. Technology Base Research Project for Electrochemical Energy Storage – Annual Report for 1990, LBL-30846 (June 1991).

11. Technology Base Research Project for Electrochemical Energy Storage – Annual Report for 1989, LBL-29155 (May 1990).

12. Technology Base Research Project for Electrochemical Energy Storage – Annual Report for 1988, LBL-27037 (May 1989).

13. Technology Base Research Project for Electrochemical Energy Storage – Annual Report for 1987, LBL-25507 (July 1988).

14. Technology Base Research Project for Electrochemical Energy Storage – Annual Report for 1986, LBL-23495 (July 1987).

15. Technology Base Research Project for Electrochemical Energy Storage – Annual Report for 1985, LBL-21342 (July 1986).

16. Technology Base Research Project for Electrochemical Energy Storage – Annual Report for 1984, LBL-19545 (May 1985).

17. Annual Report for 1983 – Technology Base Research Project for Electrochemical Energy Storage, LBL-17742 (May 1984).

18. Technology Base Research Project for Electrochemical Energy Storage – Annual Report for 1982, LBL-15992 (May 1983).

19. Technology Base Research Project for Electrochemical Energy Storage – Report for 1981, LBL-14305 (June 1982).

20. Applied Battery and Electrochemical Research Program Report for 1981, LBL-14304 (June 1982).

21. Applied Battery and Electrochemical Research Program Report for Fiscal Year 1980, LBL-12514 (April 1981).

Office of Transportation Technologies Series of 2001 Annual Progress Reports

- Office of Advanced Automotive Technologies FY 2001 Program Highlights
- Vehicle Propulsion and Ancillary Subsystems
- Automotive Lightweighting Materials
- Automotive Propulsion Materials
- Fuels for Advanced CIDI Engines and Fuel Cells
- Spark Ignition, Direct Injection Engine R&D
- Combustion and Emission Control for Advanced CIDI Engines
- Fuel Cells for Transportation
- Advanced Technology Development (High-Power Battery)
- Batteries for Advanced Transportation Technologies (High-Energy Battery)
- Vehicle Power Electronics and Electric Machines
- Vehicle High-Power Energy Storage
- Electric Vehicle Batteries R&D

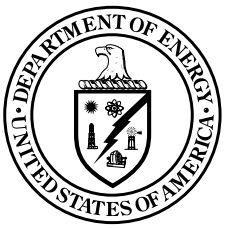

www.cartech.doe.gov

DOE/EERE/OTT/OAAT - 2001/010